THRUST MODULATED MULTIVARIABLE CONTROL OF THE GE21 ENGINE USING THE LQG/LTR METHOD

by

FRANCIS X. DUNN

BSEE, WORCESTER POLYTECHNIC INSTITUTE (1983)

SUBMITTED IN PARTIAL FULFILLMENT

OF THE REQUIREMENTS FOR THE

DEGREE OF MASTER OF SCIENCE

IN ELECTRICAL ENGINEERING

at the

MASSACHUSETTS INSTITUTE OF TECHNOLOGY

MAY 1986

Signature of Author _____

Department of Electrical Engineering
and Computer Science, May 1986

Certified By _____

Professor H. A. Spang, III
Thesis Co-Supervisor

Certified By _____

Professor M. Athans
Thesis Co-Supervisor

Accepted By _____

Professor A. C. Smith, Chairman,
Department Committee on Graduate Studies

THRUST MODULATED MULTIVARIABLE CONTROL OF THE GE21 ENGINE USING THE LQG/LTR METHOD

by

Francis X. Dunn

Submitted to the Department of Electrical Engineering and Computer Science on May 21, 1986 in partial fulfillment of the requirements for the degree of Master of Science in Electrical Engineering.

ABSTRACT

A multivariable control system for the GE21 engine operating in the Thrust Modulation Mode is designed using the Linear Quadratic Gaussian with Loop Transfer Recovery (LQG/LTR) method. A linear model of the GE21 is developed for the engine operating at maximum power without afterburner. The linear model is used to design three compensators, all using the LQG/LTR method. These designs are then used to illustrate the important characteristics and properties of the control system and to demonstrate the sucessful use of the LQG/LTR method in the design of a compensator for operating the engine in this high performance mode. The investigation of the behavior of the three compensator designs is the main topic of this research.

THESIS SUPERVISORS: Dr. H. Austin Spang III, Adjunct Professor of Electrical Engineering

Dr. Michael Athans, Professor of Systems Science and Engineering

ACKNOWLEDGEMENTS

I would like to express my thanks to my thesis supervisors, Professors H. Austin Spang III and Michael Athans for their support and guidance throughout the course of this research. I also wish to thank Mr. Petros Kapasouris whose ideas helped keep this work moving forward.

This research was carried out at the MIT Laboratory for Information and Decision Systems. Financial support was provided by the Aircraft Instruments Department of the General Electric Company and the General Electric Corporate Research and Development Center.

TABLE OF CONTENTS

LIST OF FIGURES

LIST OF TABLES

CHAPTER 1

INTRODUCTION AND SUMMARY

1.1 BACKGROUND

There has been a growing interest in increased performance control systems for jet engines [12, 14, 16, 20]. In fact, much of the recent work has used jet engines as the sample plants. Kappos et. al. [4, 39] used a linear model of the F100 to demonstrate a model reduction technique and used the LQG/LTR method for the final control design example. Pfeil et. al. [5, 41] explored the differences between a SISO design and a MIMO design using the LQG/LTR method for a control system for the T700 and Kapasouris et. al. [1, 40] investigated the differences between an LQR based design and an LQG/LTR design for the GE21.

The LQG/LTR methodology provides a step-by-step procedure for designing multivariable control systems with certain guaranteed stability and robustness properties. The initial work on the LQG/LTR based designs was done fairly recently by Doyle and Stein [21]. Robustness characterization techniques for multivariable LQG based designs has been provided by Lehtomaki [2, 32]. In addition to the design examples using jet engines, the LQG/LTR methodology has been applied to other plants, such as

submarines [15] and aircraft [33].

Since the LQG/LTR methodology is a fairly recent development, it has not been tested in many complex multivariable control system designs and has not been evaluated in industrial applications [16]. There are many techniques, such as diagonal dominance using the Inverse Nyquist array [34], Nyquist methods [42], the relative gain array [19], the linear quadratic regulator [35] and variations of these techniques [36, 37], which are more widely used as approaches to complex control system designs.

This research uses a model of an advanced jet engine, the GE21, and the LQG/LTR methodology to design a multivariable control system for operating the engine in the thrust modulation mode. Use of the singular value decomposition, which is becoming a widely used tool in the analysis of multivariable systems [1, 2, 13, 17], is employed throughout the design process.

1.2 PROBLEM DISCUSSION

Control system design for jet engines is now experiencing a need to take full advantage of all available control inputs to achieve the new and expanded performance demands of modern jet aircraft. The current control systems typically use two single-input/single-output (SISO) control loops which are spectrally separated in frequency [16]. Any additional control inputs are scheduled, open loop, based on

emperical or analytical data which defines various operating points of the engine such as ground idle, climb or cruise. This type of design has demonstrated adequate performance and, more importantly, excellent stability characteristics, with respect to actuator or sensor failures and actuator saturations, over the entire operating range of present day engines.

Conventional engine control designs, however, will not meet the more stringent performance requirements of the next generation jet engines. These advanced propulsion control systems must be capable of managing multiple engine operating modes, multiple engine thrust vectors and significant interactions with the flight control systems.

One of the many new modes of operation required of the next generation engines is termed the "Thrust Modulation Mode" [20]. The thrust modulation mode of operation provides the capability for achieving rapid thrust increases or decreases that are independent of the rotor speeds. The control system for this mode of operation would be required to hold the rotors at constant speed and vary the thrust output using the various engine geometries and other control inputs. The advantages to such a mode of operation have been identified [20], but the control system design issues involved with this mode of operation have not been fully addressed.

One of the reasons that this mode of operation has not been explored further is the lack of a systematic control

system design procedure. The design method would be required to produce a control system design which met the increased performance requirements while providing the necessary stability properties of the engine.

One approach to this control system design would be to try to extend the conventional methods which use two SISO control loops to handle multiple SISO loops, all spectrally separated in frequency. This approach could draw on proven designs of the past, but would quickly become very complicated. Indeed, simply extending this technique to the case of three SISO loops is a very complex task.

A more viable approach is to use the more recent advances in the area of multi-input/multi-output (MIMO) control system design and allow the interaction of various control inputs to enhance the loop design.

1.3 CONTRIBUTION OF THESIS

The main contribution of this thesis is to present a detailed example of a MIMO control system design using the LQG/LTR methodology. The intent of this work is to demonstrate, by example, the feasibility of using this methodology in the area of advanced jet engine control systems design with emphasis on the thrust modulation mode of operation.

The design examples describe the method used to define the linear models of the plant, different approaches to

scaling, selection of inputs and outputs for use in the control design and various issues involved in the design of an LQG/LTR based compensator. The examples also extend the work of Kapasouris [1, 40] related to the use of the singular value decomposition in selecting inputs and outputs and of Kappos [4, 39] for reducing the order of the compensator.

Other aspects of the design procedure are reviewed and design techniques, such as over designing the target loop and performing only partial recovery, are introduced and demonstrated.

It is hoped that this thesis will add to the others which demonstrate the success of the LQG/LTR methodology and will partially fulfill the need for multivariable control system design examples which use this method.

1.4 OUTLINE OF THESIS

Chapter 2 contains a description of the GE21 engine. The linear models of the plant are developed and the input/output response of the linear and nonlinear models are compared. The concept of thrust modulation is defined and the rationale for operating an engine in this mode is provided. A general overview of basic jet engine operation is also provided.

Chapter 3 discusses the issues of scaling and scaling transformations, the use of the singular value decomposition as a tool for selecting inputs and outputs for the control

design and a brief comment on the frequency response of the system. The control system design specifications are stated and the interpretation of these specifications is provided. A summary of the robustness results for MIMO control systems is also given. The final section of the chapter presents a practical discussion of the plant behavior at steady state and how one might interpret this information.

Chapter 4 presents an overview of the LQG/LTR methodology followed by the step-by-step systematic implementation of this procedure. A discussion of the limitations and constraints of this method is provided as well as a brief comment on the practical issues involved with the design.

Chapter 5 presents the detailed design examples using the GE21 and the LQG/LTR methodology. Three example designs are used to demonstrate the effects of partial and full recovery on the system parameters. The techniques of over designing the target loop and of reducing the order of the compensator are also demonstrated.

Chapter 6 contains a summary and some directions for future research.

CHAPTER 2

SYSTEM DESCRIPTION AND MODELING

2.1 INTRODUCTION

The system used for the design examples in this research is a computer model of an aircraft jet engine, the GE21. The GE21 is a double bypass variable cycle engine model intended for advanced applications. This engine does not yet exist; the computer model is used for studies of technologies expected to be available in the years 1990 - 2000 time frame. The model was provided by the General Electric Company.

This chapter contains a brief overview of general jet engine operation followed by some specific information about the GE21 model. The concept of "thrust modulation" is defined and the rationale for operating in this mode is provided.

The technique used to develop the linear models of the systems is presented and the linear model of the plant, around the appropriate operating point, is obtained. A comparison of the linear and nonlinear model input/output response is also provided.

This research initially used two engines, with different physical properties, as the actual "plants" for which the control systems were to be designed. The two engine models were of the GE21 and GE16 advanced jet engines. The models

of these engines were provided by the General Electric Company. Both engines were used during the course of the research because of the differences in physical properties of the engines. The GE21 is a double bypass variable cycle engine designed for large aircraft applications whereas the GE16 is a single bypass engine designed for smaller aircraft applications.

Although both models were used, this thesis concentrates on the operation of the GE21 engine. The reason for centering on the GE21 is that there were problems with the nonlinear model of the GE16 which cast some doubt as to the accuracy of the results. The GE21 is a more mature model and had been used in past work. The model of the GE16 available to the author is being revised; unfortunately it will be available after this research is finished. However, once the model is available, the results of this work should extend directly to use of either model.

2.2 BASIC JET ENGINE OPERATION

This section briefly describes the basic operation of axial flow jet engines. More detailed information about jet engine operation can be found in [3] and [11].

Figure 2.2-1 presents a picture of a typical production engine, the General Electric J79-15, and a cutaway view of this engine. This figure is representative of present day jet engine construction.

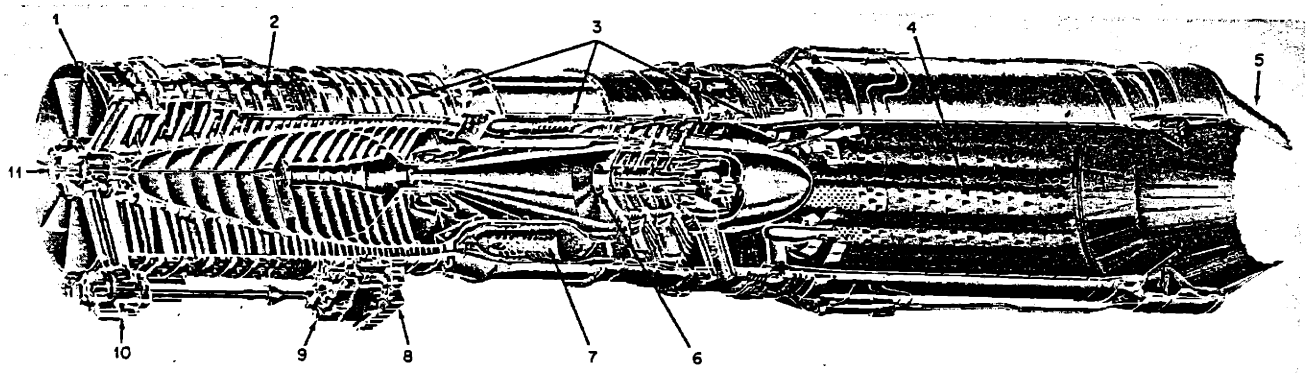

1 ANTI-ICED INLET CASE AND STRUTS
2 VARIABLE STATOR STAGES
3 SPLIT COMPRESSOR COMBUSTOR, AND TURBINE CASINGS
4 AFTERBURNER
5 VARIABLE-AREA CONVERGING-DIVERGING EXHAUST NOZZLE
6 THREE-STAGE TURBINE
7 COMBUSTION CANS
8 REAR GEARBOX
9 MAIN AND AFTERBURNER FUEL CONTROL
10 TRANSFER GEARBOX
11 FRONT GEARBOX FOR CARTRIDGE OR PNEUMATIC STARTER

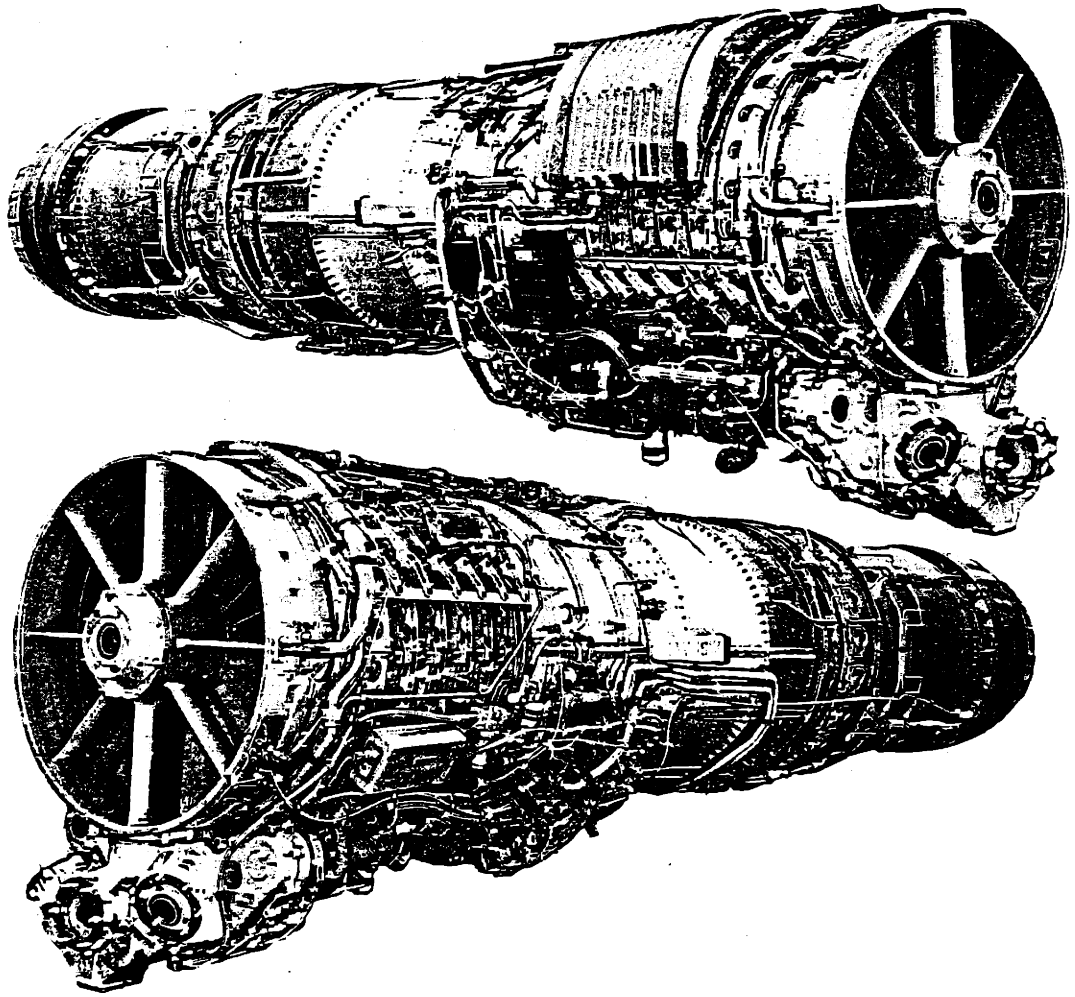

Figure 2.2-1
General Electric J79-15 Engine

The basic engine consists of six major sections. These are: 1) an inlet duct, 2) an inlet fan (or fans), 3) a compressor, 4) a combustor, 5) a turbine (or turbines) and 6) an exhaust nozzle. In addition to these major sections, each engine incorporates a series of subsystems, such as accessories, fuel, cooling, lubrication and ignition. Some engines also include a thrust augmentation system, such as water injection or afterburning, to improve engine performance based on the intended application of the engine (e.g., commercial jet liner, military cargo plane, attack fighter aircraft, etc...).

The basic operation of these axial flow jet engines is also similar. The outside air enters the engine through the inlet duct at the front of the engine. Air is directed through the inlet by the geometry of the duct. This duct geometry may be variable. Input fans may be used to provide more uniform airflow to the rest of the engine and to accelerate air around the the engine "core" through the bypass ducts and into the exhaust nozzle. In fact, a major portion of the thrust output of some engines is attributable to the air which flows around the core of the engine.

Air which does not bypass the engine "core" is directed into a compressor. The compressor usually contains many stages and is used to reduce the volume and increase the pressure of the incoming airstream. Typical compression ratios (i.e., Pout/Pin) range from 5 to 20. The compressed air is then passed into the combustor section.

The combustor usually consists of many chambers. Inside the inner chamber, aircraft fuel is vaporized and mixed with the high pressure airstream. The air/fuel mixture is then ignited by the engine ignition system. Once the initial air/fuel mixture is ignited and the engine reaches operating temperature, the ignition subsystem can be switched off and the combustion process will continue as long as the proper air/fuel ratio is maintained.

The resultant combustion causes an increase in the temperature of the gas which is proportional to the mass of the fuel consumed. There is a moderate increase in the velocity of the airstream and a small decrease in pressure. There is also a very large increase in the volume of the gas.

During the combustion process, only about 25% of the airstream is used up. The remainder of the air is used to reduce the temperature of the expanding gas before leaving the combustion chamber. The temperature of the gas must be reduced to a level which can be tolerated by the high pressure turbine stage which follows (i.e., the turbine blades must not melt or warp).

The hot, expanding gas is then passed to a turbine, or series of turbines. The turbine extracts the kinetic energy from the expanding gasses and uses this energy to turn the shafts which provide power to the compressor, the inlet fans, the engine subsystems and the aircraft accessory subsystem.

From the turbine section, the airstream is passed to the exhaust nozzle area. After leaving the turbine section,

there is still enough pressure remaining in the airstream to force the hot gasses through the exhaust nozzle at high speeds. In addition, the airstream from the engine core is mixed with the high speed airstream which was accelerated around the core by the input fans in the exhaust nozzle.

The thrust output of the engine results from taking in a large mass of air at the inlet and expelling this "air mass" through the exhaust nozzle at a much higher speed than when it entered. For maximum thrust, the gasses must be expanded completely in the exhaust nozzle and discharged into the atmosphere in an axial flow.

2.3 THRUST MODULATION

The propulsive force developed by the jet engine is measured in pounds of thrust. This force is what propels the aircraft through the air. The advances in jet aircraft design are requiring the engine to play a much larger role in the operation of the aircraft.

One of the many new modes of operation required of these advanced jet engines is termed the "Thrust Modulation Mode" [20]. This mode of operation is one in which the thrust output of the engine can be changed without changing the fan or core speeds of the engine. This type of operation provides the capability for achieving rapid thrust increases or decreases that are independent of the lower speed rotor dynamics.

The advantages to this type of operation are that it allows the engine and aircraft flight controls to work together which in turn allows for higher performance of the aircraft. Some specific examples are:

1) Shipboard Landings - this mode of operation would allow the incoming aircraft to reduce thrust for landing but would allow rapid thrust increase if the landing had to be aborted.

2) Terrain Following - this mode would allow the flight control system to modulate thrust as required to follow the desired course.

3) Threat Avoidance - this mode of operation would allow a much higher degree of manuverability to assist the pilot with avoidance of dangerous assaults.

The concept of thrust modulation is relatively straight forward. By adjusting the various engine parameters, such as the air bypass ratio, the nozzle area, the fuel flow and the inlet and compressor guide vane angles, the thrust output of the engine can be changed and the speeds can, in principle, be held constant. The task is to determine just how to vary these parameters and to arrive at a systematic approach to designing a control system that maintains the stability of the engine while operating in the mode required.

Before addressing the detailed issues involved in the design, a general overview of the nonlinear models of jet engines is provided in the following section.

2.4 GENERAL DESCRIPTION OF THE NONLINEAR COMPUTER MODELS

This research used computer models of two different jet engines. The set up, variable naming conventions and operation of these models basically follow the accepted practices outlined in [28] and [29].

Each section of the engine is given a number which is called the "station designator." Variable names usually consist of one or two letters followed by the appropriate station designator. Figure 2.4-1 shows a typical layout of "stations" in a jet engine. Some examples of nomenclature system are given in Table 2.4-1.

Variable Name Starting Letter	Variable Type	Example
"T"	TEMPERATURE	T42
"P"	PRESSURE	P3
"PS"	STATIC PRESSURE	PS3
"W"	FLOW	W42
"WF"	FUEL FLOW	WF36
"A"	AREA	A8
"AE"	EFFECTIVE AREA	AE96
"STP"	STATOR POSITION	STP48

Table 2.4-1
Example of Variable Nomenclature

The specific variable of interest for each of the engine models used are discussed in more detail in the appropriate sections of this thesis.

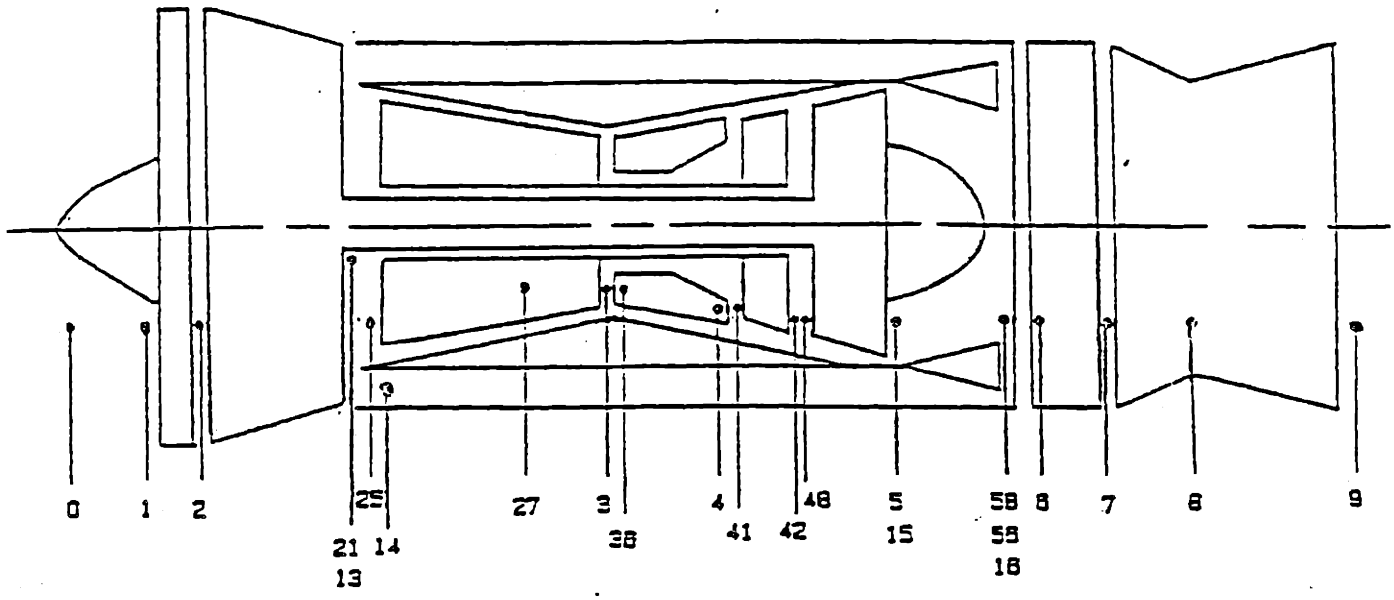

PLANE	DEFINITION
AMB	Free Stream Air Conditions
1	Engine/Inlet Interface (before anti-icing air enters primary stream)
2	Fan Rotor Inlet (after anti-icing air enters primary stream)
13	Fan Tip Discharge
14	Bypass Duct Entrance
15	Mixer Cold Chute Inlet
16	Mixer Cold Chute Exit
21	Fan Hub Discharge
25	High Pressure Compressor Inlet
27	High Pressure Compressor Interstage Bleed Extraction Station (5th stage)
3	High Pressure Compressor Discharge (after bleed extraction)
36	Combustor Inlet
4	Combustor Exit
41	High Pressure Turbine Inlet (after re-introduction of non-chargeable nozzle cooling flow)
42	High Pressure Turbine Exit (after re-introduction of rotor cooling flow)
49	Low Pressure Turbine Inlet
5	Low Pressure Turbine Exit (after re-introduction of cooling flow)
56	Mixer Hot Chute Exit
58	Combined Fan and Core Streams at Point of Mixing
6	Augmentor Inlet (AFT of flameholders)
7	Augmentor Exit
8	Primary Exhaust Nozzle Throat
9	Exhaust Nozzle Exit

Figure 2.4-1
Jet Engine Station Designators

2.5 GE21 DESCRIPTION

2.5.1 OVERVIEW OF GE21 OPERATION

The GE21 is a dual rotor, double bypass variable cycle jet engine. The engine consists of of two blocker fans, two variable area bypass inlets (VABI), a multistage compressor, a combustor, a high pressure turbine, a low pressure turbine, a variable area inner exhaust nozzle, a variable area outer exhaust nozzle and variable stator positions on the fans and turbines. The outline sketch (envelope) of this engine is shown in Figure 2.5-1. A cutaway diagram which depicts the physical configuration of the engine is shown in Figure 2.5-2.

The operation of this engine is similar to the basic description given in section 2.2. The unique features of this engine are the variety of control inputs available. In addition to the traditional variable stators, fuel control and variable exhaust nozzle area, this engine provides many other variable geometries and engine parameters for use in controlling the engine. Some of these are the Forward Variable Area Bypass Inlet (VABI), the Rear VABI, two variable area exhaust nozzles and variable stators on the inlet fan, compressor and low pressure turbine. Many engines contain some combinations of these controls, but few contain all of them and none dynamically adjust all these controls simultaneously, in a closed-loop sense, in the engine control

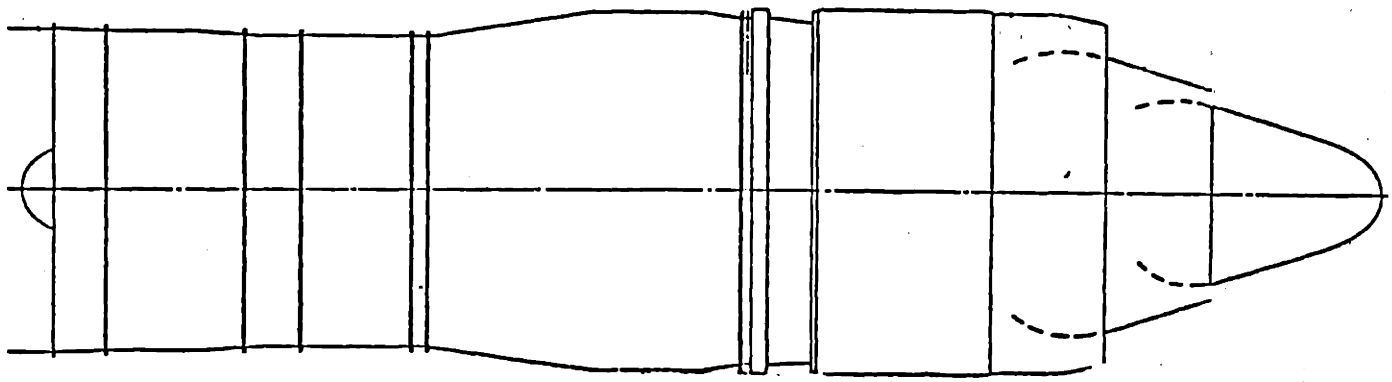

Figure 2.5-1
Envelope of GE21 Engine

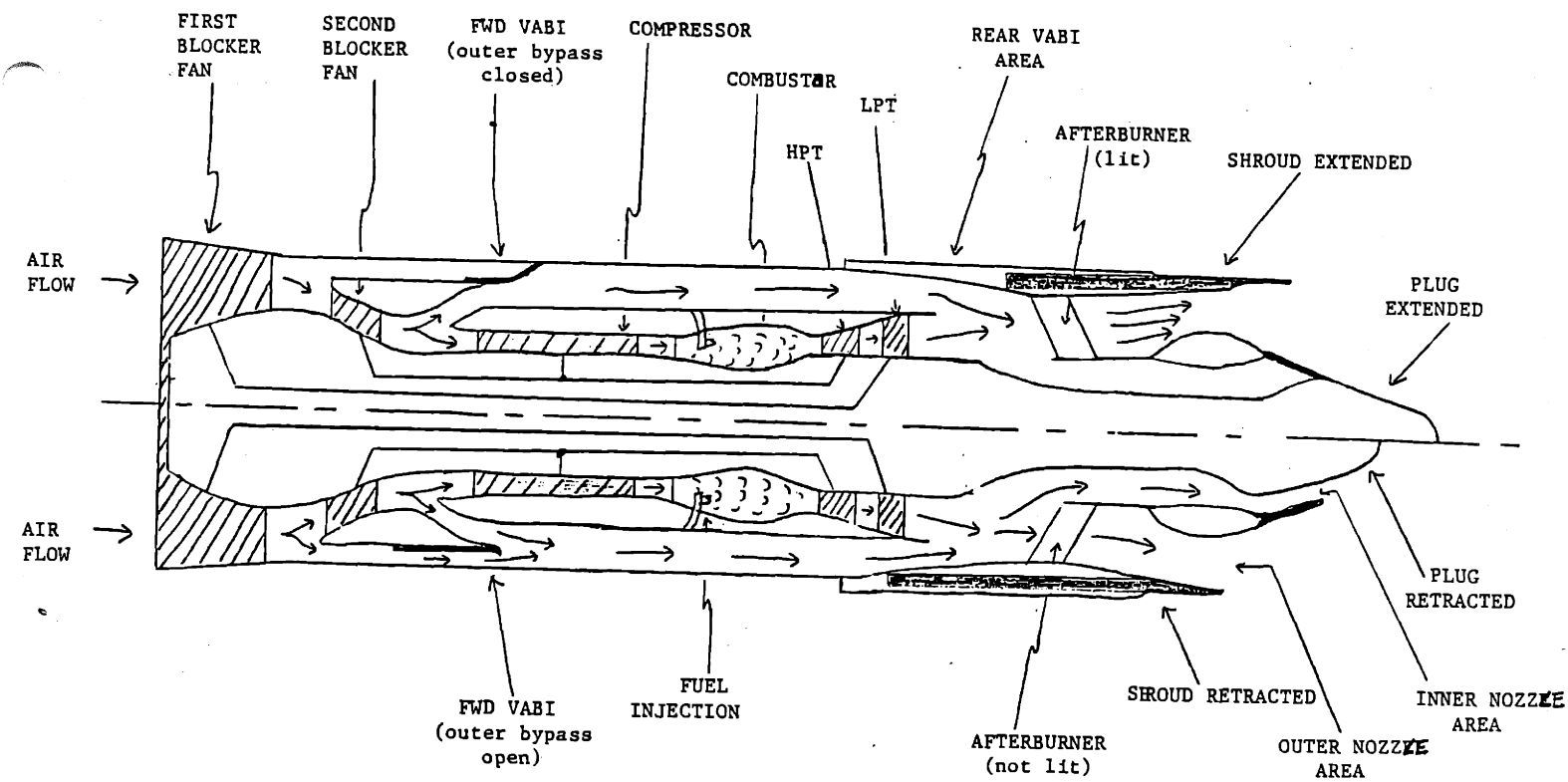

Figure 2.5-2
Cut-Away View of GE21 Engine

system.

Many of these control inputs have been made possible by recent advances in jet engine design. The availability of all these controls is the feature of advanced jet engines, such as the GE21, which allows operation in the various modes, including the thrust modulation mode.

2.5.2 GE21 NONLINEAR DYNAMIC MODEL

A nonlinear dynamic computer model of the GE21 engine will be used as the "true" plant throughout this control system design examples. The linear models required for the system design will be derived from this nonlinear model. This computer model is assumed to be a good approximation of the actual engine operation and it is reasonable to assume that a control system designed for the computer model will be useful in controlling the actual engine. In the frequency domain, the model is assumed to be valid up to a frequency range of approximately 50 rad/sec. Above this range, high frequency unmodeled dynamics are assumed to predominate.

A block diagram representation of the engine modeled by the computer code is shown in Figure 2.5-3. This diagram loosely follows the SAE standards in [28] and [29] for station designations and nomenclature as described in section 2.4. A complete list of the variables for the GE21 is given in appendix A.

2.5.3 GE21 INPUT/OUTPUT DESCRIPTION

The nonlinear computer model of the GE21 provides eight independent control variables, which can be used to control the engine operation, two state variables and a variety of output variables to select from.

2.5.3.1 GE21 CONTROL VARIABLES

The available control variables for the GE21 are tabulated in Table 2.5-1.

VARIABLE NAME	UNSCALED UNITS	DESCRIPTION
STP22	SQ. IN.	SECOND BLOCKER FAN STATOR POSITION
STP48	SQ. IN.	LOW PRESSURE TURBINE STATOR POSITION
AE96	SQ. IN.	FORWARD VABI EFFECTIVE AREA
AE16	SQ. IN.	REAR VABI EFFECTIVE AREA
A8	SQ. IN.	OUTER NOZZLE AREA
A88	SQ. IN.	INNER NOZZLE AREA
WF36	PPH	MAIN BURNER FUEL FLOW
WF6	PPH	AFTERBURNER FUEL FLOW

Table 2.5-1
Available Control Variables for the GE21

The control variable WF6 represents the afterburner fuel flow. The afterburner is used to augment the engine thrust by injecting fuel into the expanding gasses in the exhaust nozzle and igniting the fuel/air mixture. This control will not be used for this research and WF6 will be set to zero.

The remaining seven independent input variables can be used in the control design. This implies that seven output

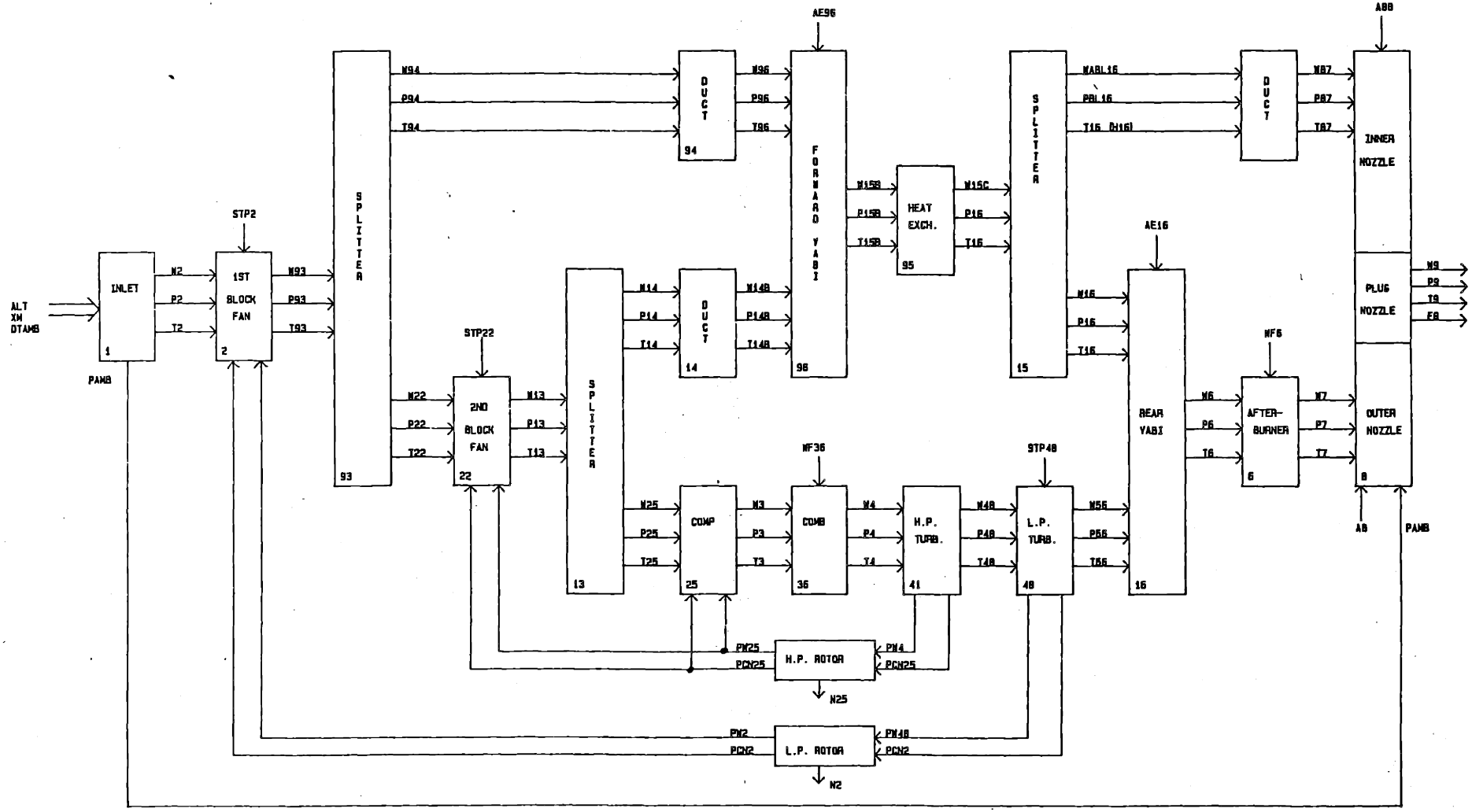

Figure 2.5-3
Block Diagram of GE21 Engine

variables can be controlled independently.

2.5.3.2 GE21 STATES

The GE21 has basically two dynamic state variables (actuators and sensors not included). These states are the fan speed, N2, and core speed, N25.

2.5.3.3 GE21 OUTPUT VARIABLES

As shown in Figure 2.5-3, there are a variety of outputs to select from. The choice of the output variables is dependent on the intended purpose of the control design; the choices for this design example are discussed in section 3.3.1 There are some general issues to consider when selecting the output variables to control. These are:

a) can the variable be physically measured?

b) can the operational and performance constraints be maintained by controlling the chosen variables?

c) are there specific outputs that you must control?

Previous research with the GE21 model has provided the initial sorting of output variables [1]. The initial selections are tabulated in Table 2.5-2.

These initial choices are the variables which are used to start the design task. In addition to the variables above, the net thrust, with symbol FG, is used as a "measured" output for this research.

VARIABLE NAME	UNSCALED UNITS	DESCRIPTION
N2	RPM	LOW PRESSURE ROTOR SPEED
N25	RPM	HIGH PRESSURE ROTOR SPEED
T42	^{o}R	SENSED HIGH PRESSURE TURBINE TEMP.
PS3	PSIA	STATIC PRESSURE AT COMBUSTOR OUTPUT
DPQP3	--	COMPRESSOR PRESSURE RATIO
DPQP13	--	SECOND BLOCKER FAN PRESSURE RATIO
DPQP93	--	FIRST BLOCKER FAN PRESSURE RATIO

Table 2.5-2
Output Variables for the GE21

2.5.4 THRUST MEASUREMENT

Neither the GE21, the GE16 nor any other present day engine provide a direct means to measure the thrust developed by an engine once the engine is installed in an aircraft [11]. The thrust output of an engine is generally calculated using various engine parameters such as the engine core speed, the exhaust gas temperature and the engine pressure ratio.

While this is the case for present day engines, work is progressing in the area of thrust measurement. Since the goal of this research is to provide a design example which demonstrates that thrust modulation is feasible and that there is a technique which can be used to design a control system for this mode of operation, thrust will be used as a direct measurement.

Although it was not a goal of this research, various combinations of output variables were used in an attempt to

attain an equivalent thrust measure from variables which could truly be measured. In actual operation, the core speed, N2, is often used as the main thrust measurement parameter. Since the control design used in this research holds the speeds constant, this parameter could not be used. No other physically measurable output, or combination of measureable outputs, was found to replace the use of N2 in determining the thrust of the engine. Another approach may be to use, in the feedback path, a model of the engine which provides a "calculated thrust" value based on some set of measured outputs. It may be possible to then use this value as the "measured" thrust of the engine. This method was briefly attempted, unsuccessfully, in this research. The nonlinear computer model does provide the calculated value of the engine thrust output based on the physics of the engine. This parameter, called "net thrust," is not available on a "real" engine but was used as a "measured" output for this research. Again, since it was not a goal of this research, the issue of developing an equivalent thrust measure on actual engines was left to the jet engine designers.

2.5.5 PHYSICAL CONSTRAINTS

Every physical system has a set of physical constraints which cannot be violated during the system operation. For jet engines such as the GE21, these constraints range from observing a maximum low pressure rotor speed of 6000 rpm to

keeping the sensed high pressure turbine temperature below 2800°F. The maximum physical values of the variables used on the GE21 engine are given in appendix C.

2.6 LINEAR MODEL DESCRIPTION

2.6.1 INTRODUCTION

The dynamics of both jet engines are described by nonlinear equations relating the state vector $\underline{x}(t)$, the input control vector $\underline{u}(t)$ and the system output vector $\underline{y}(t)$ in the form:

$$d/dt[\underline{x}(t)] = \underline{f}(\underline{x}(t),\underline{u}(t))$$

$$\underline{y}(t) = \underline{g}(\underline{x}(t),\underline{u}(t))$$

The state variables of a system are associated with the energy storage elements of the system. For jet engines, the dynamic state variables are typically temperatures, pressures and inertia terms. Since the temperatures and pressures change much more quickly than the inertia terms, the former are generally modelled as direct feed through terms in the linear system equations. Thus, only the inertia terms are used as state variables in the linear models.

Prior to the design of a linear compensator, the nonlinear model must be linearized about a certain equilibrium point. These equilibrium points for jet engines are called "operating points" and refer to the specific mode of operation for the engine (e.g., ground idle, take-off,

climb and cruise). The operating points for the GE21 were provided by the General Electric Company.

The linear model about each operating point takes the form:

$$d/dt[\delta\underline{x}(t)] = \underline{A}\ \delta\underline{x}(t) + \underline{B}\ \delta\underline{u}(t)$$

$$\underline{y}(t) = \underline{C}\ \delta\underline{x}(t) + \underline{D}\ \delta\underline{u}(t)$$

where

$$\underline{A} = \partial\underline{f}(\underline{x}(t),\underline{u}(t))/\partial\underline{x}(t) \mid \underline{x}_o,\underline{u}_o$$

$$\underline{B} = \partial\underline{f}(\underline{x}(t),\underline{u}(t))/\partial\underline{u}(t) \mid \underline{x}_o,\underline{u}_o$$

$$\underline{C} = \partial\underline{g}(\underline{x}(t),\underline{u}(t))/\partial\underline{x}(t) \mid \underline{x}_o,\underline{u}_o$$

$$\underline{D} = \partial\underline{g}(\underline{x}(t),\underline{u}(t))/\partial\underline{u}(t) \mid \underline{x}_o,\underline{u}_o$$

and

$$\delta\underline{x}(t) = \underline{x}(t) - \underline{x}_o$$

$$\delta\underline{y}(t) = \underline{y}(t) - \underline{y}_o$$

$$\delta\underline{u}(t) = \underline{u}(t) - \underline{u}_o$$

and

$$\underline{f}(\underline{x}_o,\underline{u}_o) = \underline{0}.$$

The partial derivatives are approximated by $\partial z/\partial t = \Delta z/\Delta t$, and these are obtained numerically via computer iteration of the nonlinear model.

2.6.2 GE21 LINEAR MODEL RESPONSE

Using the procedure outlined in the previous section, the GE21 model was linearized about a set of operating points. There were a total of 9 "operating points" which

defined various modes of engine operation (e.g., ground idle, climb, cruise etc...). The equilibrium condition of interest in this research is the condition of maximum power without afterburner, also called operating point 9 for this model. The numerical values of the system matrices for this linearization at operating point 9 are given in Appendix B.

Once the linear models were developed, the input/output responses of the linear and nonlinear models were compared. For "small" deviations about the chosen equilibrium point (i.e., operating point 9), the response of the linear model tracked the response of the nonlinear model quite closely. Note that the transient responses may be very different, but the error between the model responses is more critical at steady state for this research. The evaluation of the plant capabilities and the initial selections of inputs and outputs is based on the assumption that the linear model is accurate in steady state operation.

Figure 2.6-1 shows the amount of deviation in response between the linear and nonlinear model responses for small perturbations around operating point 9. These plots were generated by perturbing the input controls individually with both positive and negative deviations about this equilibrium point. All the variables have been normalized using the maximum physical values of each parameter. The percentage deviations of each of the variables shown in Figure 2.6-1 are calculated as follows:

$$\% \text{ Change} = \frac{\text{Perturbed Value} - \text{Value at Op. Point}}{\text{Maximum Physical Value}}$$

In the figure, the curve labeled "1" is the nonlinear model response and the curve labeled "2" is the response of the linear model.

2.6.3 SENSOR AND ACTUATOR LINEAR MODELS

The computer model of the GE21 engine does not contain any actuator or sensor dynamics and there was no need to add any actuators or sensors to the model for this research. There are a few typical actuator and sensor models which have been used on previous work with jet engines. These models are provided, for reference, in Appendix D.

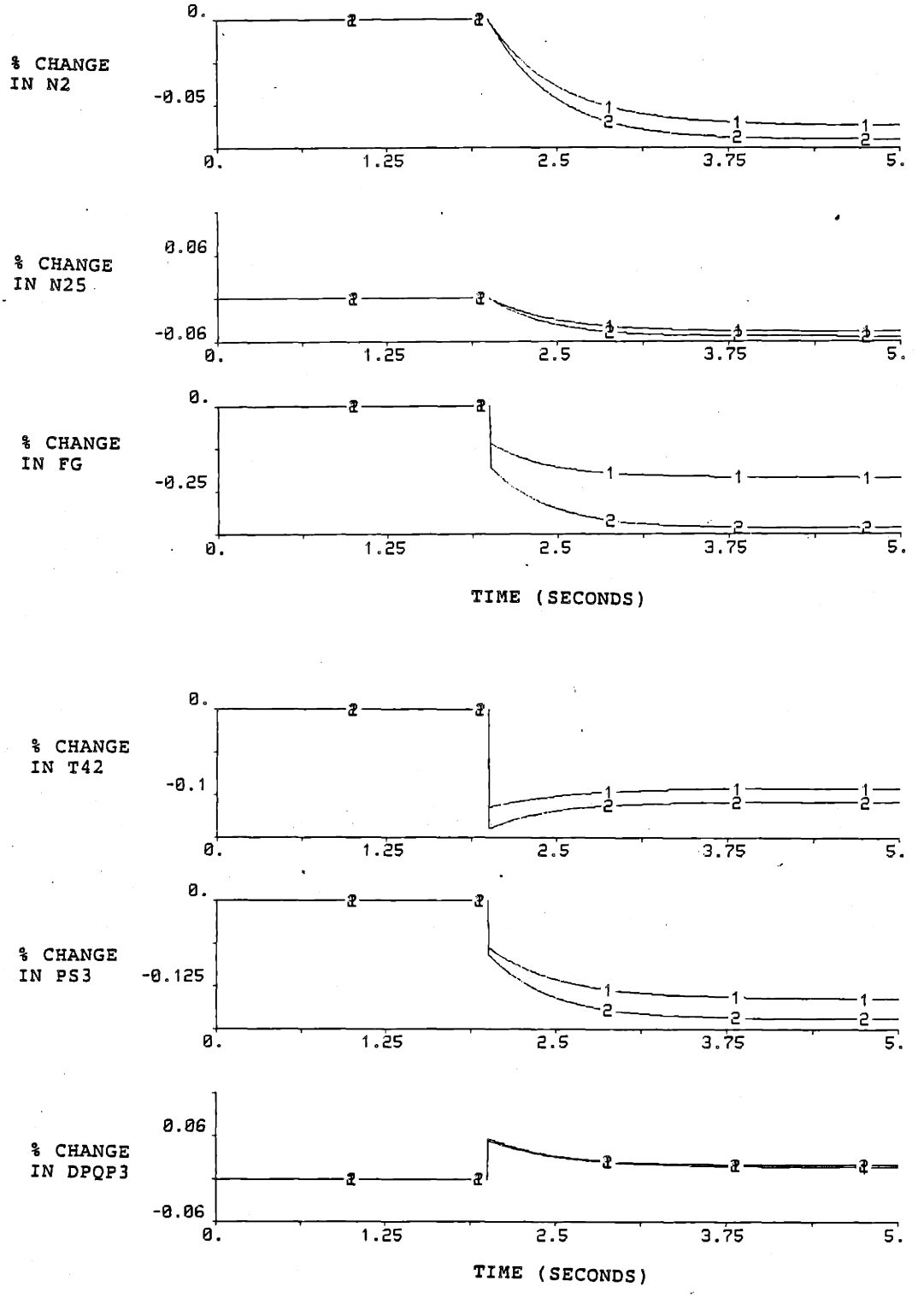

Figure 2.6-1
Nonlinear (1) vs. Linear (2) Model Response To -30% Step Change In WF36

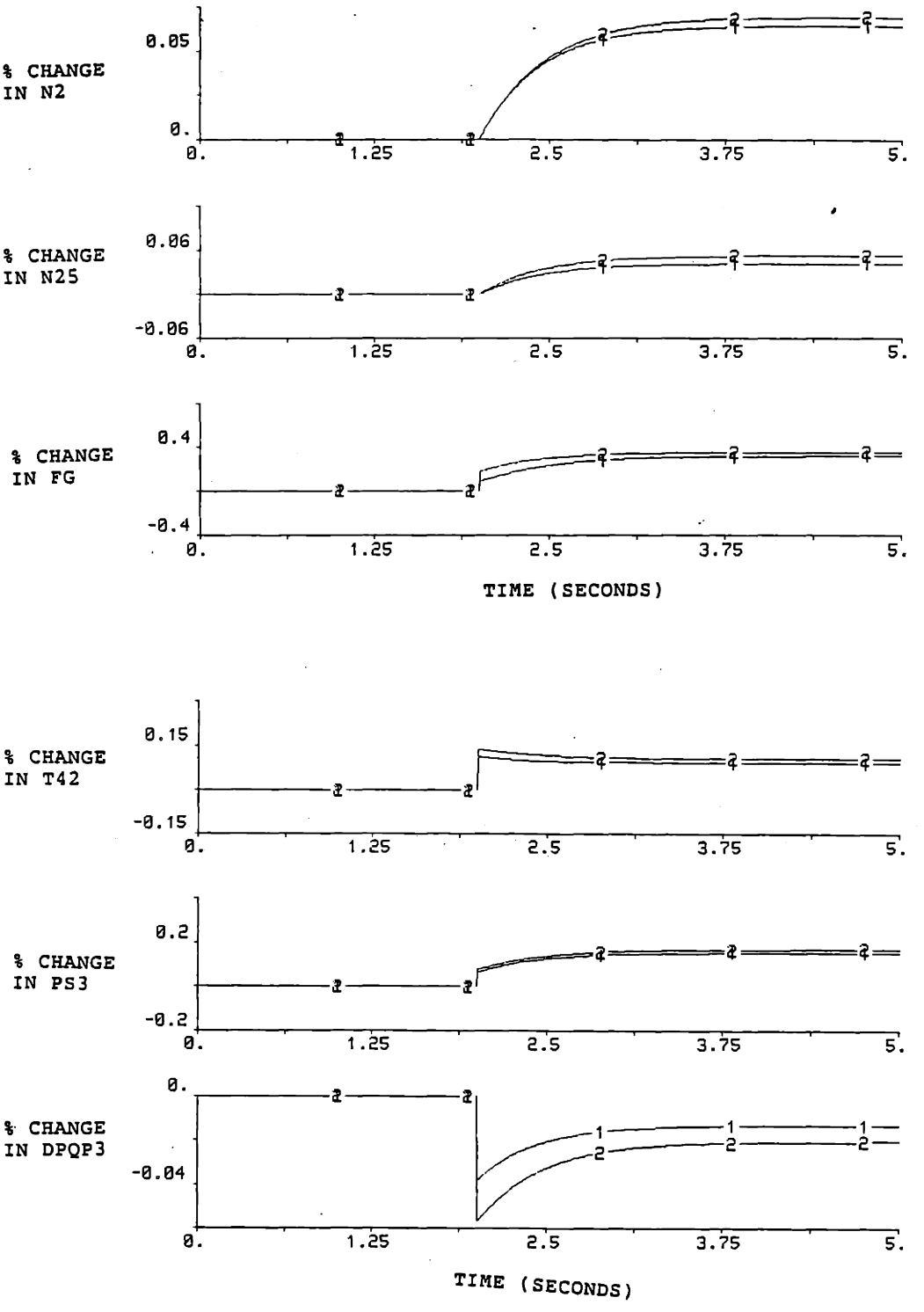

Figure 2.6-1 (Continued)
Nonlinear (1) vs. Linear (2) Model Response To +30% Step Change In WF36

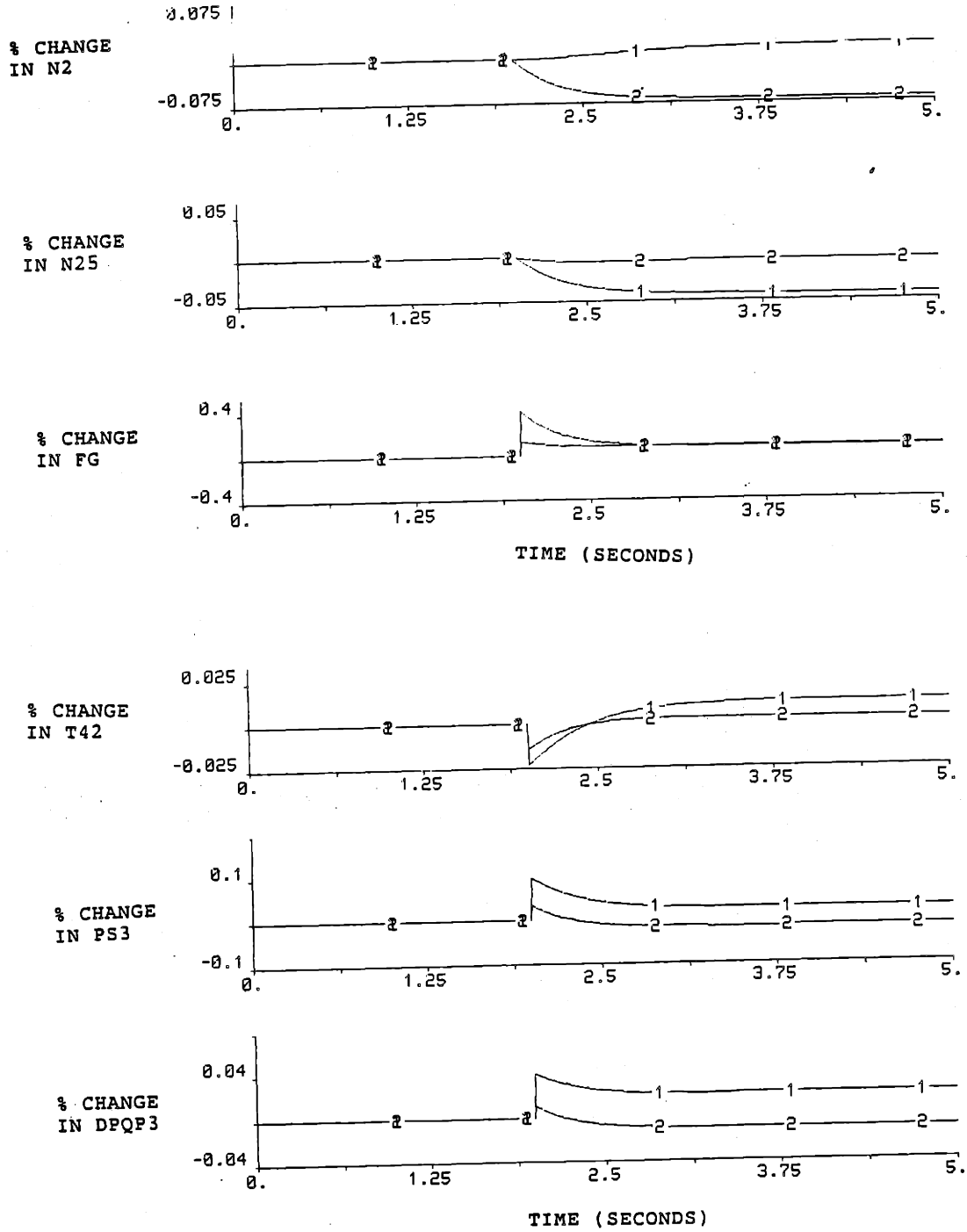

Figure 2.6-1 (Continued)
Nonlinear (1) vs. Linear (2) Model Response To -20% Step Change In A8

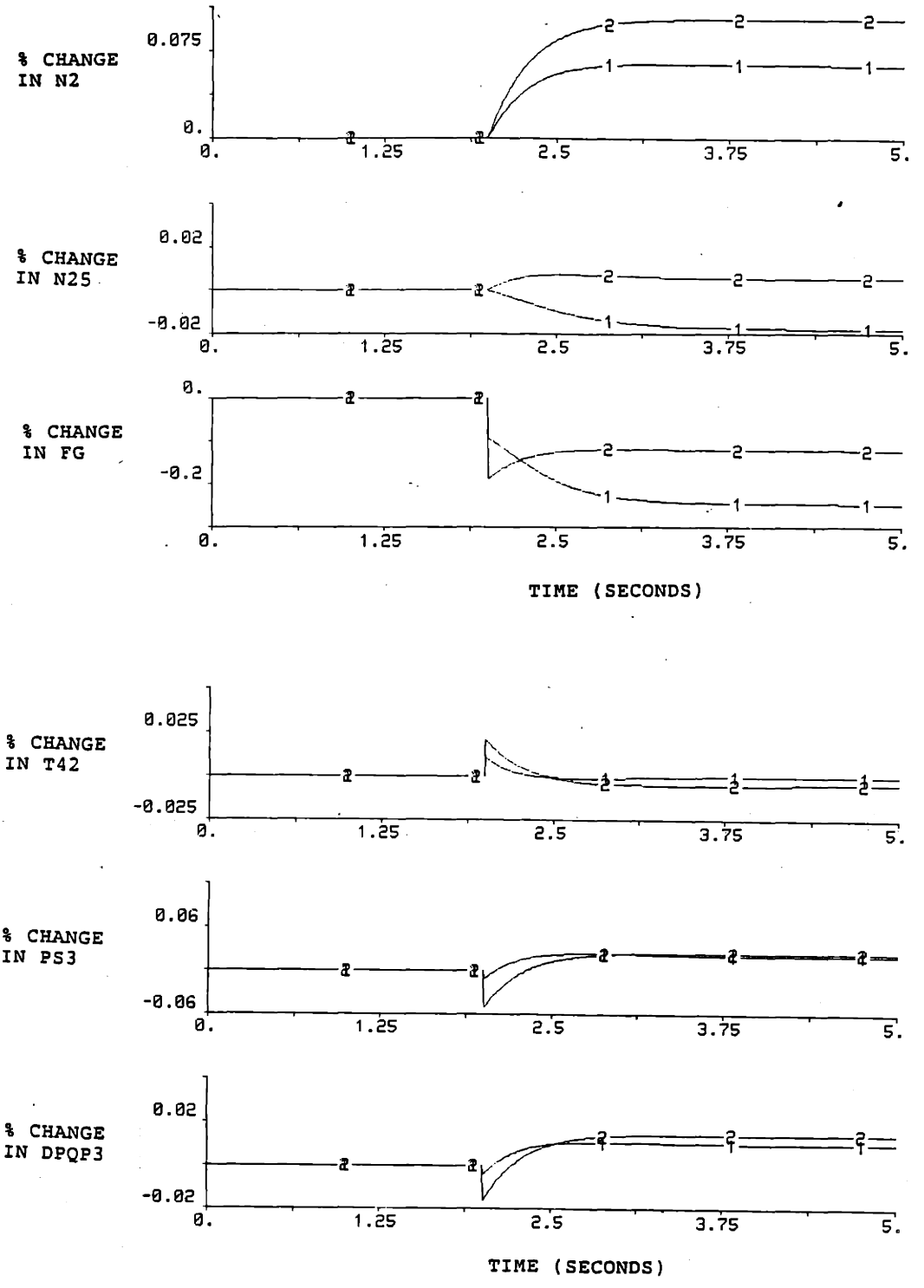

Figure 2.6-1 (Continued)
Nonlinear (1) vs. Linear (2) Model Response To +20% Step Change In A8

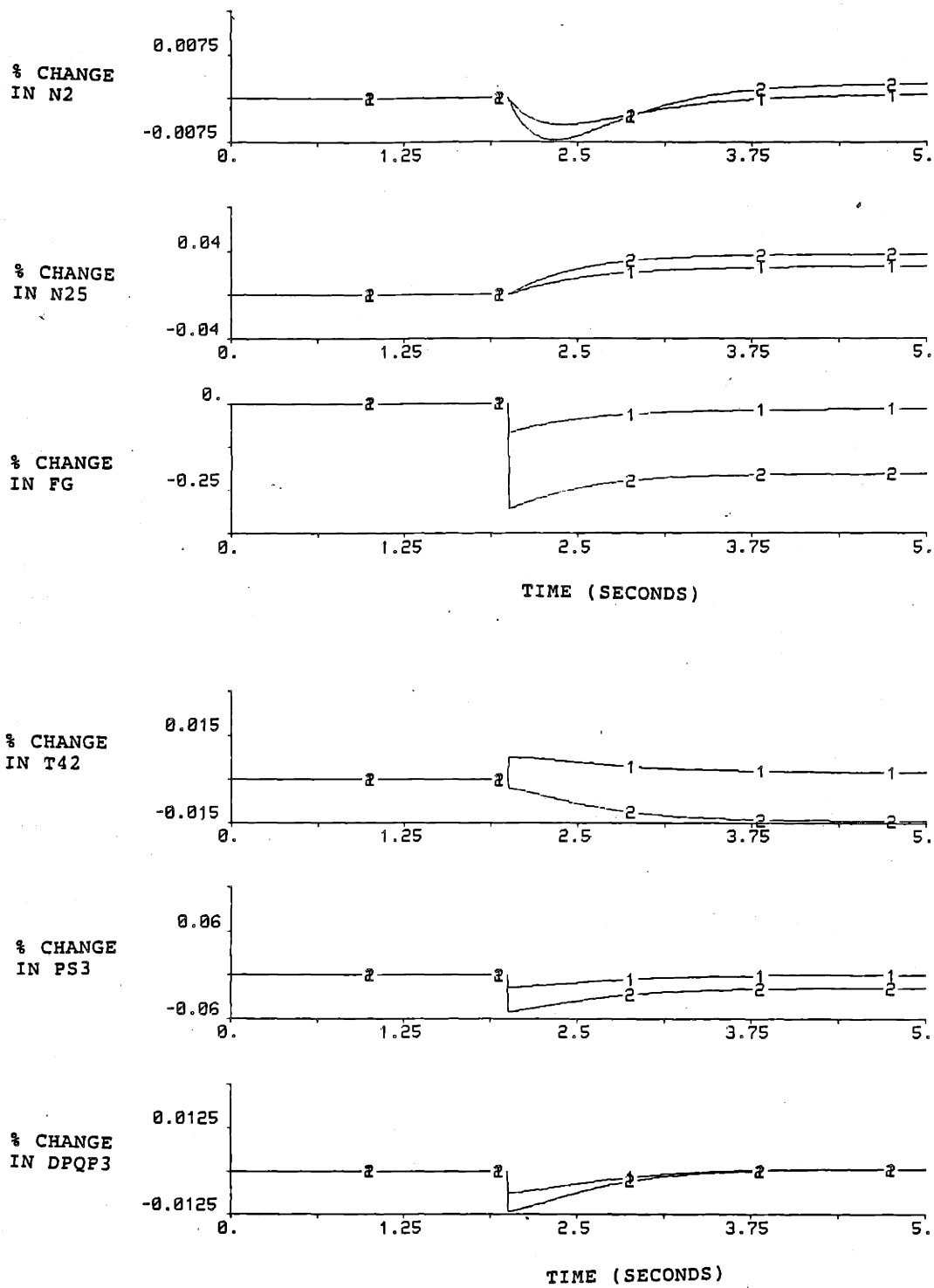

Figure 2.6-1 (Continued)
Nonlinear (1) vs. Linear (2) Model Response To -30% Step Change In AE96

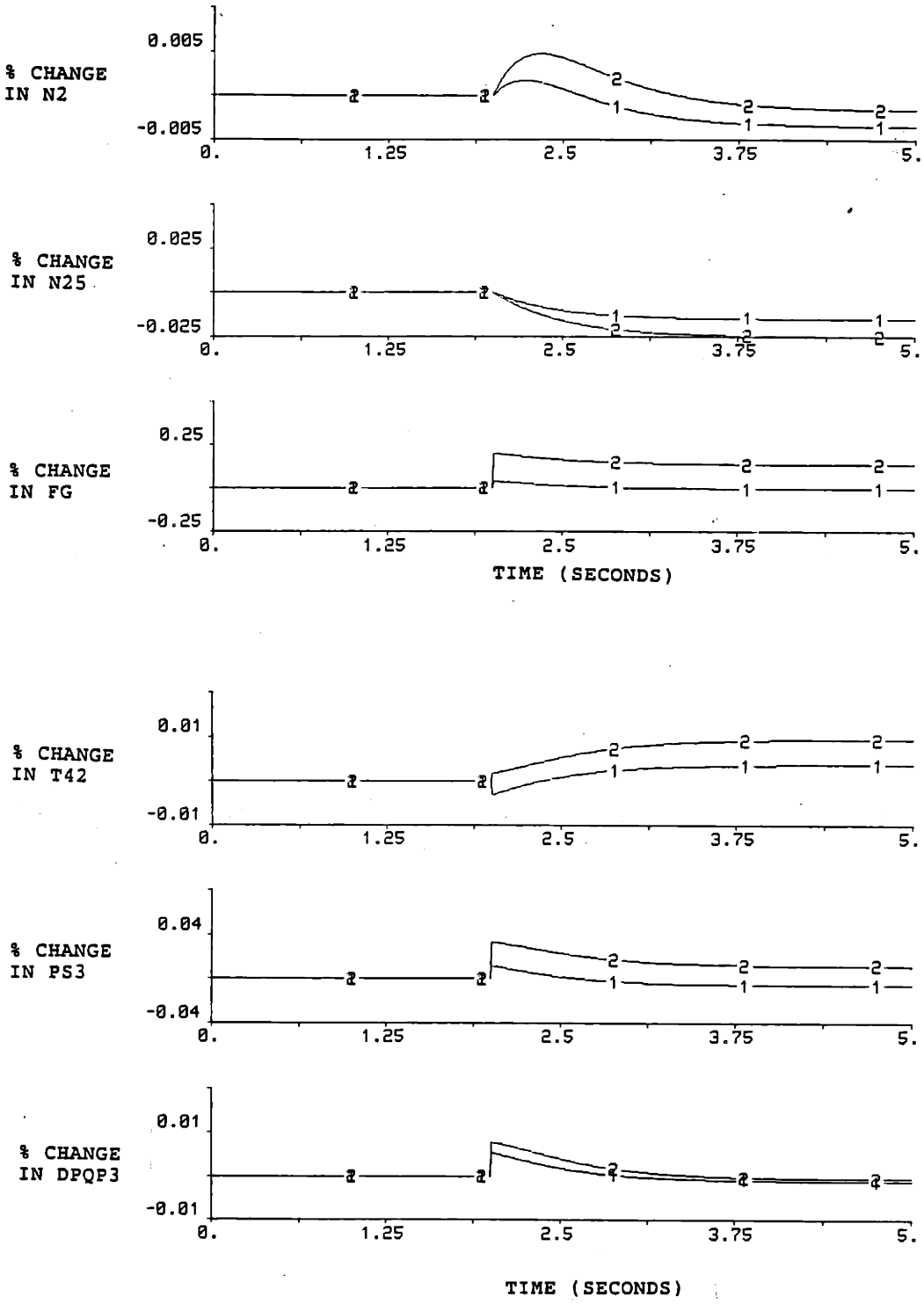

Figure 2.6-1 (Continued)
Nonlinear (1) vs. Linear (2) Model Response To +30% Step Change In AE96

2.7 SUMMARY

This chapter has presented a general description of the example system used in this research. The basic operation of jet engines was briefly reviewed and description of the computer model used to represent the GE21 were discussed. The definition of "Thrust Modulation" was provided and the rationale for operating the engine in this mode was discussed. A linear model of the GE21 operating at maximum power without afterburner was derived and a comparison of the input/output response of the linear and nonlinear models for perturbations of the control inputs about the equilibrium point was presented.

CHAPTER 3

LINEAR MODEL ANALYSIS AND DESIGN SPECIFICATIONS

3.1 INTRODUCTION

In order to use the present design techniques, an infinite-dimensional nonlinear model must be converted into a linear, finite-dimensional model which is valid over some frequency range of interest. The control design is then based on this nominal linear model but must provide closed loop stability and the required performance when connected to the actual engine.

This chapter will investigate the important issues involved in the use of the models which were developed in Chapter 2. More specifically, issues such as scaling, selection of input and output variables and types of modelling errors will be examined. The last section in this chapter will present the performance requirements for the proposed control system.

The reader already familiar with the concepts of scaling, singular value decomposition and its application to the selection of input and output variables and sources of modelling error in MIMO control design may wish to skip to the last section for a summary of the performance specifications applicable to this design.

3.2 SCALING

Any model of a physical system will be described by quantities which have some set of units. The choice of these units is, for the most part, arbitrary and the person who creates the model generally chooses units which are comfortable to work with. The choice of units may not be the best one for exploiting the particular physical behavior of the system. For example, the jet engines describe fuel flow in pounds per hour (PPH) and the nozzle area in square inches (IN^2). At operating point 9 in the GE21 engine, a 1000 unit increase in fuel flow corresponds to an increase of approximately 3% from nominal while an increase of 1000 units in nozzle area corresponds to an increase of approximately 88% from nominal. Obviously, this system of units used does not equally demonstrate the physical interactions of the system.

To more accurately reflect the physical interactions of the system, some sort of scaling is necessary. A transformation to a more appropriate set of units may be made, such as measuring fuel flow in tons per hour, or some type of normalizing may be performed which would remove all the units from the system description. The only "catch" to these scaling transformations is that they are all case dependent.

There is no well-defined, systematic procedure available to assist the designer in selecting "optimum" scale factors.

There are some empirical and semiempirical methods which have been used successfully by designers to select scale factors for many systems. One method of scaling is called the equilibrium method [26]. The basic idea of of this method is to scale the input, output and state variables so that the maximum entry in each row and each column of the system transfer function matrix (TFM) is of the same magnitude. This method may work well for some systems, however the major disadvantage to this method is that the order of scaling (i.e., row scaling followed by column scaling or column scaling followed by row scaling) can change the system response. For a more detailed explanation of the equilibrium method of scaling see [26] and for an example of the effects of the order of scaling on the results see [17].

Another approach to scaling is called the geometric method [24]. The basic idea of this method is to scale each row or column of the system TFM by the geometric mean of its largest and smallest elements. Again, the order of scaling affects the results.

There are still other methods which attempt to minimize certain properties of the system. One method determines that the system TFM is well scaled if the variability of the entries in the matrix is minimal [27]. Other methods of scaling attempt to minimize the condition number of the system TFM.

In the context of using the LQG/LTR methodology for a compensator design, there have been various types of scaling

used based on the particular plant to be controlled. For example, in [5] the plant was a turboshaft jet engine used on a helicopter and the scale factors represented the maximum expected deviations of the variable from the nominal operating points. In [1], the plant was the GE21 axial flow turbofan jet engine used in large aircraft applications and the scale factors represented the maximum physical values of the variables. A forward swept wing aircraft was used as the plant in [33] and the scale factors were selected based on the physical significance of each of the control surfaces. And in [15], the plant was a submarine and, for scale factors, a set of "weights" were selected which made certain variables more important in the design (i.e., they had a larger contribution to the scaled input, output or state vectors) and minimized the contribution of other variables.

These are all valid approaches to the problem of scaling. However, since these are only empirical methods, each method could provide a different result when applied to different plants. The final word here is that scaling is a case dependent issue. All of the above methods can assist the designer in selecting scale factors. However, once the system has been scaled, the designer must combine physical knowledge of the system with aquired intuition in order to determine the scale factors selected are appropriate for the design.

Ideally, the scale factors are selected such that the scaled system truly exhibits the physical behavior of the

system. For physical systems such as jet engines, a general rule of thumb has been to use the following:

$$z_{iscaled} = z_i / z_{iref}$$

where

z_{iref} = a physically significant deviation of z (in the same direction as z).

Using past work as a guide [1, 5], the method of scaling used for this research was to use the maximum physical values of the input, output and state variables as the scale factors (i.e., $z_{iscaled} = z_i / z_{imax}$ and z represents an input, output or state variable). Other possible methods of scaling were investigated during the course of the research, such as using the equilibrium points as scale factors or using a perturbation about the equilibrium point as the scale factors, but the use of the maximum physical value of each variable as the scale factor seemed to best suit this application.

The maximum physical values of the variables and the value of each variable at the 9 operating points of the GE21 engine are given in Appendix C. Once the method of scaling is selected, a scaling transformation is then applied to the system matrices.

3.2.1 SCALING TRANSFORMATION

A scaling transformation of a given linear system is one where the input, output and state variables are transformed by diagonal matrices with positive elements along the

diagonals. If $\underline{x}$, $\underline{u}$ and $\underline{y}$ are the original state, input and output vectors, then the scaled vectors are:

$$\underline{x}_s = \underline{S}_x\underline{x}, \quad \underline{u}_s = \underline{S}_u\underline{u}, \quad \text{and} \quad \underline{y}_s = \underline{S}_y\underline{y}. \tag{3.1}$$

This type of scaling leads to the following transformation of system matrices:

$$\begin{aligned} \underline{A}_s &= \underline{S}_x\underline{A}\,\underline{S}_x^{-1} \\ \underline{B}_s &= \underline{S}_x\underline{B}\,\underline{S}_u^{-1} \\ \underline{C}_s &= \underline{S}_y\underline{C}\,\underline{S}_x^{-1} \\ \underline{D}_s &= \underline{S}_y\underline{D}\,\underline{S}_u^{-1} \end{aligned} \tag{3.2}$$

and the scaled system transfer function matrix becomes:

$$\underline{G}_s = \underline{S}_y\underline{G}\,\underline{S}_u^{-1}. \tag{3.3}$$

The values of the elements on the diagonal represent the scale factors used for each variable. The numerical values of the unscaled system matrices, the matrices used as scale factors and the scaled system matrices (all at operating point 9) are presented in Appendix B.

It is easy to verify that using these diagonal scaling matrices will not change the eigenvalues of the system (i.e., the eigenvalues of the scaled system will be the same as the eigenvalues of the unscaled system). However, the singular values of the system [6, 13], which are important in the design of the control system, are definitely affected by the scale factors used in a particular design.

3.3 SINGULAR VALUE ANALYSIS AND INPUT/OUTPUT COUPLING

The use of the singular value decomposition (SVD) in multivariable control design has become a basic tool [1, 2, 4, 5, 17]. Recent work has extended the use of this tool to assist the designer in determining the degree of input/output coupling, or relative controllability [1, 18], which exists between certain combinations of inputs and the corresponding combinations of outputs. This technique has been used in this research to select inputs and outputs.

Before proceeding too far, a word about singular values and scaling. It is well known that scaling affects the singular values of a system [2, 4, 13, 18]. This section provides an example which demonstrates the effects of scaling on the systems used for this research. Unfortunately, the analysis depends on the scale factors chosen; it does not tell the designer whether or not the "correct" scale factors have been selected. Here again, the designer must examine the results and decide, based on physical intuition and knowledege of the system, whether or not the results make sense.

The method of using the SVD to determine input/output coupling is relatively straight forward. The overall (linear) system transfer function matrix (TFM) is given by:

$$\underline{G}(s) = \underline{C}\ (s\underline{I}-\underline{A})^{-1}\ \underline{B} + \underline{D} \qquad (3.4)$$

and

$$\underline{y}(s) = \underline{G}(s)\ \underline{u}(s). \qquad (3.5)$$

In steady state ($s=j\omega=0$) the TFM becomes:

$$\underline{G}(0) = \underline{C}\ (-\underline{A})^{-1}\ \underline{B} + \underline{D} \tag{3.6}$$

and

$$\underline{y}(0) = \underline{G}(0)\ \underline{u}(0). \tag{3.7}$$

The design procedure outline in the following chapters relies on the models be accurate in steady state. It is for this reason that the following analysis concentrates on steady state approach.

The SVD of $\underline{G}(0)$ is given by (note that $\underline{W}$ is used to represent the left singular vectors instead of the traditional symbol $\underline{U}$ in order to avoid confusion between these vectors and the system input vector):

$$\underline{G}(0) = \underline{W}\ \underline{\Sigma}\ \underline{V}^T \tag{3.8}$$

and

$$\underline{y}(0) = [\underline{W}\ \underline{\Sigma}\ \underline{V}^T]\ \underline{u}(0). \tag{3.9}$$

Recall that W and V are unitary matrices so $\underline{W}^T=\underline{W}^{-1}$ and $\underline{V}^T=\underline{V}^{-1}$. Rearranging the above equation yields:

$$\underline{W}^T\ \underline{y}(0) = \underline{\Sigma}\ [\underline{V}^T\ \underline{u}(0)] \tag{3.10}$$

Equation (3.10) more clearly exposes the relationship between the combination of plant outputs defined by $\underline{v}^T\underline{u}(0)$ and the combination of plant inputs defined by $\underline{w}^T\underline{y}(0)$, where the lower case symbols are used to identify vectors within the larger matrices.

The above input/output relations are related through a diagonal matrix $\underline{\Sigma}$ which demonstrates the degree of coupling between them. The larger the entry in $\underline{\Sigma}$ which corresponds to a particular input/output pair, the stronger the coupling (or equivalently, the higher the gain). Figures 3.0-1 and 3.0-2 illustrate this relationship more clearly. In Figure 3.0-1, the superscript H represents the complex conjugate transponse

of the matrix. In Figure 3.0-2, the singular values are assumed to be ordered from maximum to minimum (i.e., $\sigma_{max}=\sigma_1$ and $\sigma_{min}=\sigma_n$).

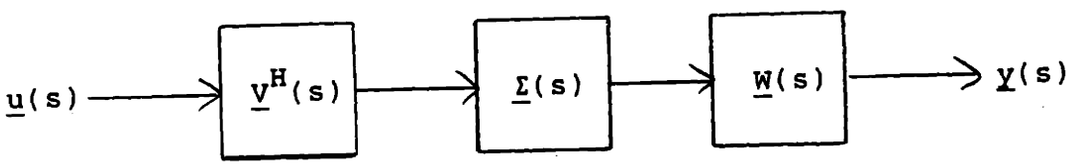

Figure 3.0-1
Visual Representation of the SVD

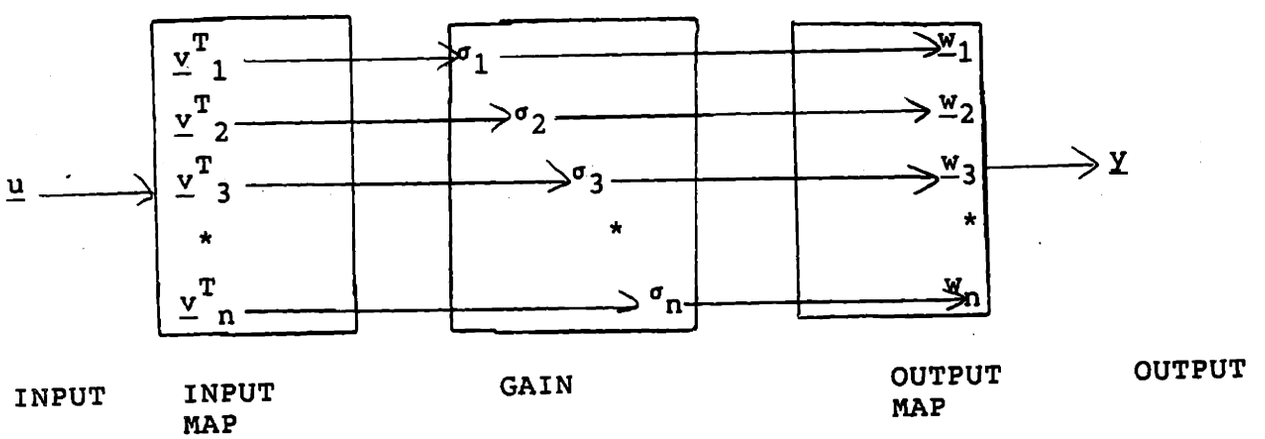

Figure 3.0-2
Geometric Illustration of Input/Output Coupling in Steady State

The above SVD is then used to demonstrate the coupling between inputs and outputs. The linear combination of inputs $\underline{v}^T\underline{u}(0)$ are evaluated. The relative contribution of each plant input to the total linear combination is best view as a percentage, thus the individual entries of $\underline{v}^T$ are viewed as percentages of the sum of the (absolute value) of the entries. A similar breakdown is performed for the outputs. The degree of interaction is then defined by the magnitude of

the singular value associated with the input/output combination. This technique is demonstrated by example in the following section.

3.3.1 SVD ANALYSIS OF INPUT/OUTPUT COUPLING OF THE GE21

The GE21 engine provides 7 control inputs and 7 outputs as shown in Table 3.3-1.

CONTROL INPUTS	PLANT OUTPUTS
WF36 (Main Fuel Flow)	N2 (LP Rotor Speed)
STP22 (Fan Stator Position)	N25 (HP Rotor Speed)
STP48 (LPT Stator Position)	FG (Net Thrust)
A8 (Outer Nozzle Area)	T42 (HP Turbine Temp.)
A88 (Inner Nozzle Area)	PS3 (Static Pressure)
AE16 (Rear VABI Area)	DPQP3 (Comb. Press. Ratio)
AE96 (Forward VABI Area)	DPQP13 (Fan Press. Ratio)

Table 3.3-1
Control Inputs and Plant Outputs for GE21

Since there are 7 inputs and 7 outputs in the GE21, the plant TFM will be a 7 x 7 matrix. This implies that there will be seven singular values for this TFM for all frequency. The open loop, unscaled frequency response of the GE21 is shown in Figure 3.3-1. The scaled plant frequency response is shown in Figure 3.3-2. In both Figures, the singular values are given in dB. Notice that the "distance," in dB, between the maximum and minimum singular value of the scaled plant is much smaller than that of the unscaled plant. This indicates that the interaction of inputs and outputs in the scaled system is stronger, or that the system is more tightly coupled, than the unscaled system. Actually, the physical

coupling of the system has not changed - the scaled system simply highlights or accentuates the physical interaction of the "true" system. The numerical values of the unscaled system, scaled system and scale factor matrices are presented in Appendix B.

From the frequency responses shown in Figures 3.3-1 and 3.3-2, it is clear that the scaling of the plant inputs, outputs and states definitely affects the SVD of the system. It is for this reason that the selection of scale factors is of such importance in the design process; the remainder of the design depends on the "correctness" of the response of the scaled system.

The technique described in section 3.3 can either be used to select the "best" combination of inputs and outputs to use in the control design or can be slightly more specialized (i.e., if the desired outputs are known, then the technique can be used to select the best combination of inputs to control them).

We start by identifying the outputs we must control. The intent of the control design is to vary thrust (FG) while holding the fan and core speeds constant (N2 and N25). Therefore we must definitely control these three. In addition, the engine must not stall during its operation and the turbine temperature must stay below a predetermined limit ($2800^{o}F$).

If we assume that the stall margins and turbine

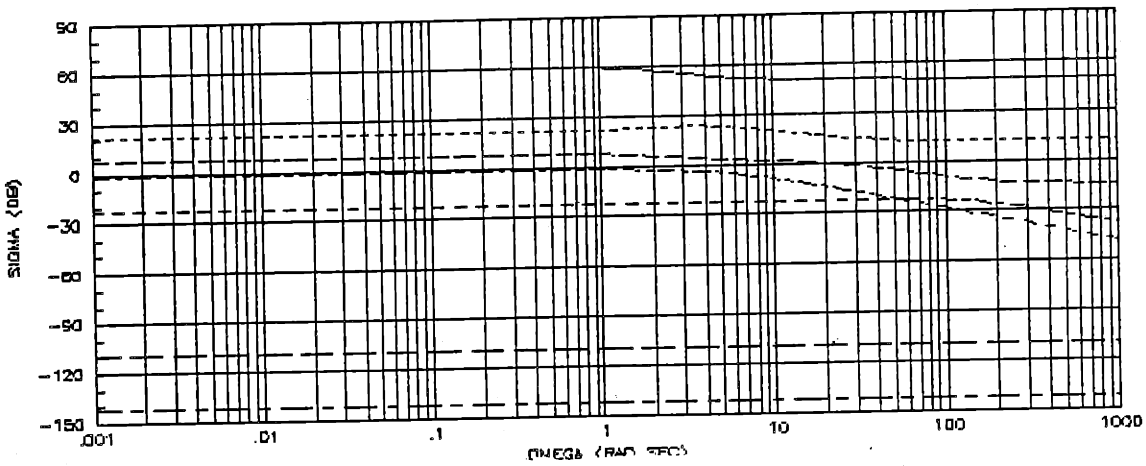

Figure 3.3-1
Open Loop Frequency Response of Unscaled 7 x 7 System

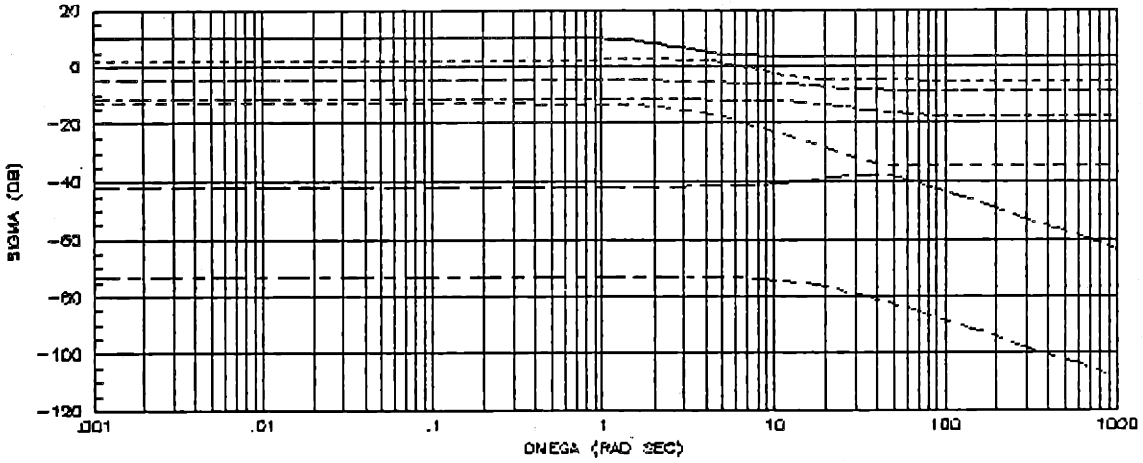

Figure 3.3-2
Open Loop Frequency Response of Scaled 7 x 7 System

temperature remain within the specified limits, then we are left with 3 outputs which must be controlled. So, as a target reduced system, we are looking for the best combination of inputs which will control the outputs Y=[N2 N25 FG]'.

3.3.1.1 SCALED 7 X 7 SYSTEM

The SVD of G(0) for the scaled 7 x 7 system is given in Figure 3.3-3. As mentioned earlier, the easiest representation of this type of analysis is as a percentage of the total value. This is the representation shown in Figure 3.3-3.

The values of the smallest singular values are almost zero, indicating some linear dependence of those combinations of inputs and outputs on the previous combinations. For this particular selection of input and output variables, this can be interpreted as a weak input/output interaction. From Figure 3.3-3, it can be seen that the largest contributions to these "weak" control combinations are STP22 and AE16. Since these controls appear to be relatively weak, they can be dropped. Two outputs should also be dropped in order to have a square plant. Again, from Figure 3.3-3, the variables DPQP3 and DPQP13 are dropped and the SVD of G(0) for the 5 x 5 system is calculated.

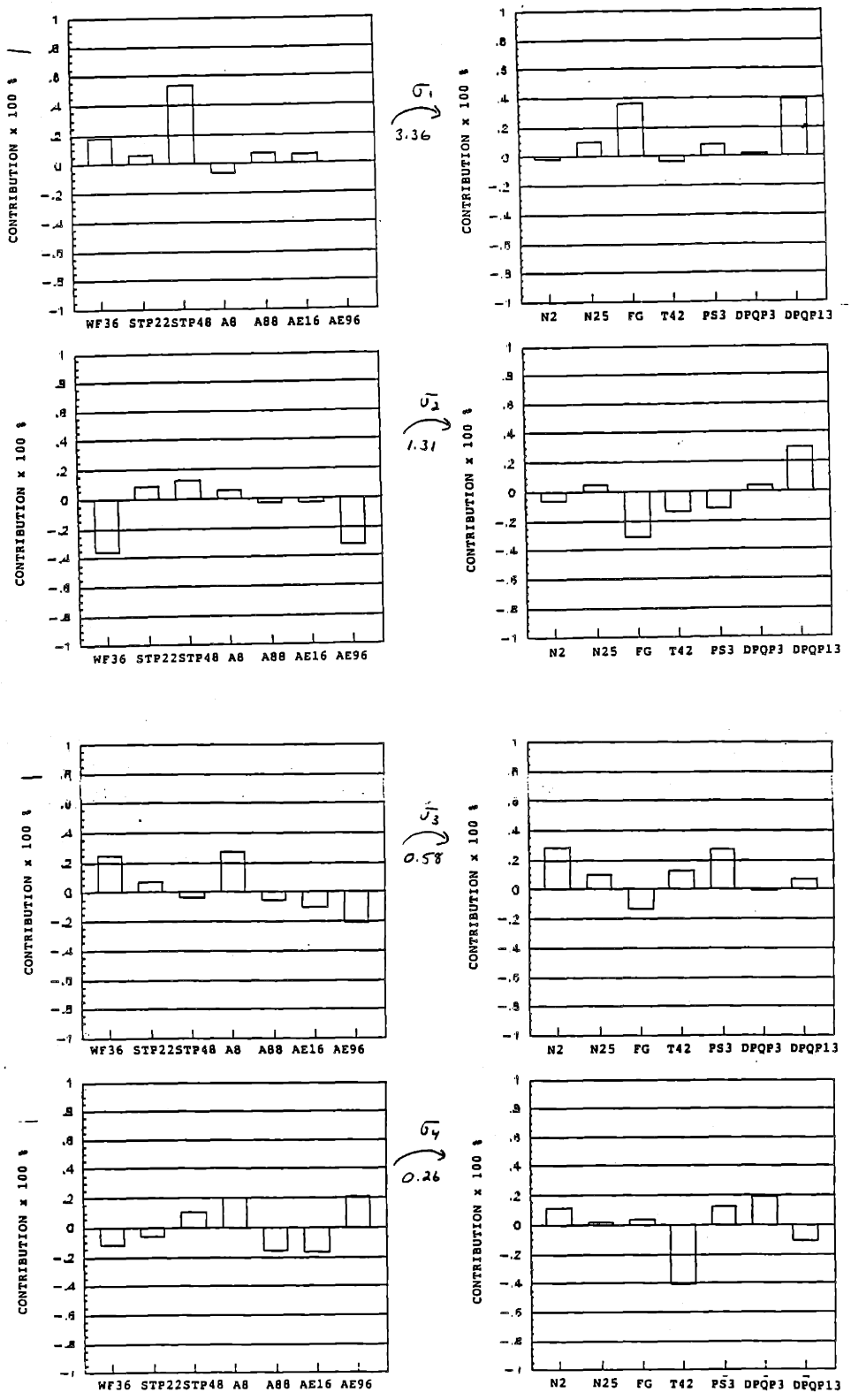

Figure 3.3-3
Singular Value Decomposition of Scaled 7 x 7 System TFM at D.C.

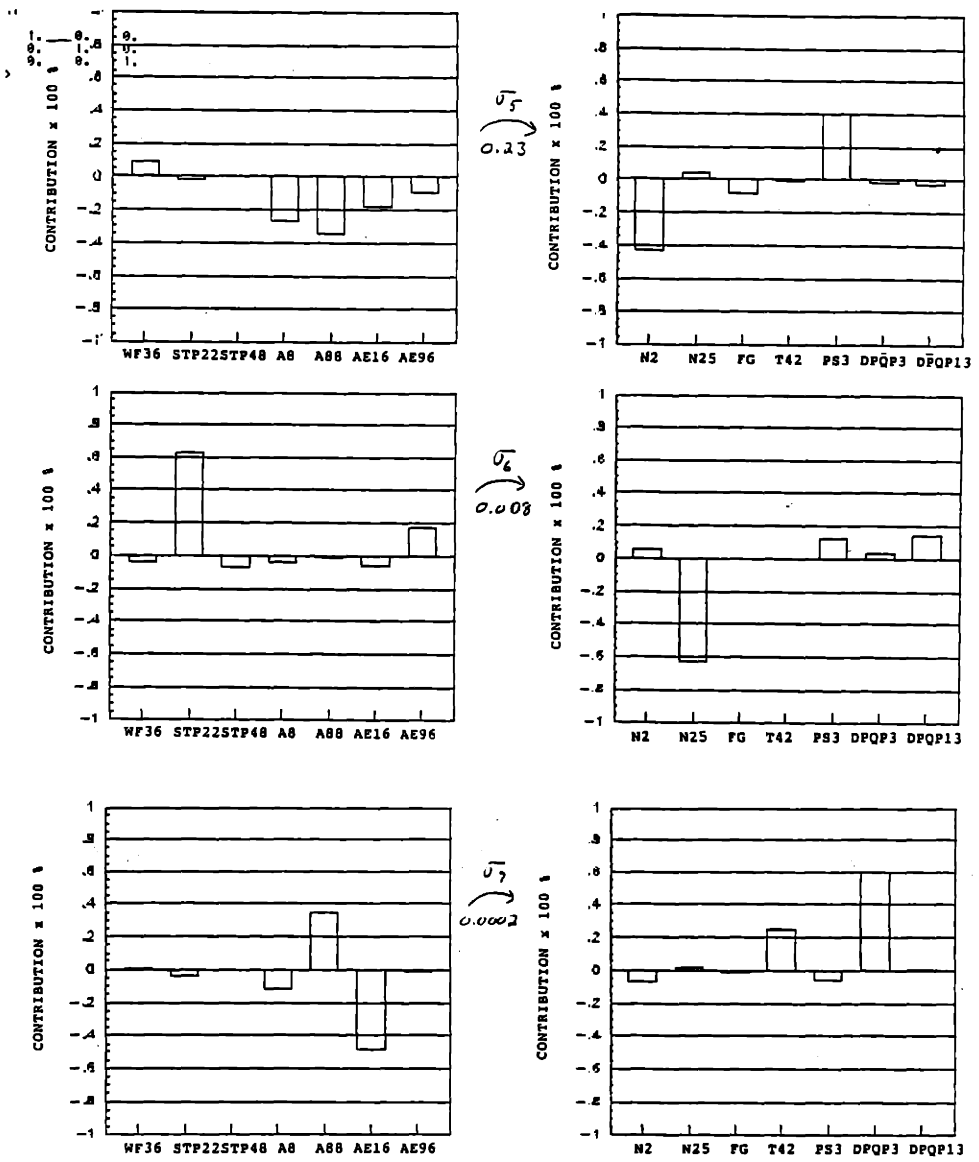

Figure 3.3-3 (Continued)
Singular Value Decomposition of Scaled 7 x 7 System TFM at D.C.

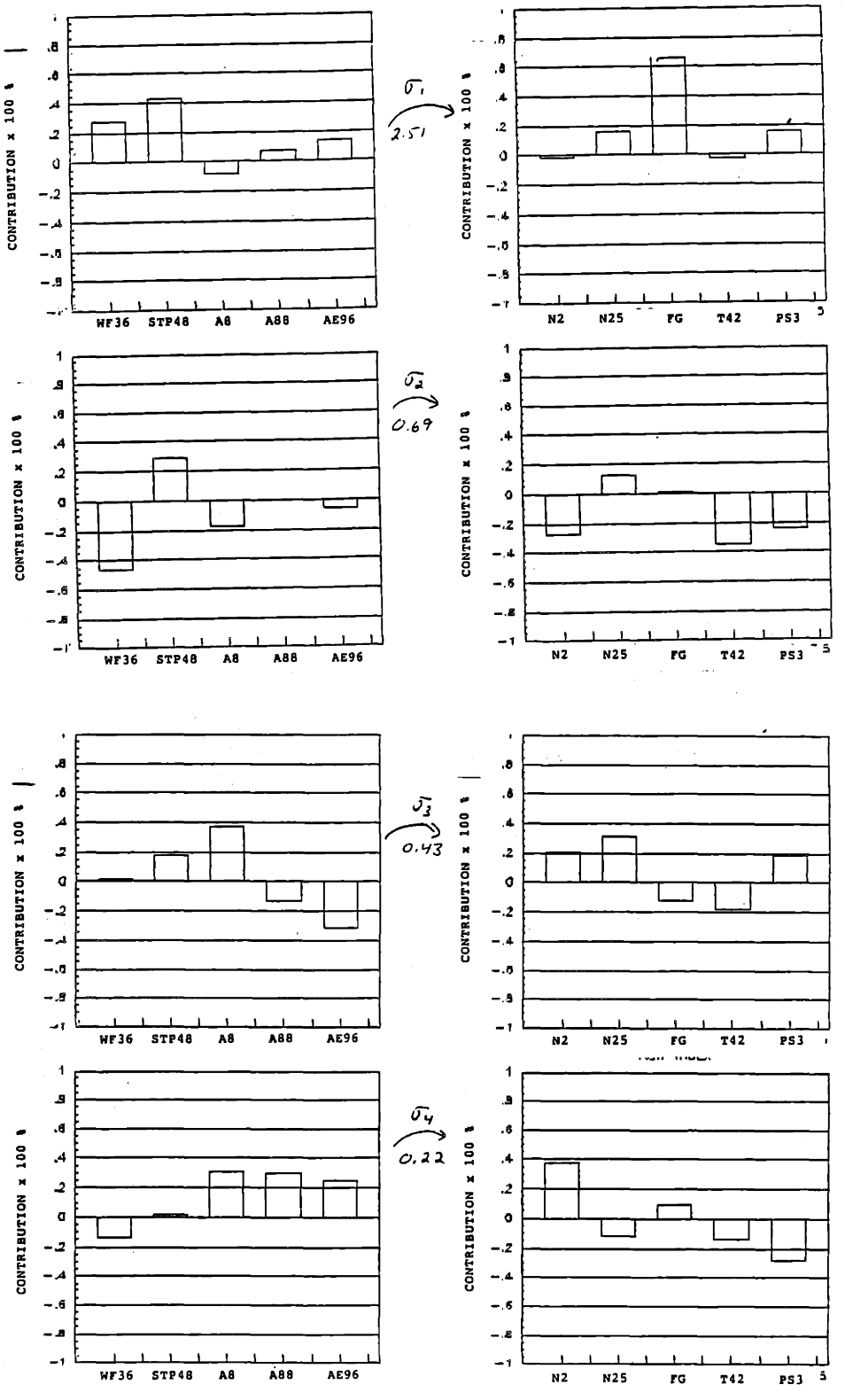

Figure 3.3-4
Singular Value Decomposition of Scaled 5 x 5 System TFM at D.C.

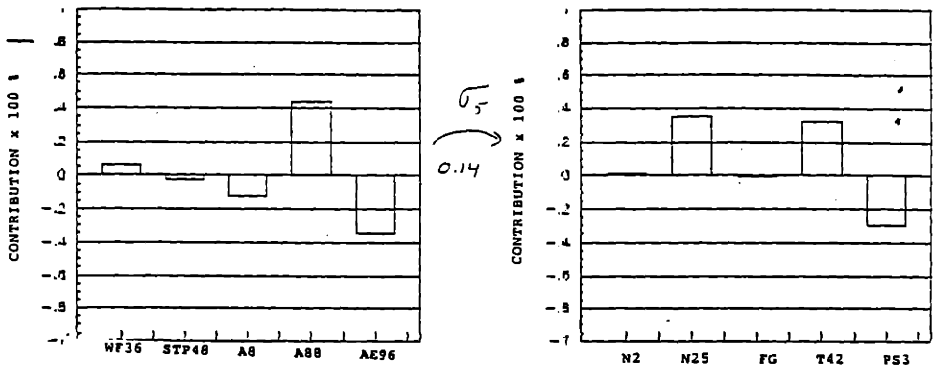

Figure 3.3-4 (Continued)
Singular Value Decomposition of Scaled 5 x 5 System TFM at D.C.

3.3.1.2 SCALED 5 X 5 SYSTEM

The results of the SVD of the 5 x 5 system are presented in Figure 3.3-4. The singular values of the reduced system are now much closer together, ranging from σ_{max}=2.5 down to σ_{min}=0.1435. The reduction of the system to 3 x 3 is still the goal, so more inputs must be eliminated. The largest contribution to the "weakest" linear combination of inputs is A88, so this input is dropped. The largest contribution to the weakest output is PS3, so this output is dropped.

3.3.1.3 SCALED 4 X 4 SYSTEM

The SVD of $\underline{G}(0)$ for the reduced 4 x 4 system is shown in Figure 3.3-5. Now the system appears very tightly coupled and there is no clear-cut input or output to drop. Now the task is to try all possible combinations of 3 inputs and define the target outputs as N2, N25 and FG. Repeat the SVD

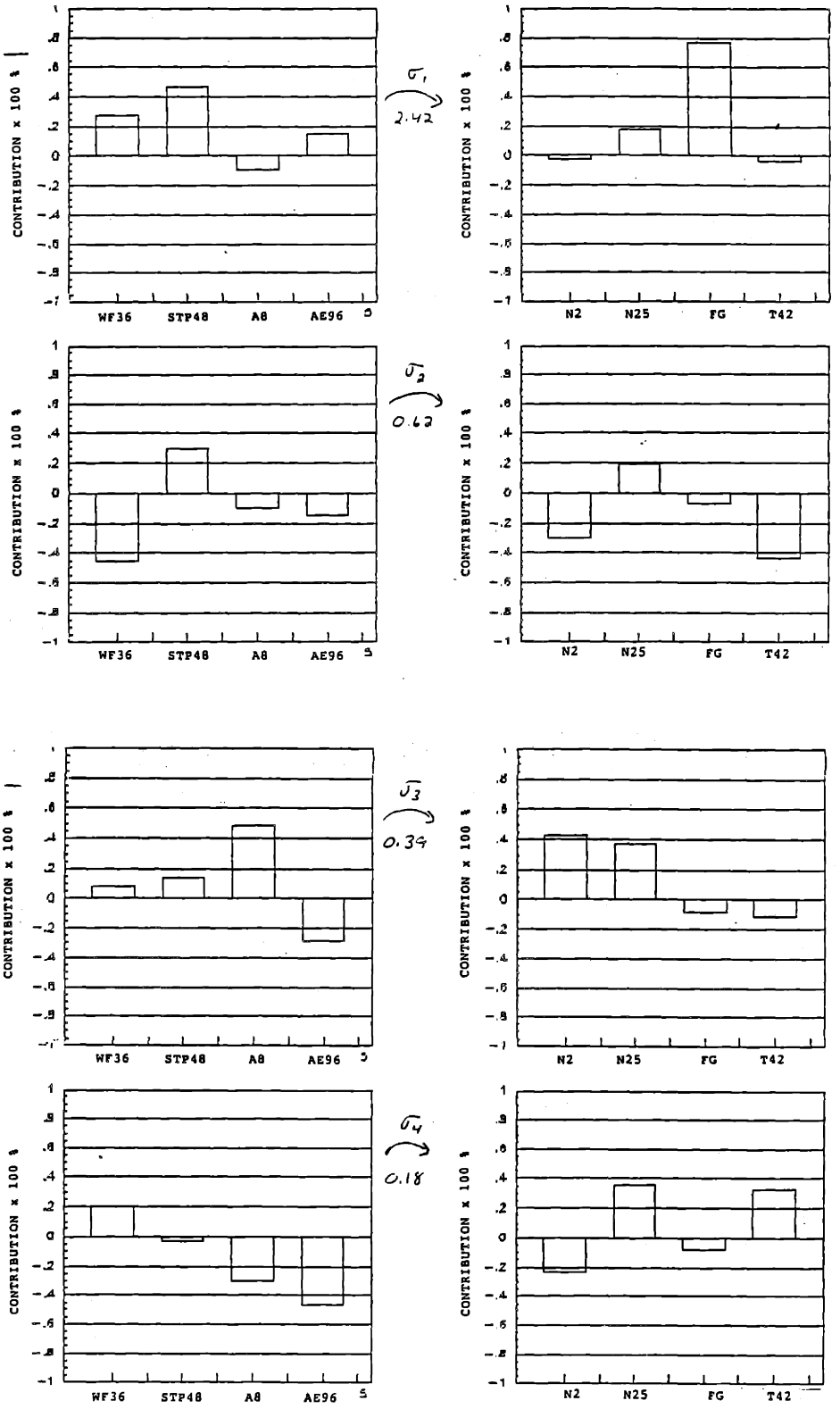

Figure 3.3-5
Singular Value Decomposition of Scaled 4 x 4 System TFM at D.C.

on the 3 x 3 systems until the minimum "spread" of singular values is obtained. The singular values for three cases are tabulated in Table 3.3-1. The condition number, $\sigma_{max}/\sigma_{min}$, is a good measure of the system coupling. From Table 3.3-1, it is clear that the most tightly coupled system is obtained when the inputs WF36, A8 and AE96 are used to control N2, N25 and FG as outputs.

The frequency response of the initial reduced 5 x 5 system is shown in Figure 3.3-6. The frequency response of

INPUT COMBINATIONS	WF36, A8, AE96	WF36, STP48, AE96	WF36, STP48, A8
SINGULAR VALUES	1.44 0.42 0.17	2.38 0.38 0.21	2.34 0.44 0.21
$\sigma_{max}-\sigma_{min}$	1.27	2.17	2.13
$\sigma_{max}/\sigma_{min}$	8.47	11.33	11.14

Table 3.3-1
Singular Value Analysis of Different Input Combinations

the final reduced 3 x 3 system is shown in Figure 3.3-7. Notice that the frequency response of the reduced systems shows that the singular values are closer together for all frequencies, not simply at s=0 where the steady state analysis was performed. This implies that the input and output combinations are tightly coupled over all frequency and that the loop will be easier to "shape," in the frequency domain, for the control design.

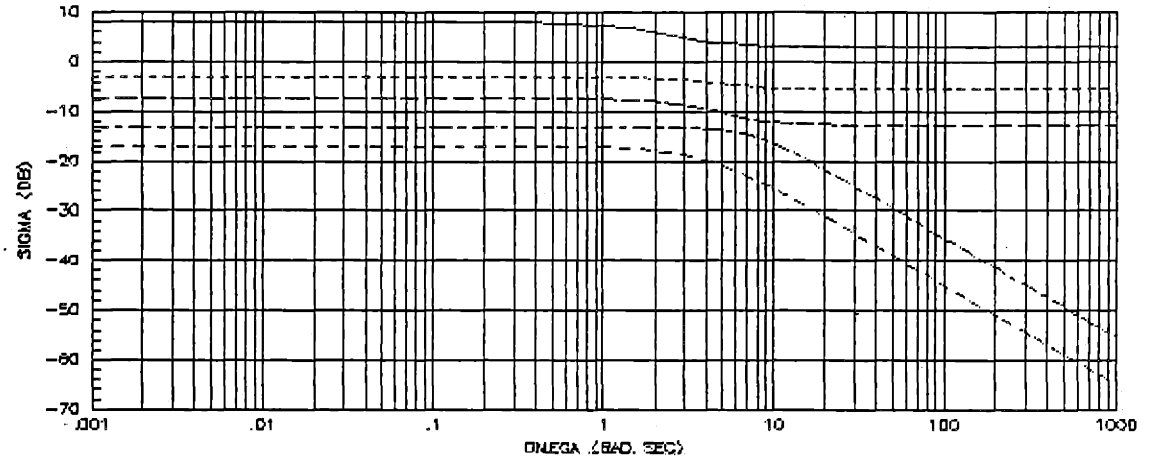

Figure 3.3-6
Open Loop Frequency Response of Scaled 5 x 5 System

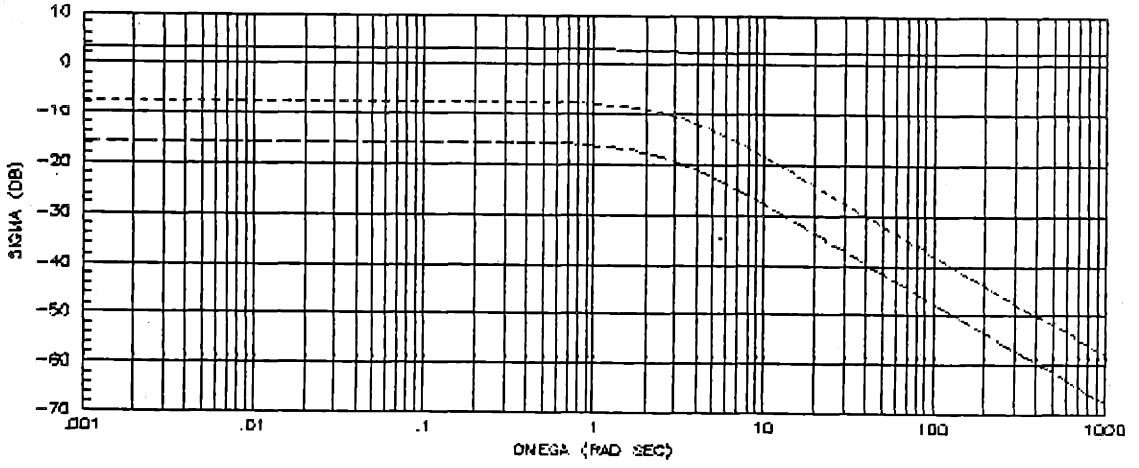

Figure 3.3-7
Open Loop Frequency Response of Scaled 3 x 3 System

3.3.2 COMMENT ON PLANT FREQUENCY RESPONSE

A brief comment on the response characteristics of the plant is in order. From Figure 3.3-7, the reduced (3 x 3) plant has 3 singular value responses. In two of the output directions, the frequency response indicates cut-off frequencies at approximately 2.5 rad/sec. Since this roll-off has a slope of -20 dB/decade, the plant appears to have single poles in these directions. This agrees, intuitively, with the fact that the plant has 2 states.

The third direction of the output space does not roll-off. This also makes sense, intuitively, since the linear model developed in Chapter 2 contains a feedthrough "D" matrix. This implies that in a certain direction, the effects of the plant input, u(t), will be seen directly at the plant output.

None of the response curves display a lead term, indicating that the system has no transmission zeros. A more detailed desrciption of the frequency response and related issues is provided in Chapter 5.

3.4 SCALED 3 X 3 LINEAR MODEL OF GE21

In the preceeding sections, a 7 x 7 linear model of the GE21 has been reduced down to a 3 x 3 linear model using the singular value decomposition technique. The models being used have all been scaled using the maximum physical value of

each variable as the scale factors (see section 3.2.1). The reduced 3 x 3 model uses the inputs, outputs and states listed in Table 3.4-1.

INPUT	STATE	OUTPUT
WF36 (Fuel Flow)	N2 (LP Speed)	N2
A8 (Outer Nozzle Area)	N25 (HP Speed)	N25
AE96 (FWD VABI Area)		FG (Thrust)

Table 3.4-1
Scaled 3 x 3 Linear Model of GE21 used for Target Designs

The state-space system matrices for this scaled, reduced system are:

$$\underline{A} = \begin{bmatrix} -3.4272 & 1.7566 \\ -0.3110 & -1.9281 \end{bmatrix} \qquad \underline{C} = \begin{bmatrix} 1.0000 & 0.0000 \\ 0.0000 & 1.0000 \\ 0.5211 & 2.6808 \end{bmatrix}$$

$$\underline{B} = \begin{bmatrix} 0.4909 & 1.1449 & 0.1894 \\ 0.4148 & 0.1405 & -0.2414 \end{bmatrix} \qquad \underline{D} = \begin{bmatrix} 0.0000 & 0.0000 & 0.0000 \\ 0.0000 & 0.0000 & 0.0000 \\ 0.5954 & -0.6348 & 1.0206 \end{bmatrix}$$

3.5 CONTROL SYSTEM DESIGN SPECIFICATIONS

The physical constraints of the GE21 engine were described in sections 2.5. In addition to the limitations described in these sections, the following performance specifications will be used to evaluate the control system design:

1. Zero steady-state error to constant command inputs and/or constant disturbances (modelled at th plant output).

2. Errors to sinusoidal command inputs and/or output disturbances should be less than 1% below frequencies of 0.5 rad/sec.

3. Errors to sinusoidal sensor noises should be less than 3% at frequencies of 2000 rad/sec.

4. Crossover frequency (loop bandwidth) should be approximately 10 rad/sec.

5. Change Thrust from the nominal value at the operating point to the 50% of this value in less than 0.5 seconds.

3.5.1 INTERPRETATION OF THE DESIGN SPECIFICATIONS

The basic feedback control structure used for this design is shown in Figure 3.5-1. This structure is a unity gain feedback configuration and the notation used is defined in Table 3.5-1.

SYMBOL	DEFINITION
$\underline{r}(s)$	Command Input Vector
$\underline{u}(s)$	Plant Input Vector
$\underline{y}(s)$	Plant Output Vector
$\underline{e}(s)$	Tracking Error Vector
$\underline{d}(s)$	Output Disturbance Vector
$\underline{n}(s)$	Sensor Noise Vector
$\underline{K}(s)$	Linear Compensator Transfer Matrix
$\underline{G}(s)$	LTI Plant Transfer Matrix

Table 3.5-1
Notation For Control Loop Design

From Figure 3.5-1, the following frequency domain transfer function relation is easily verified:

$$\underline{y}(s) = [\underline{I} + \underline{G}(s)\underline{K}(s)]^{-1}\underline{G}(s)\underline{K}(s)\ \underline{r}(s) + [\underline{I} + \underline{G}(s)\underline{K}(s)]^{-1}\ \underline{d}(s) + [\underline{I} + \underline{G}(s)\underline{K}(s)]^{-1}\ \underline{n}(s) \qquad (3.15)$$

or

$$\underline{y}(s) = \underline{C}(s)\ \underline{r}(s) + S(s)[\underline{d}(s) + \underline{n}(s)] \qquad (3.16)$$

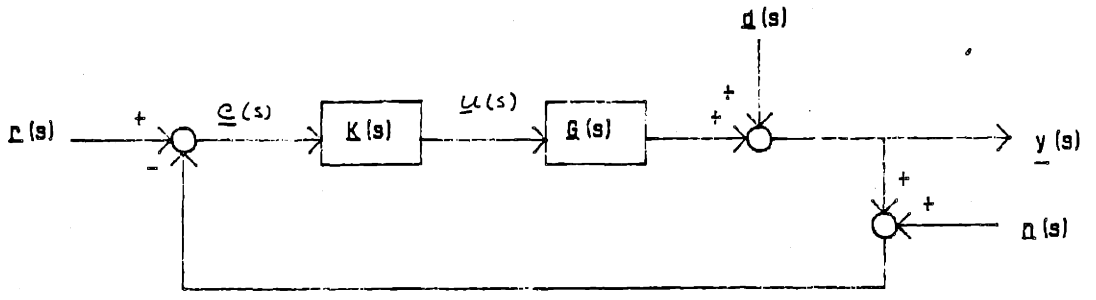

Figure 3.5-1
MIMO Feedback Control Loop Structure

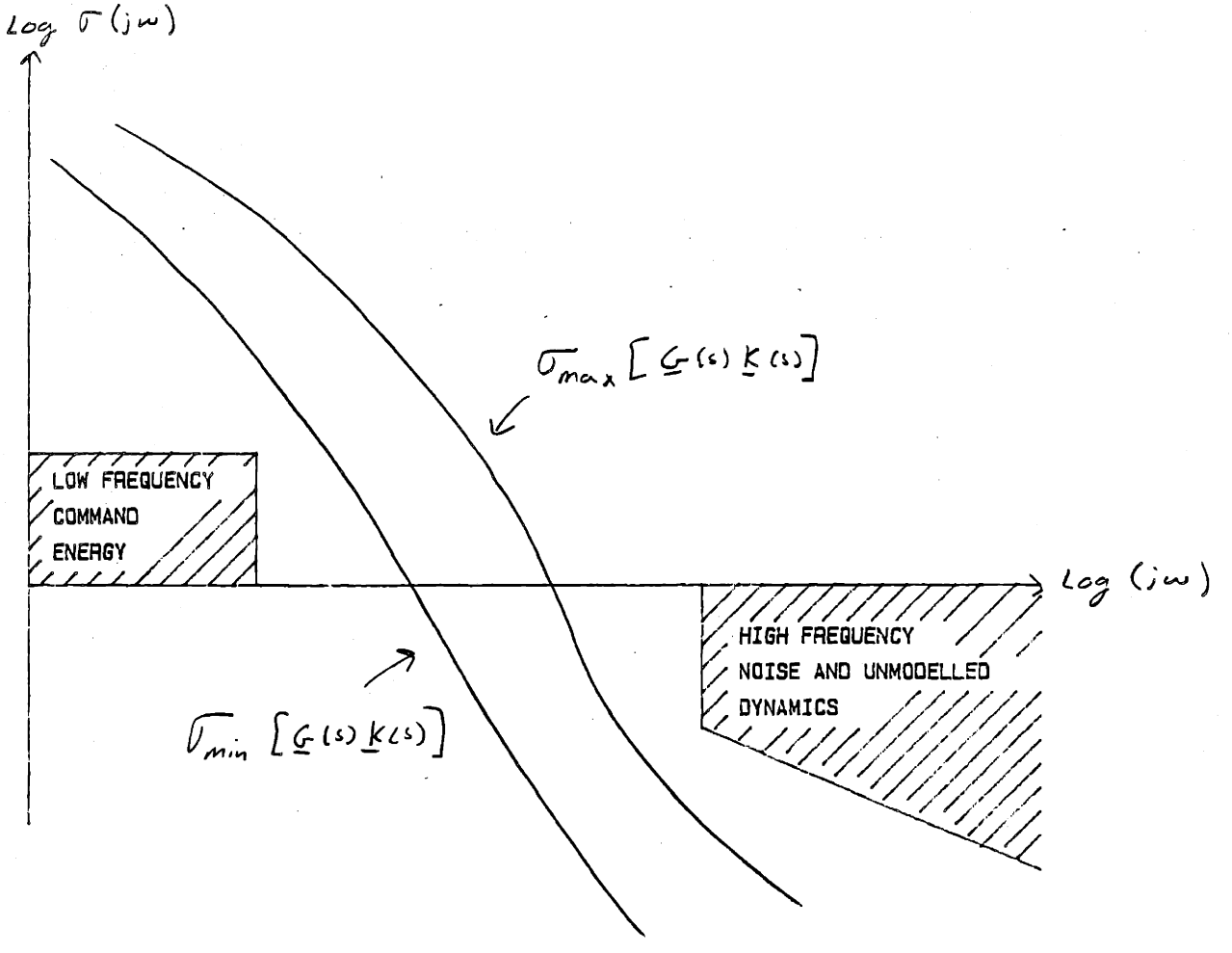

Figure 3.5-2
MIMO Bode Diagram Illustrating the
Singular Value Requirements for G(s)K(s)

where $\underline{C}(s)$ is referred to as the Closed Loop Transfer Function Matrix (TFM) and S(s) is called the Sensitivity TFM.

The specifications are given in terms of the tracking error. From Figure 3.5-1, the expression for $\underline{e}(s)$ is:

$$\underline{e}(s) = \underline{S}(s)[\underline{r}(s) - \underline{d}(s)] + \underline{C}(s)\,\underline{n}(s). \tag{3.17}$$

For the jet engine systems being used here, the disturbance and noise energy is typically at higher frequencies, starting from the specified point of 2000 rad/sec. The Command input energy is typically in the low frequency range below this point.

At steady state, the noise and disturbance inputs are approximately zero and for zero steady state error the expression for the tracking error becomes

$$\underline{e}(s)|_{s=0} = \underline{S}(s)\,\underline{r}(s)|_{s=0} = \underline{0}. \tag{3.18}$$

The above expression implies that $\underline{S}(s)=\underline{0}$ when $s=j\omega=0$ which implies that

$$|\underline{G}(s)\underline{K}(s)| \to \infty \text{ as } s \to 0. \tag{3.19}$$

For infinite gain at d.c., the compensator will require additional free integrators which add dynamics to the loop. To have less than 1% error for command inputs below 0.05 rad/sec implies that

$$\underline{e}(s)|_{s\leq 0.05} \geq (0.01\ \underline{I})[\underline{r}(s)]|_{s\leq 0.05} \Rightarrow \underline{S}(s) \geq 0.01\ \underline{I} \tag{3.20}$$

and

$$\underline{S}(s)=[\underline{I} + \underline{G}(s)\underline{K}(s)]^{-1}=0.01\ \underline{I}$$

$$\Rightarrow [\underline{I} + \underline{G}(s)\underline{K}(s)]|_{s\leq 0.05} = 100\underline{I} \tag{3.21}$$

or

$$\underline{G}(s)\underline{K}(s)|_{s\leq 0.05} \simeq 100\underline{I}. \tag{3.22}$$

Stating this requirement in terms of the frequency response of the system yields:

$$20\log|\underline{G}(s)\underline{K}(s)|_{s\leq 0.05} \geq 20\log|100\underline{I}| = 20\log|100| = 40 \text{ dB}$$

or

$$\sigma_{min}(\underline{G}(s)\underline{K}(s))|_{s\leq 0.05} \geq +40 \text{ dB}. \qquad (3.23)$$

A similar analysis can be performed for the requirement that the error due to sensor noise be less than 3% for frequencies above 2000 rad/sec and the condition to meet is

$$\sigma_{max}(\underline{G}(s)\underline{K}(s))|_{s\geq 2000} \leq -30 \text{ dB}. \qquad (3.24)$$

The crossover frequency will be adjusted in the design process. This type of requirement requires a certain degree of interpretation by the designer. For example, if the singular values of the frequency response are spread at crossover, compliance with all of the above requirements simultaneously may be difficult. Typically the designer will accept a lower crossover frequency in order to meet the sensor noise rejection requirements.

A type of Bode plot for this multivariable design is shown in Figure 3.5-2. This figure depicts the requirements graphically, similar to the familar single-input/single output case.

3.6 PLANT BEHAVIOR AT STEADY STATE

Before proceding directly into the controller design, it is wise to verify that the plant being used can physically perform as required. One method of evaluating the plant

capabilities is to investigate the steady state behavior.

At this point in the design process, the designer should have confidence in the linear model of the plant which is being used. The analysis performed in Chapter 2 and the comparison of the input/output responses should allow the designer to "trust" the model which is being used.

From the linear model, the open loop TFM is

$$\underline{y}(s) = \underline{G}(s)\ \underline{u}(s) \tag{3.25}$$

and at $s=j\omega=0$ this reduces to

$$\underline{y}(0) = \underline{G}(0)\ \underline{u}(0). \tag{3.26}$$

Rearranging the above expression yields

$$\underline{u}(0) = \underline{G}^{+}(0)\ \underline{y}(0) \tag{3.27}$$

where $^{+}$ represents the pseudo inverse of the plant TFM. If $\underline{G}(0)$ is square and invertible, then the above expression uses the standard matrix inverse.

The requirements are that the scaled output vector $\underline{y}$ = [N2 N25 FG]^{T} change from the initial value of $\underline{y}_i$ = [0 0 0]^{T} to the final value of $\underline{y}_f$ = [0 0 -0.5]^{T}. Substituting the numerical values into equation (3.27) yields

$$\underline{u}(0) = \begin{bmatrix} 0.3844 & 2.2997 & 0.4208 \\ 2.6750 & -1.6901 & -0.2737 \\ 0.9289 & -5.0196 & 0.5640 \end{bmatrix} \begin{bmatrix} 0.0 \\ 0.0 \\ -0.5 \end{bmatrix} \tag{3.28}$$

and

$$\underline{u}(0) = \begin{bmatrix} -0.21 \\ 0.13 \\ -0.28 \end{bmatrix} \begin{matrix} \%WF36 \\ \%A8 \\ \%AE96 \end{matrix} \tag{3.29}$$

The above expression for $\underline{u}(0)$ indicates that WF36 must drop 21% from its nominal value, A8 must increase 13% from nominal and AE96 must decrease 28% from nominal. In terms of

the actual changes in control inputs, fuel flow must change from 40,400 pph down to 31,916 pph; the nozzle area must increase from 1,131 in^2 to 1278 in^2; and the forward VABI must allow less air to flow through the engine core by reducing the effective area from 385 in^2 down to 277 in^2. These values are within the acceptable limits of control inputs which suggests that the plant can perform as required.

In addition to the steady state gain analysis, further insight into the plant characteristics can be gained by investigating the SVD of the plant TFM at $s=j\omega=0$. For this system

$$\underline{G}(0) = \underline{W}\ \underline{\Sigma}\ \underline{V}^T \quad ; \text{ all entries real at d.c. (3.30)}$$

$$= \begin{bmatrix} 0.07 & -0.96 & -0.29 \\ 0.06 & -0.28 & 0.96 \\ 0.99 & 0.09 & -0.04 \end{bmatrix} \begin{bmatrix} 1.44 & 0.00 & 0.00 \\ 0.00 & 0.42 & 0.00 \\ 0.00 & 0.00 & 0.17 \end{bmatrix} \begin{bmatrix} 0.84 & -0.41 & 0.35 \\ -0.26 & -0.88 & -0.40 \\ 0.47 & 0.24 & -0.85 \end{bmatrix}$$

If unit length input control vectors, in the directions corresponding to the singular values given above, are applied to this plant, the output space is spanned by the following three vectors:

$$\underline{w}_1 = \begin{bmatrix} 0.1028 \\ 0.0871 \\ 1.4344 \end{bmatrix} \qquad \underline{w}_2 = \begin{bmatrix} -0.3997 \\ -0.1182 \\ 0.0358 \end{bmatrix} \qquad \underline{w}_3 = \begin{bmatrix} -0.0478 \\ 0.1598 \\ -0.0063 \end{bmatrix}$$

The plant output vector is $\underline{y} = [N2 \quad N25 \quad FG]^T$. The vector $\underline{w}_1$ shows the output direction corresponding to the maximum singular value of $\sigma_{max}=1.44$ and $\underline{w}_3$ shows the output direction corresponding to the minimum singular value of $\sigma_{min}=0.17$.

The above SVD provides valuable insight into the characteristics of the plant. For example, the following conclusions can be obtained from the above SVD:

1. The maximum output direction is obtained when N2, N25 and FG move in the same direction. Also, the magnitude of the thrust variation can be quite large in this direction. This can be seen from the size and sign of the entries in $\underline{w}_1$.

2. The minimum output direction is obtained when N2 and N25 move in opposite directions, as seen from the entries of $\underline{w}_3$.

3. The "middle" output direction is obtained when N2 and N25 move in the same direction but FG moves in the opposite direction, as determined from the entries in $\underline{w}_2$. Also note that the change in FG will be very small if required to operate in this mode.

All of the above information makes sense intuitively for this plant. Jet engines typically vary thrust by adjusting the core speed and, since the turbines are located behind the compressor, both speeds will tend to move in the same direction. This checking of mathematical results against physical intuition is an important part of the design.

The above steady state analysis indicates that the plant can perform as required. The steady state analysis does not provide any information as to the transient response of the system (i.e., overshoot, response time) of the system. The transient response characteristics of the system are obtained from time domain simulations.

3.7 SUMMARY

This chapter has presented a discussion of scaling of the plant input, output and state variables and the effects of scaling on the response of the plant. Various techniques used to scale systems were reviewed and the rationale for using the maximum physical values of the system parameters as scale factors for the design examples in this research was discussed.

The use of the singular value decomposition (SVD) as a tool for evaluating the input/output coupling of the plant was discussed and the technique was used to select the "best" combination of inputs and outputs for the designs in this research.

A summary of the robustness results for MIMO control systems was presented. The types of errors involved with the stability-robustness of a system model were briefly presented and a few example error types were given.

The control system design specifications were presented followed by a detailed discussion of the meaning and interpretation of these requirements. In addition, the evaluation of the system behaivor at steady state was suggested as a quick method of determining whether or not the plant could perform the required task. Both the plant transfer function matrix (TFM) and the SVD of the plant TFM were shown to provide valuable information regarding the response characteristics of the plant in steady state.

CHAPTER 4

COMPENSATOR DESIGN USING THE LQG/LTR METHOD

4.1 INTRODUCTION

This chapter presents a general discussion of the Model Based Compensator (MBC) and the Linear Quadratic Gaussian with Loop Transfer Recovery (LQG/LTR) methodology. Emphasis is placed on the perfromance and recovery at the plant output. The step-by-step procedure for designing an LQG/LTR compensator is presented followed by a discussion of the properties, constraints and practical issues involved with these compensator designs.

4.2 LQG/LTR DESIGN METHODOLOGY OVERVIEW

The LQG/LTR design methodology provides the designer with a step-by-step methodical procedure for designing (linear) multivariable feedback control sytems with certain guaranteed stability and robustness properties [2, 13, 22, 23, 25]. This procedure uses the so-called Model Based Compensator (MBC) in the feedback control loop [13]. The basic control structure of the MBC is shown in Figure 4.2-1.

The control system is based on designing a linear compensator, based on a linear time-invariant (LTI) plant

model, and then substituting the nonlinear plant into the loop in place of the linear model. Insofar as the linear model was a "good" approximation to the nonlinear plant in the defined operating range, the control design will behave as expected.

The nominal linear model of the plant is given by:

$$d/dt\ [\underline{x}(t)] = \underline{A}\ \underline{x}(t) + \underline{B}\ \underline{u}(t) + \underline{L}\ \underline{\xi}(t) \qquad (4.1)$$

$$\underline{y}(t) = \underline{C}\ \underline{x}(t) + \underline{\theta}(t) \qquad (4.2)$$

where the $\underline{\xi}(t)$ is a white noise process representing plant disturbances and $\underline{\theta}(t)$ is a white noise process representing sensor and actuator noises. The plant disturbance noise, $\underline{\xi}(t)$, is assumed to have zero mean and unit intensity, in other words

$$E[\underline{\xi}(t)\underline{\xi}^T(t)] = \underline{I}\delta(t-\tau)$$

where the symbol E represents the expectation operator. The sensor noise, $\underline{\theta}(t)$, is assumed to have zero mean and intensity given by:

$$E[\underline{\theta}(t)\underline{\theta}^T(t)] = \underline{\Theta}\delta(t-\tau).$$

The open loop plant transfer function matrix (TFM) is given by:

$$\underline{G}(s) = \underline{C}(s\underline{I}-\underline{A})^{-1}\underline{B} \qquad (4.3)$$

and the MBC TFM is given by:

$$\underline{K}(s) = \underline{G}(s\underline{I}-\underline{A}+\underline{BG}+\underline{HC})^{-1}\underline{H} \qquad (4.4)$$

The MBC derives its name from the fact that the $\underline{A}$, $\underline{B}$ and $\underline{C}$ matricies of the plant appear explicitly in the compensator formulation (see Figure 4.2-1). The design of the compensator and control loop reduces to the selection of the

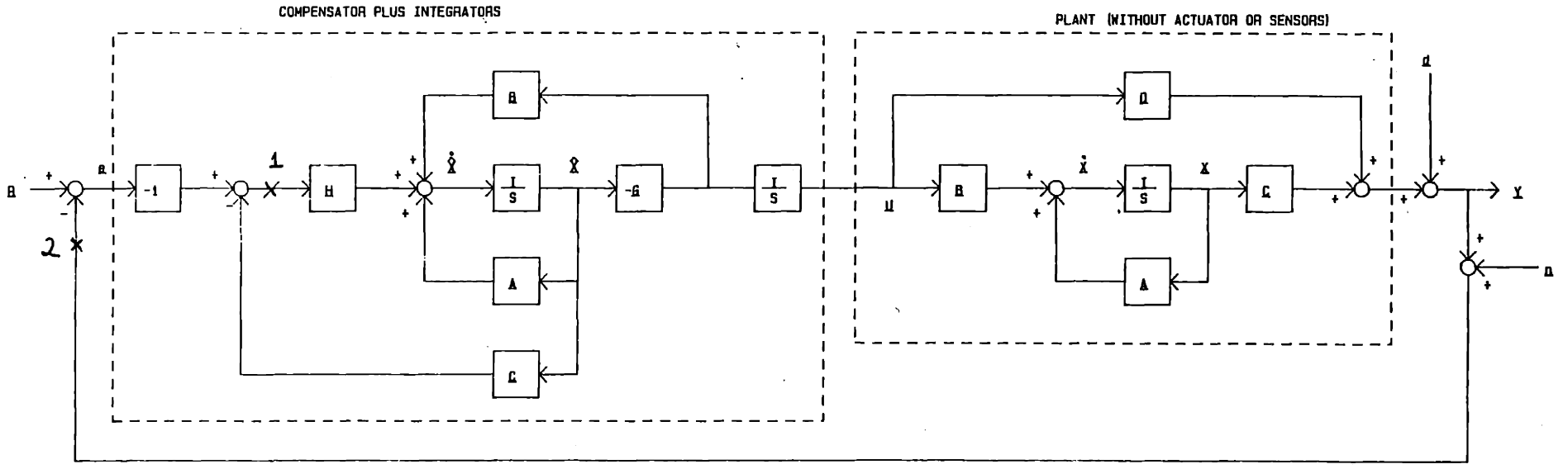

Figure 4.2-1
Structure of the Model Based Compensator in a MIMO Feedback Loop

parameters $\underline{H}$ and $\underline{G}$ which meet the control system design specifications.

The basis of this technique is to design a target loop by selecting either $\underline{H}$ or $\underline{G}$ and then "recovering" this loop by adjusting the other parameter and using the Kwakernaak "sensitivity" recovery method [30].

The compensator design method used in this research is to fix $\underline{H}$ and then vary $\underline{G}$ to recover the loop. The parameter $\underline{H}$ is selected using a variation of the Kalman Filter design technique. The parameter $\underline{G}$ is selected using the solution to the linear quadratic regulator problem which minimizes the cost functional

$$J = \int_0^\infty (\underline{x}^T \underline{Q} \underline{x} + \underline{u}^T \underline{R} \underline{u})\, dt.$$

The parameter $\underline{H}$ is referred to as the "filter gain matrix" and the parameter $\underline{G}$ is referred to as the "control gain matrix." These matricies are computed as follows:

$$\underline{\text{Filter Gain}}: \quad \underline{H} = \underline{K}\, \underline{C}^T\, \underline{\Theta}^{-1} \tag{4.5}$$

$$\underline{\text{Control Gain}}: \quad \underline{G} = \underline{R}^{-1}\, \underline{B}^T\, \underline{P} \tag{4.6}$$

where $\underline{K}$ and $\underline{P}$ are solutions to the algebraic Riccati equations (ARE):

Filter Algebraic Riccati Equation (FARE)

$$\underline{A}\, \underline{K} + \underline{K}\, \underline{A}^T + \underline{L}\, \underline{L}^T - \underline{K}\, \underline{C}^T\, \underline{\Theta}^{-1}\, \underline{C}\, \underline{K} = \underline{0} \tag{4.7}$$

Control Algebraic Riccati Equation (CARE)

$$\underline{A}^T\, \underline{P} + \underline{P}\, \underline{A} + \underline{Q} - \underline{P}\, \underline{B}\, \underline{R}^{-1}\, \underline{B}^T\, \underline{P} = \underline{0} \tag{4.8}$$

Although the filter gain matrix is computed using the Kalman Filter design techniques, the optimal estimation interpretation of the Kalman Filter is discarded and the

matrices $\underline{L}$ and $\underline{\Theta}$ are used as design parameters to achieve the required system frequency response. Similarly, the quantities $\underline{Q}$ and $\underline{R}$ in the CARE are used as design parameters for shaping the LQG loop.

Referring to Figure 4.2-1, the loop transfer function matricies (LTFM) at points (1) and (2) in the loop are given by:

$$\text{LTFM at (1)} = \underline{C}\ \underline{\Phi}(s)\ \underline{H} = \underline{G}_{KF}(s) \tag{4.9}$$

$$\text{LTFM at (2)} = \underline{G}\ \underline{\Phi}(s)\ \underline{B} = \underline{G}_{LQ}(s) \tag{4.10}$$

where $\underline{\Phi}(s) = (s\underline{I} - \underline{A})^{-1}$.

By appropriate choices of $\underline{L}$, $\underline{\Theta}$, $\underline{Q}$ and $\underline{R}$ and proper solution of the respective ARE, it is possible to shape $\underline{G}_{KF}(s)$ and $\underline{G}_{LQ}(s)$ in the frequency domain to achieve the desired responses. The frequency domain properties of $\underline{G}_{KF}(s)$ and $\underline{G}_{LQ}(s)$, as shown by the singular values of the frequency responses, are compared to the design specifications given in section 3.5. The selection of these design parameters is discussed below.

For the designs used in this research, the requirements are that the loop shapes are "good" at the plant output, or point (1) in Figure 4.2-1. A "good" loop shape will insure good command following and disturbance rejection, as required by the design specifications.

The LQG/LTR method, as used in this research, is outlined in the following steps:

1. Choose $\underline{H}$ which shapes $\underline{G}_{KF}(s)$ in the frequency domain to satisfy the performance and design specifications using the parameter definition:

$$\underline{\Theta} = \upsilon \underline{I} \qquad (4.11)$$

and the parameter $\underline{L}$ is selected as described in section 4.3.

2. Choose $\underline{G}$ which recovers the shape of $\underline{G}_{KF}(s)$ using the parameter definitions:

$$\underline{R} = \rho \underline{I} \qquad (4.13)$$

$$\underline{Q} = \underline{C}^T \underline{C} \qquad (4.14)$$

As $\rho \to 0$, the shape of the frequency response of $\underline{G}_{LQ}(s)$ will approach that of $\underline{G}_{KF}(s)$ which represents the desired response.

The LQG/LTR design procedure is illustrated by example in the following sections. First, however, we discuss the restrictions and properties of the LQG/LTR procedure.

4.2.1 PROPERTIES AND RESTRICTIONS OF THE LQG/LTR PROCEDURE

Before "blindly" applying the LQG/LTR design procedure, there are certain constraints which must be observed. These constraints are listed below.

1. $[\underline{A}, \underline{B}]$ is controllable
2. $[\underline{A}, \underline{C}]$ is observable
3. $\underline{G}(s)$ is strictly minimum phase

and for a stable system:

4. $\mathrm{Re}\{\lambda_i(\underline{A}-\underline{B}\underline{G})\} < 0$

5. $\mathrm{Re}\{\lambda_i(\underline{A}-\underline{H}\underline{C})\} < 0$

and for the design:

6. $\nu > 0$

7. $\rho > 0$.

Under the above conditions, the linear control system has the following guarenteed properties:

1. $\sigma_{min}[\underline{I} + \underline{G}(s)\underline{K}(s)] \geq 1$
2. $\sigma_{min}[\underline{I} + (\underline{G}(s)\underline{K}(s))^{-1}] \geq 1/2$

} as $\rho \to 0$ in LTR

3. guaranteed closed loop stability

The SISO equivalent of the above expressions is a guaranteed gain margin of ± 6 dB and a guaranteed phase margin of $\pm 60^{o}$.

Note that if the plant does have right half plane transmission zeros, the recovery procedure may work, especially if the zeros are much higher in frequency than the crossover of the system. The recovery is not guaranteed, however, and more work in the area of nonmimimum phase plants is needed.

4.3 DESIGN OF THE TARGET LOOP

The LQG/LTR design procedure starts with a target design which meets the design specifications (section 3.5). One of those specifications is that there be zero steady state error to constant command inputs. In view of the fact of a finite loop gain at d.c., see Figure 3.3-7, a dynamic augmentation of the original plant will be necessary in order to provide

very high (infinite) loop gain at s=0.

The control structure used will be that shown in Figure 4.3-1. Integrators are added to all plant input channels. These integrators, although modelled as part of the plant, will physically be located within the compensator. The relationship between the nominal plant and the augmented plant is given by:

$$\underline{G}_a(s) = [\underline{G}_p(s)][\underline{I}/s] \tag{4.15}$$

A block diagram and the frequency response of the augmented are shown in Figure 4.3-1.

The state space representation of the augmented system is given by the following system of equations:

$$\begin{bmatrix} \dot{\underline{x}}_p \\ \underline{u}_s \end{bmatrix} = \begin{bmatrix} \underline{A}_p & \underline{B}_p \\ \underline{0} & \underline{0} \end{bmatrix} \begin{bmatrix} \underline{x}_p \\ \underline{u}_p \end{bmatrix} + \begin{bmatrix} \underline{0} \\ \underline{I} \end{bmatrix} \underline{u}_s \tag{4.16}$$

or

$$\dot{\underline{x}}_a = \underline{A}_a \underline{x}_a + \underline{B}_a \underline{u}_s \tag{4.17}$$

and

$$\underline{y} = [\underline{C}_p \quad \underline{D}_p] \begin{bmatrix} \underline{x}_p \\ \underline{up} \end{bmatrix} = \underline{C}_a \underline{x}_a \tag{4.18}$$

with $\underline{D}_a = \underline{0}$.

The design of the target Kalman Filter loop is based on the selection of a scalar, υ, and a matrix, $\underline{L}$, which provide the desired frequency response characteristics for the singular values of the transfer matrix $\underline{G}_{KF}(s)$. Based on the zero steady state error requirement, the target design uses

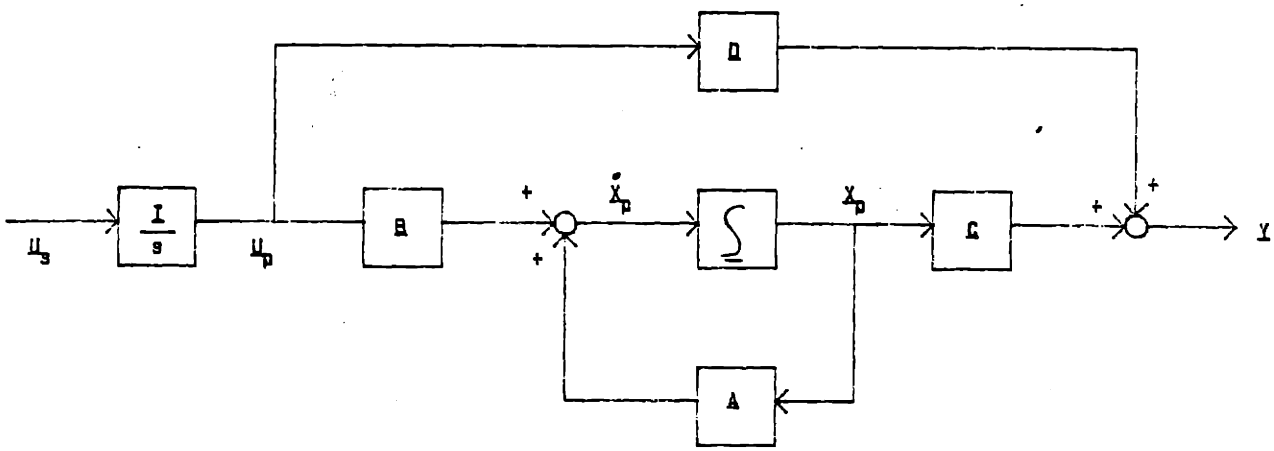

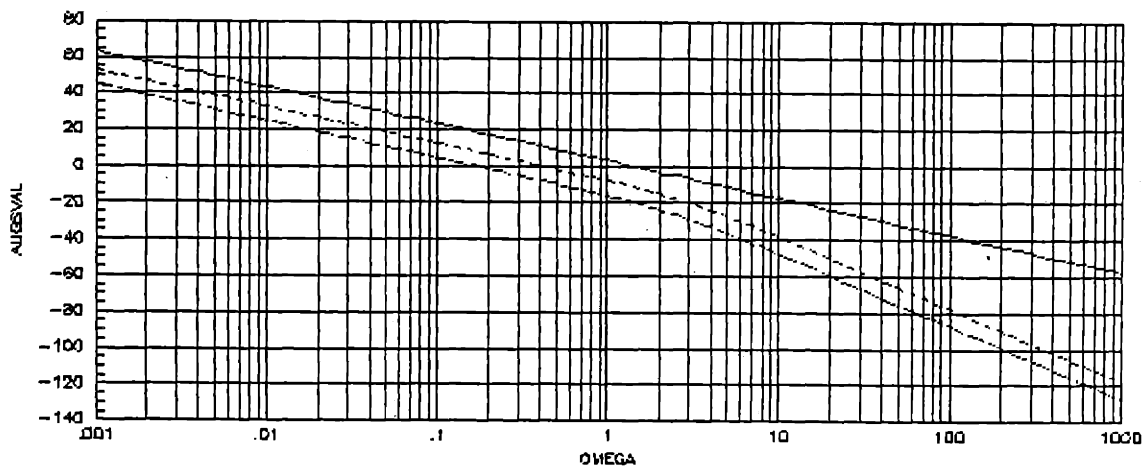

Figure 4.3-1
Augmented Plant Structure and Open Loop Frequency Response
of Augmented Plant

the augmented system as the nominal plant.

The technique for designing the target loop using the Kalman Filter concept is based on the Kalman Frequency Domain Equality which states:

$$[\underline{I}+\underline{G}_{KF}(s)][\underline{I}+\underline{G}_{KF}(-s)]^T = \underline{I}+(1/\upsilon)\underline{G}_{fol}(s)\underline{G}_{fol}(-s) \quad (4.19)$$

Far from the crossover region (at $s=j\omega\to 0$ and at $s=j\omega\to\infty$ the approximation for this expression becomes:

$$\underline{G}_{KF}(s) \simeq (1/\upsilon)^{1/2}\underline{G}_{fol}(s) \quad (4.20)$$

The auxillary function $\underline{G}_{fol}(s)$ is defined as:

$$\begin{aligned}\underline{G}_{fol}(s) &= \underline{C}_a(s\underline{I}-\underline{A}_a)^{-1}\underline{L} \\ &= [\underline{D}_p\ \underline{C}_p]\left[s\underline{I} - \begin{pmatrix} \underline{0} & \underline{0} \\ \underline{B}_p & \underline{A}_p \end{pmatrix}\right]^{-1}\begin{bmatrix} \underline{L}_L \\ \underline{L}_H \end{bmatrix}\end{aligned} \quad (4.21)$$

The design parameter $\underline{L}$ is used to shape the singular values of of $\underline{G}_{fol}(s)$ and, using the approximation in equation (4.20), the frequency response of $\sigma(\underline{G}_{KF}(s))$. The above partitioning of $\underline{L}$ allows the designer to match the singular values of the target design at high and low frequency. To see how to select $\underline{L}$, expand equation (4.20) as follows:

$$\underline{G}_{fol}(s) = [\underline{D}_p\ \underline{C}_p]\begin{bmatrix} \underline{I}/s & \underline{0} \\ (s\underline{I}-\underline{A}_p)^{-1}\underline{B}_p/s & (s\underline{I}-\underline{A}_p)^{-1} \end{bmatrix}\begin{bmatrix} \underline{L}_L \\ \underline{L}_H \end{bmatrix} \quad (4.22)$$

Expanding the above expression yields:

$$\underline{G}_{fol}(s) = (\underline{I}/s)(\underline{D}_p+\underline{C}_p(s\underline{I}-\underline{A}_p)^{-1}\underline{B}_p)\underline{L}_L + \underline{C}_p(s\underline{I}-\underline{A}_p)^{-1}\underline{L}_H. \quad (4.23)$$

At low frequency, the first term of equation (4.23) dominates and

$$\lim_{s=j\omega\to 0}\underline{G}_{fol}(s) = (\underline{D}_p+\underline{C}_p(-\underline{A}_p)^{-1}\underline{B}_p)\underline{L}_L. \quad (4.24)$$

To match the singular values at low frequencies, set

$$(\underline{D}_p+\underline{C}_p(-\underline{A}_p)^{-1}\underline{B}_p)\underline{L}_L = \underline{I} \tag{4.25}$$

and

$$\underline{L}_L = (\underline{D}_p+\underline{C}_p(-\underline{A}_p)^{-1}\underline{B}_p)^T[(\underline{D}_p+\underline{C}_p(-\underline{A}_p)^{-1}\underline{B}_p)(\underline{D}_p+\underline{C}_p(-\underline{A}_p)^{-1}\underline{B}_p)^T]^{-1}.$$

If the plant is square (i.e., same number of inputs and outputs), then this reduces to

$$\underline{L}_L = (\underline{D}_p+\underline{C}_p(-\underline{A}_p)^{-1}\underline{B}_p)^{-1}. \tag{4.27}$$

It is also interesting to note that emperical evidence suggests that if any of the above inverses do not exist, then using the pseudo inverse of these matricies appears to yield satisfactory results. That is

$$\underline{L}_L = (\underline{D}_p+\underline{C}_p(-\underline{A}_p)^{+}\underline{B}_p)^{+}, \tag{4.28}$$

where $^+$ indicates the pseudo inverse, appears to be a suitable definition for the paramater $\underline{L}_L$.

At high frequencies, the dominant terms in equation (4.23) are given by

$$\lim_{s=j\omega\to\infty} \underline{G}_{fol}(s) = \underline{D}_p\underline{L}_L + \underline{C}_p\underline{L}_H \tag{4.29}$$

and to match the singular values set

$$\underline{D}_p\underline{L}_L + \underline{C}_p\underline{L}_H = \underline{I}. \tag{4.30}$$

Solving for $\underline{L}_H$ yields

$$\underline{L}_H = \underline{C}_p(\underline{C}_p\underline{C}_p^T)^{-1}[\underline{I}-\underline{D}_p\underline{L}_L] \tag{4.31}$$

or

$$\underline{L}_H = \underline{C}_p^{+}[\underline{I}-\underline{D}_p\underline{L}_L]. \tag{4.32}$$

The design parameter $\underline{L}$ in equation (4.12) is defined by the partitioned matrix

$$\underline{L} = \begin{bmatrix} \underline{L}_L \\ \hline \underline{L}_H \end{bmatrix} \qquad (4.33)$$

and defines the shape of the response of $\sigma(\underline{G}_{fol}(s))$. The value of the scalar υ is used to adjust the crossover frequency of the target design to meet the requirements.

The design of the target loop is now an iterative procedure. The design steps are:

1. Define $\underline{M}=\underline{L}\,\underline{L}^T$ in the FARE (equation 4.7).
2. Choose an initial value of υ.
3. Solve for $\underline{H}$ in equation (4.5).
4. Plot the frequency response of $\sigma(\underline{G}_{KF}(s))$.
5. Decide if the frequency response in step 4 meets the frequency domain design requirements. If the frequency response requirements are met, then the target loop design is nearly complete. If the design requirements are not met, then select another value of υ and repeat steps 3, 4 and 5.
6. Simulate the time response of the target loop to verify that the time domain (i.e., overshoot and response time) specifications are also met. If these requirements are also met, the the target loop design is finished. If not, adjust the design parameters and repeat the above procedure.

Once the target loop is designed, the recovery procedure is applied.

4.4 THE RECOVERY PROCEDURE

The object of the recovery step in the design process is to select values for the scalar ρ which force the frequency response of the open loop TFM ($\underline{G}(s)\underline{K}(s)$) to be the same as the frequency response of the target loop. That is, the frequency response of $\sigma(\underline{G}(s)\underline{K}(s))$ would have matched singular

values at d.c., infinite gain at d.c., fall at -20 dB/decade, have the same crossover frequency as the target loop and, at some frequency above crossover, would roll off at -40 dB/decade.

The recovery procedure is:

1. Pick a starting valus of ρ.
2. Solve the CARE (equation 4.8) using ρ and $\underline{Q}=\underline{C}_a^T\underline{C}_a$.
3. Solve for the control gain $\underline{G}$ in equation 4.6.
4. Plot the frequency response of $\sigma(\underline{G}_a(s)\underline{K}(s))$.
5. Decide if the target loop has been adequately recovered. If recovered, the recovery step is complete. If not, reduce the value of ρ and repeat steps 2, 3, 4 and 5.

A more theoretical discussion of the LTR procedure can be found in [13, 23]. Discussions on the limits of achievable performance of this technique can be found in [31].

4.5 SOME PRACTICAL ISSUES

When applying the LQG/LTR procedure, there are some important practical issues to keep in mind. The first is that as the value of υ or ρ approach zero, the individual entries in the filter gain matrix $\underline{H}$ and the control gain matrix $\underline{G}$ get very large. This, in turn, implies that the compensator "$\underline{A}$" matrix ($\underline{A}_c=\underline{A}-\underline{B}\underline{G}-\underline{H}\underline{C}$) may contain entries which become very large. Since the compensator must eventually be implemented with a computer, the designer should watch these enteries to insure that they will not cause computational problems when implemented with the computer.

Another issue is that the recovery procedure will create some very high frequency poles in the overall design. These poles may require very small (impractical) time steps for the numerical integration procedures used in the computer implementation of the control system. There are methods of "dropping" these poles [4], and one technique is demonstrated in the design examples.

4.6 SUMMARY OF ROBUSTNESS RESULTS

At this point, a brief discussion of "robustness" is in order. The robustness of a linear system refers to the stability properties of the closed-loop system in the presence of model uncertainty. More specifically, the robustness of the system refers to the extent to which the elements of the loop transfer function matrix can vary from their nominal values before the closed-loop system goes unstable.

The important robustness results for multivariable control systems were derived by Lehtomaki [2, 32]. These results state that the error, $\underline{E}(s)$, between the true plant, $\tilde{G}(s)$, and the nominal plant, $\underline{G}(s)$, provides a measure of the stability robustness of the system. The errors are split into two catagories, relative error and absolute error. Relative errors correspond to multiplicative or division errors and absolute errors correspond to additive or subtractive errors.

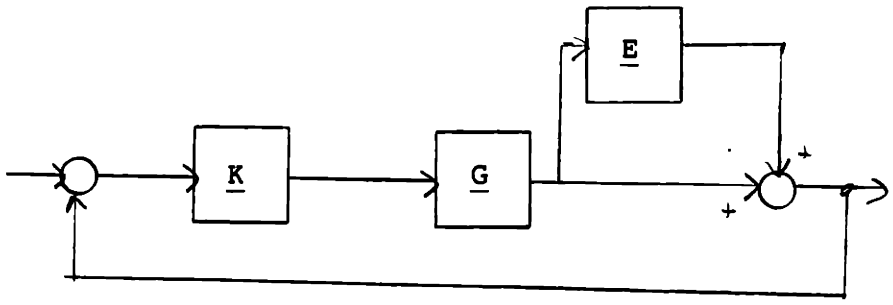

Figure 4.6-1
Block Diagram Representation of Multiplicative Error

The errors which most concern the control system designer are the relative errors. A block diagram of the multiplicative error representation is shown in Figure 4.6-1. The multiplicative error is defined by

$$\underline{E}(s) = (\underline{\tilde{G}}(s) - \underline{G}(s))\underline{G}^{-1}(s) \qquad (4.34)$$

Using the above definition of model error, it can be shown that if the singular value inequality of (4.35) holds, then the closed-loop system is guaranteed stable [2].

$$\sigma_{max}[\underline{E}(s)] < \sigma_{min}[\underline{I} + (\underline{G}(s)\underline{K}(s))^{-1}] \qquad (4.35)$$

For most physical systems, including the one used for this research, the modelling error is often difficult or impossible to quantify. However, even if the modelling error is not known, the above inequalities can still provide valuable information regarding the maximum size of the error the system can tolerate. This error relationship provides a

conservative bound for the system error; a system may still be closed-loop stable even if the above bounds are crossed. In the latter case, system stability would have to be determined through extensive simulation and testing.

4.7 SUMMARY

This chapter has presented the step-by-step procedure for designing an LQG/LTR compensator with recovery at the plant output. The need for dynamic augmentation of the original plant was presented and the method of selecting design parameters based on the augmented plant was given. The properties and restrictions as well as some practical issues related to the LQG/LTR procedure were discussed. A brief overview of some basic robustness results was also presented.

CHAPTER 5

COMPENSATOR DESIGN FOR THE GE21

5.1 INTRODUCTION

The requirements for the compensator design for the GE21 were given in section 3.5. The main performance requirement is to be able to vary thrust from the nominal value at the operating point down to 50% of the nominal value and back up again. The response time of this thrust modulation is given as 0.5 seconds.

This chapter illustrates the procedure for designing the LQG/LTR compensator for the GE21. Three sample trial designs are used in the example. The three sample designs all use the same operating point, but illustrate different methods of applying the LGQ/LTR procedure and interpreting the results.

The first design used a target loop with a 10 rad/sec crossover but the LTR procedure only recovers the loop to 3 rad/sec. The second example fully recovers the target loop to 10 rad/sec. The third design used a target loop with a crossover of 100 rad/sec and a recovered loop of 10 rad/sec. The three designs are referred to as simply the first, second and third design and these are shown in Table 5.1-1.

DESIGN	TARGET CROSSOVER	RECOVERY CROSSOVER
FIRST	10 radians/sec	3 radians/sec
SECOND	10 radians/sec	10 radians/sec
THIRD	100 radians/sec	10 radians/sec

Table 5.1-1
Three Design Examples Summary

5.2 GE21 MODEL REVIEW

The compensator designs presented in the following sections are all based on the 3 x 3 scaled linear model of the GE21 developed in Chapter 3. The order of the inputs, outputs and states for the linear model is given in Table 5.2-1.

INPUTS	STATES	OUTPUTS
WF36 (Fuel Flow)	N2 (LP Speed)	N2
A8 (Outer Nozzle Area)	N25 (HP Speed)	N25
AE96 (FWD VABI Area)		FG (Thrust)

Table 5.2-1
Order of Inputs, States and Outputs for GE21 Linear Model

The input, state and output variables are all scaled using the maximum physical value of each variable. Both the linear model and the nonlinear computer model have been scaled and only the scaled systems are used in the simulations. The scaled 3 x 3 system matrices were presented in section 3.4. The scale factors are provided in Appendix C and all other system matrices are provided in Appendix B.

The compensator provides the engine main fuel flow input, WF36, the outer nozzle area adjustment, A8, and the forward VABI control, AE96, as control inputs to the plant. For the nonlinear simulations, a total of 7 control inputs

are required by the model. The 4 control inputs not provided by the compensator are set to the respective values at the operating point where the model was linearized and held constant. The operating point of the engine for all the simulations in this section is defined at sea level static conditions as maximum power without afterburner, also called "operating point 9" for the GE21 engine. The inputs and outputs for the nonlinear model are listed in Table 5.2-2. The steady state values of the variables at the different engine operating points were provided by the General Electric Company and are listed in Appendix C.

INPUTS	OUTPUTS
WF36	N2
STP22	N25
STP48	FG
A8	T42
A88	PS3
AE16	DPQP3
AE96	DPQP13

Table 5.2-2
Order of Inputs and Outputs for GE21 Nonlinear Model

There are no actautors or sensors used in any of the simulations in this section.

5.3 GE21 CONTROLLER DESIGN

In order to meet the response time requirement of 0.5 seconds, the initial target loop was designed with a crossover frequency of 10 rad/sec. A 10 rad/sec crossover implies a 0.1 second time constant and, from classical control theory, within 5 time constants the loop should reach

its final steady state value.

The parameter $\underline{L}$ was calculated using equation (4.33) and the scalar ν was varied until $\sigma_{min}(\underline{G}_{KF}(s))$ had a crossover of 10 rad/sec. The frequency response of $\sigma(\underline{G}_{KF}(s))$ is shown in Figure 5.3-1 with ν=0.01. Notice that the singular values of $\underline{G}_{KF}(s)$ are matched at high and low frequencies.

The recovery procedure (section 4.4) was then applied and the scalar ρ was varied to try to recover the loop. As an interim step in the design, the loop was only partially recovered. With ρ=0.0001, $\sigma_{min}(\underline{G}_a(s)\ \underline{K}(s))$ has a crossover frequency of 3 rad/sec. The frequency response of the open loop TFM is shown in Figure 5.3-2. The frequency response of the closed loop TFM for this step is shown in Figure 5.3-3.

The value of ρ was then reduced until the target loop was fully recovered. With $\rho=10^{-6}$, the open loop frequency response is shown in Figure 5.3-4 and the closed loop frequency response is shown in Figure 5.3-5.

From Figure 5.3-4 we can see that when the loop is fully recovered, the singular values of the open loop frequency response are more tightly matched than when the loop is only partially recovered as shown in Figure 5.3-2. This indicates that the open loop response to commands in all directions is the same in the fully recovered design but the response may vary in the partially recovered design depending on the direction of the commanded input.

In the closed loop systems, the partially recovered

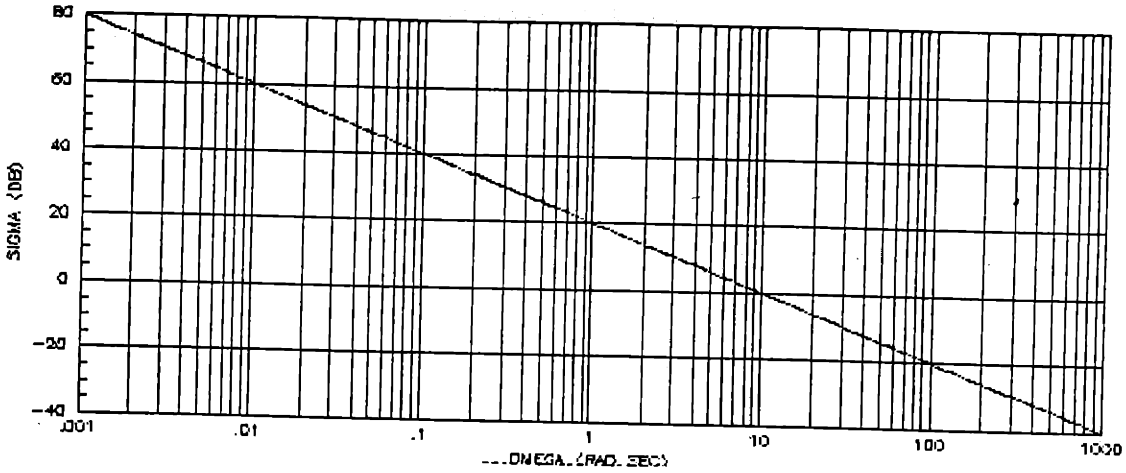

Figure 5.3-1
Open Loop Frequency Response of Target Loop, $\underline{G}_{KF}(s)$ - First Design
$(\nu=0.01)$

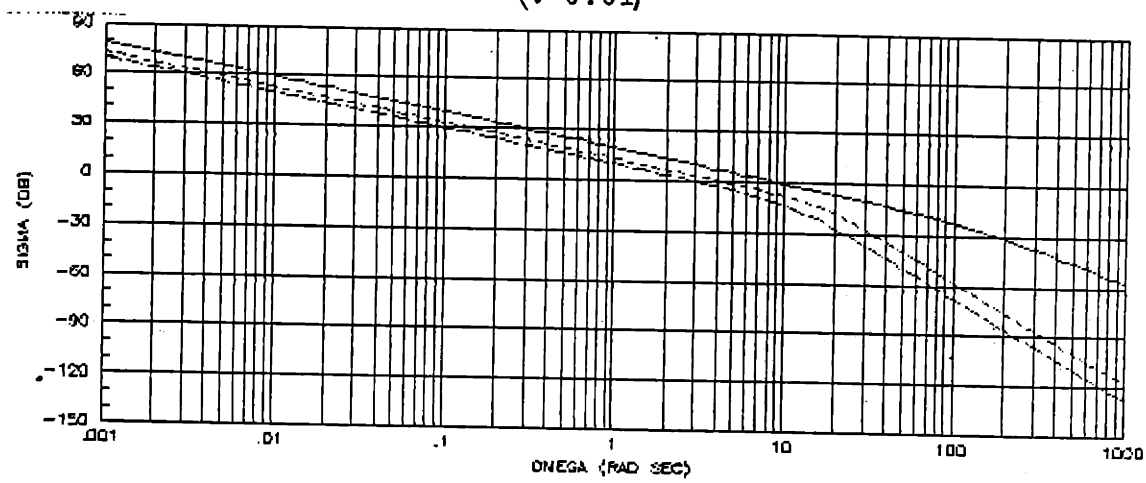

Figure 5.3-2
Frequency Response of $\underline{G}_a(s)\underline{K}(s)$ - First Design
$(\nu=0.01,\ \rho=0.0001)$

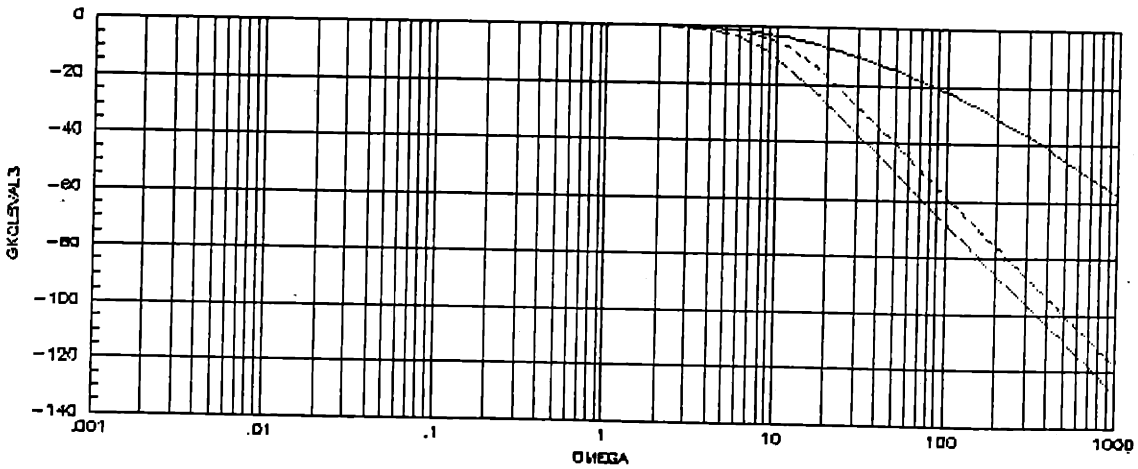

Figure 5.3-3
Frequency Response of $[I+\underline{G}_a(s)\underline{K}(s)]^{-1}\underline{G}_a(s)\underline{K}(s)$ - First Design
$(\nu=0.01,\ \rho=0.0001)$

design has singular values which start to drop off before the 10 rad/sec crossover. This indicates that the response to commands is these directions will be slower than the response of the commands in other directions. When the loop is recovered fully, the frequency response of the closed loop system is more tightly matched through the 10 rad/sec crossover region which indicates a more uniform response to commands in all directions, up to the cut-off frequency of 10 rad/sec.

The third trial used a value of $\nu=10^{-4}$ and $\rho=10^{-6}$ which creates a target loop with a crossover 100 rad/sec (see Figure 5.3-6) and the recovered loop has $\sigma_{min}(\underline{G}_a(s)\ \underline{K}(s))$ crossover at 10 rad/sec. The frequency responses of the open loop and closed loop TFMs are shown in Figures 5.3-7 and 5.3-8.

The third design has frequency response characteristics similar to those of the first design with respect to the roll-off in different directions of commands. The difference between the first and third design is that the direction of minimum response in the closed loop design is still at 0 dB at 10 rad/sec. This indicates that the overall response of the third design would be faster than either the first or the second design, which was the original intent of the third design.

The frequency responses of the compensators plus integrators are shown in Figures 5.3-9 thru 5.3-11. Notice that the responses of all the compensators "flatten out" at

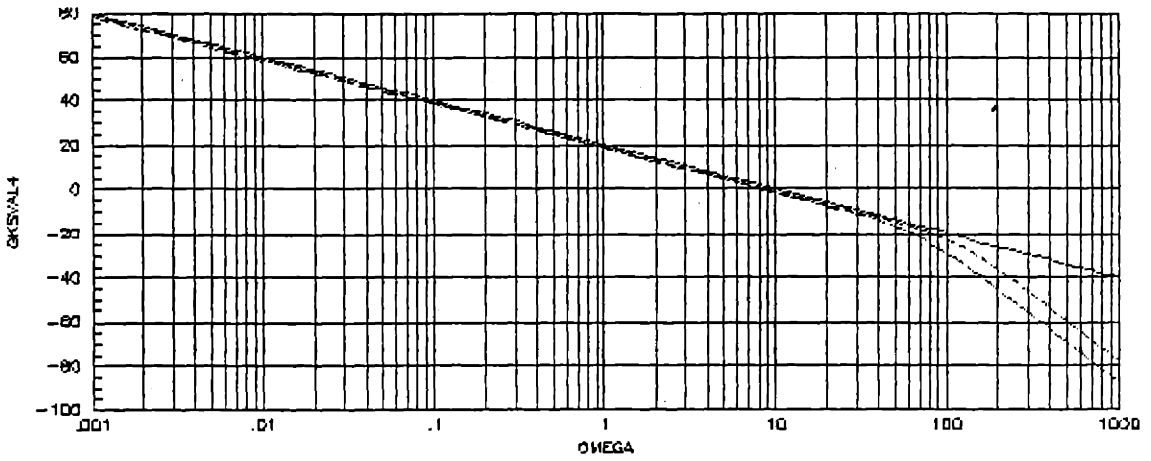

Figure 5.3-4
Frequency Response of $\underline{G}_a(s)\underline{K}(s)$ - Second Design

$\left(\nu=0.01,\ \rho=10^{-6}\right)$

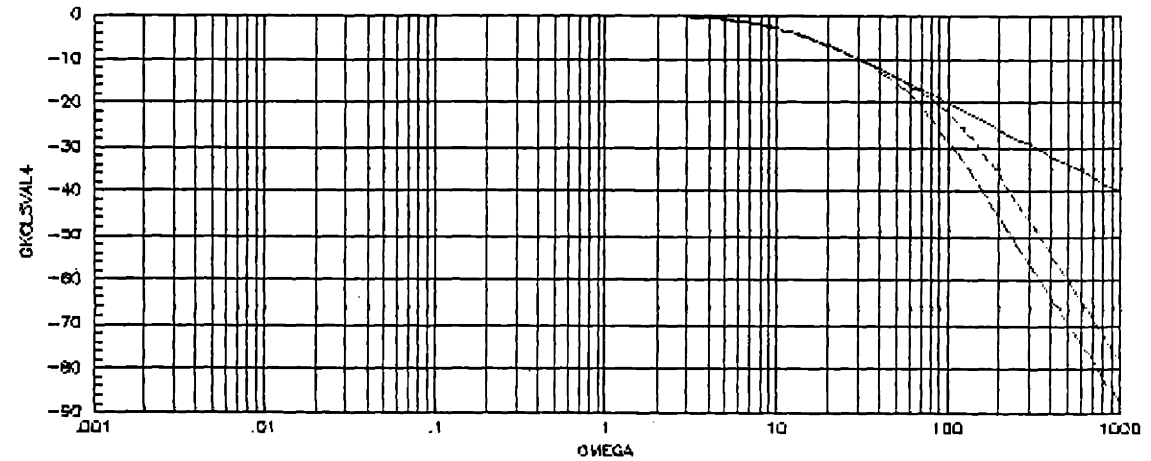

Figure 5.3-5
Frequency Response of $[I+\underline{G}_a(s)\underline{K}(s)]^{-1}\underline{G}_a(s)\underline{K}(s)$ - Second Design

$\left(\nu=0.01,\ \rho=10^{-6}\right)$

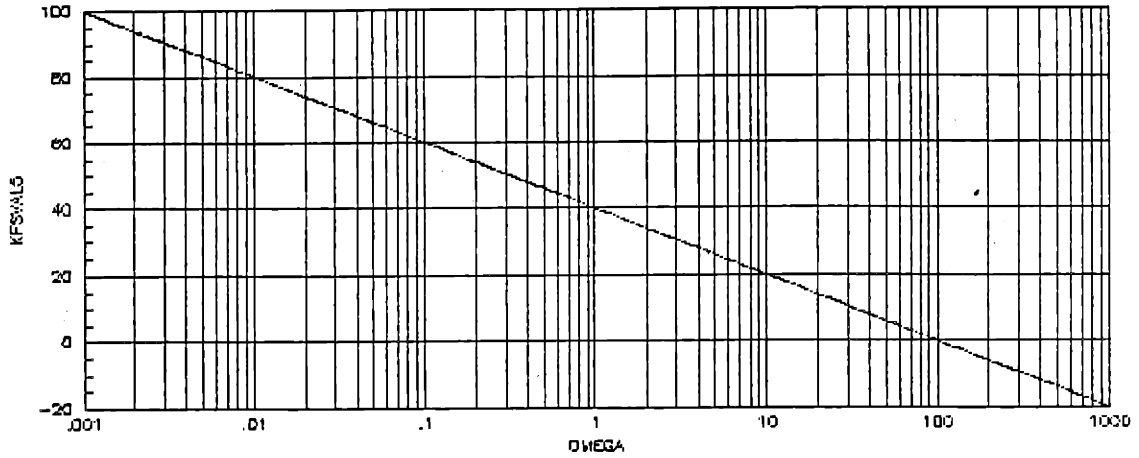

Figure 5.3-6
Open Loop Frequency Response of Target Loop, $\underline{G}_{KF}(s)$ - Third Design
$\left(\nu=10^{-4}\right)$

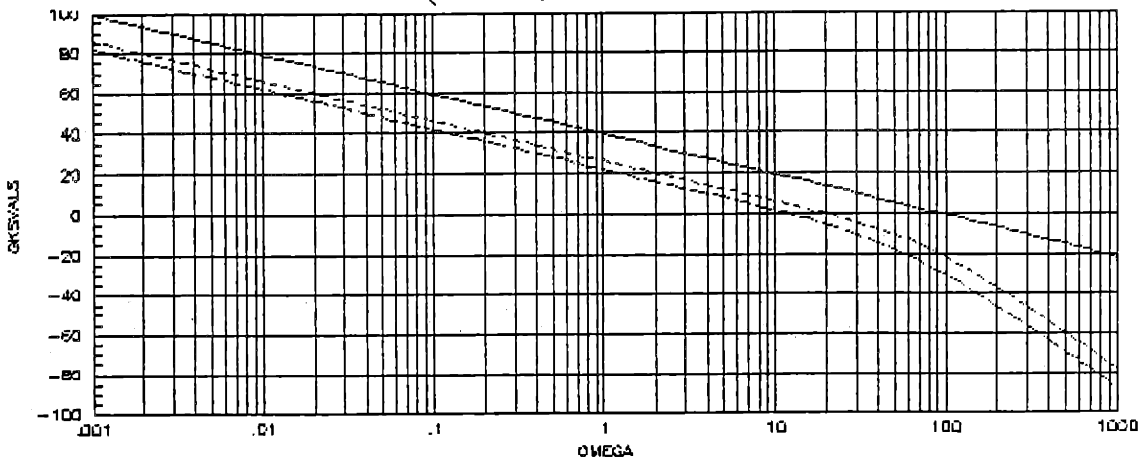

Figure 5.3-7
Frequency Response of $\underline{G}_a(s)\underline{K}(s)$ - Third Design
$\left(\nu=10^{-4},\ \rho=10^{-6}\right)$

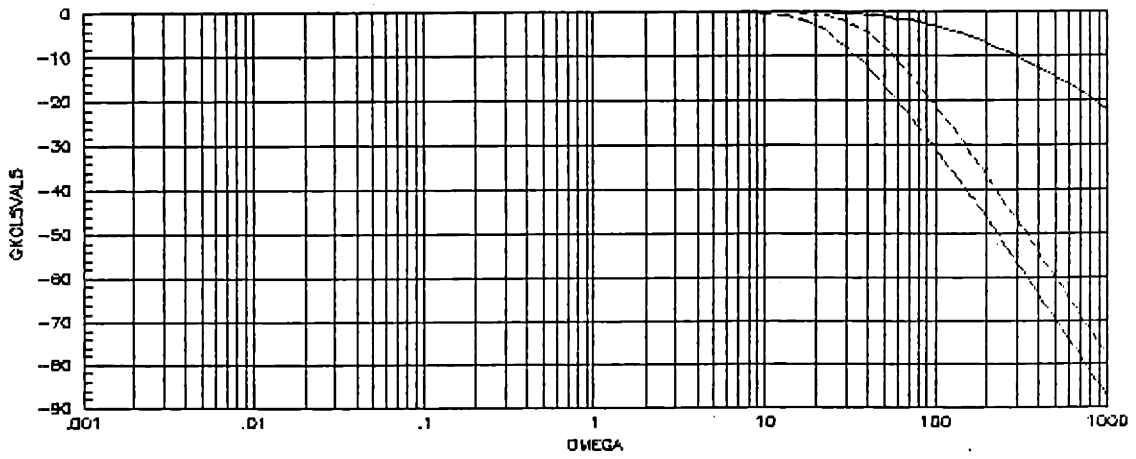

Figure 5.3-8
Frequency Response of $[I+\underline{G}_a(s)\underline{K}(s)]^{-1}\underline{G}_a(s)\underline{K}(s)$ - Third Design
$\left(\nu=10^{-4},\ \rho=10^{-6}\right)$

around 2 rad/sec then roll-off again at some higher frequency. This is due to the zeros of the compensator which are created by the design process. The roll-off begins at the higher frequency poles which are also created in the design process. These poles and zeros are discussed again in section 5.5. Also note that the large gain at d.c. is due to the free integrators which were added to the plant inputs during the design. These integrators are physically located within the compensator and provide the "infinite" gain at d.c. which is required by the design specifications.

The frequency response of the sensitivity TFM (section 3.5.1) for each loop are shown in Figures 5.3-12 thru 5.3-14. These plots suggest that the loops which are not recovered fully are more sensitive to disturbances in certain directions than the fully recovered loop, as indicated by the magnitude of the sensitivity response at the 10 rad/sec crossover. In addition, notice that the faster loop, Figure 5.3-14, is more sensitive than the other loops at 20 rad/sec in certain directions (also note that the scale on this figure is different than that on the previous two).

The frequency response of the command input to control TFM (i.e., from $\underline{r}$ to $\underline{u}$ in Figure 3.5-1) for each loop are shown in Figure 5.3-15 through 5.3-17. The designer should check this response to insure that the control inputs to the plant are not overly sensitive to noise or disturbances in certain directions or at certain frequencies. From Figures 5.3-15 through 5.3-17, we notice that the singular values,

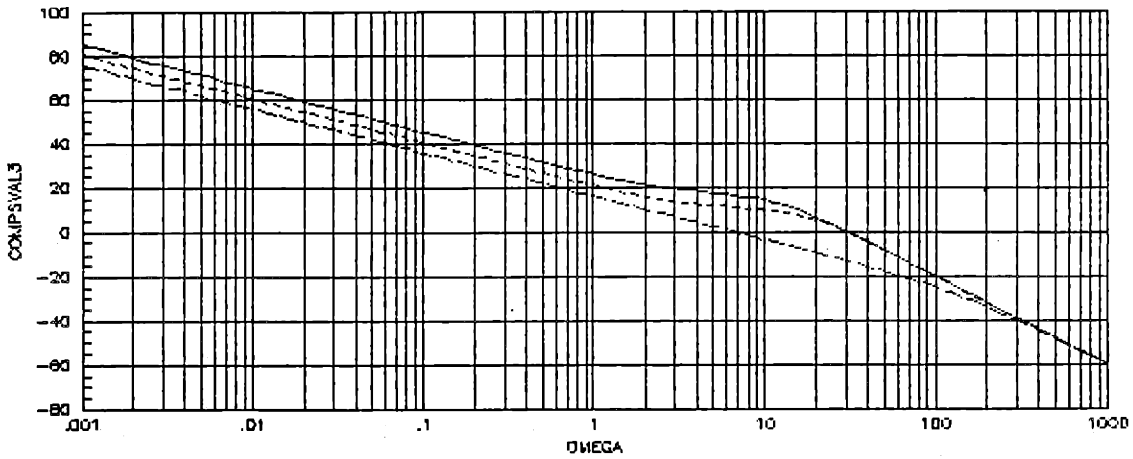

Figure 5.3-9
Frequency Response of Compensator, $\underline{K}(s)\underline{I}/s$ - First Design
$(\nu=0.01,\ \rho=0.0001)$

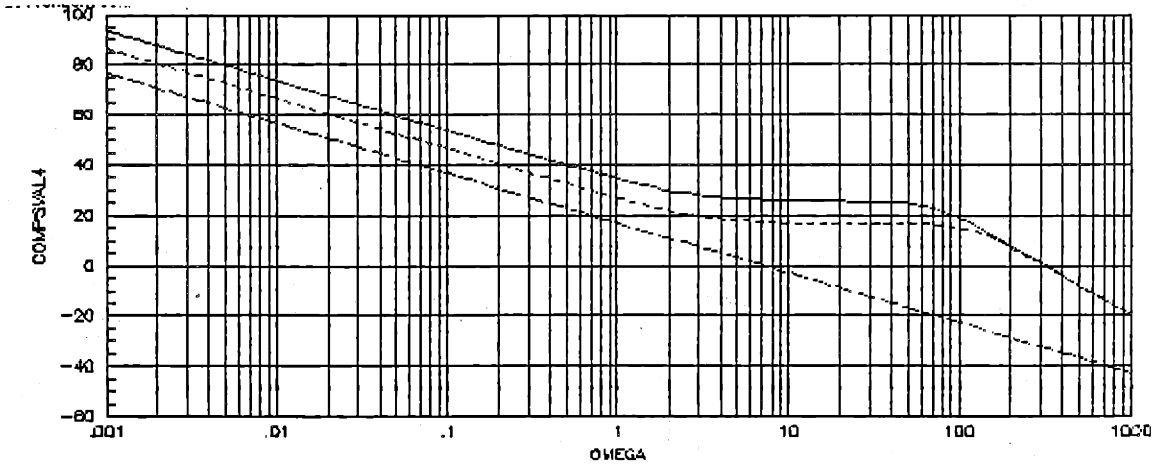

Figure 5.3-10
Frequency Response of Compensator, $\underline{K}(s)\underline{I}/s$ - Second Design
$(\nu=0.01,\ \rho=10^{-6})$

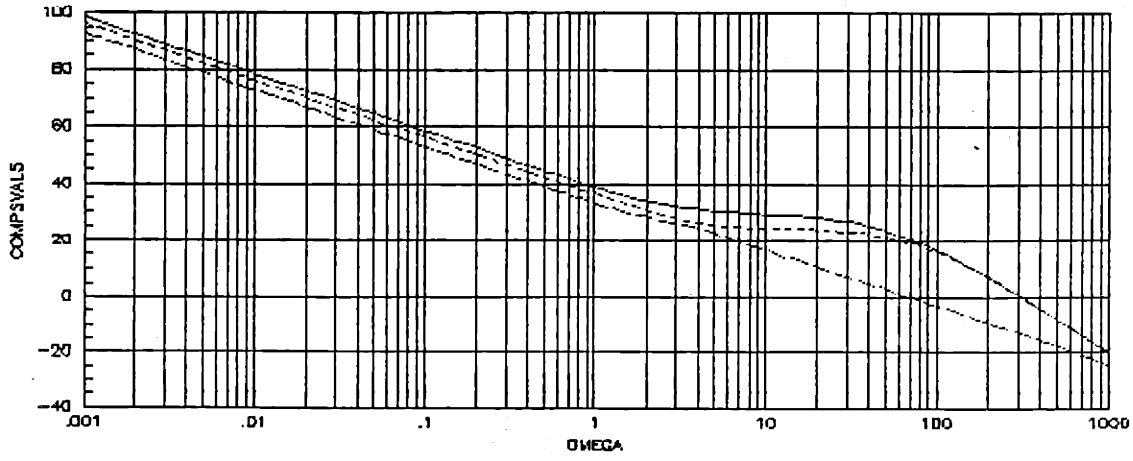

Figure 5.3-11
Frequency Response of Compensator, $\underline{K}(s)\underline{I}/s$ - Third Design
$(\nu=10^{-4},\ \rho=10^{-6})$

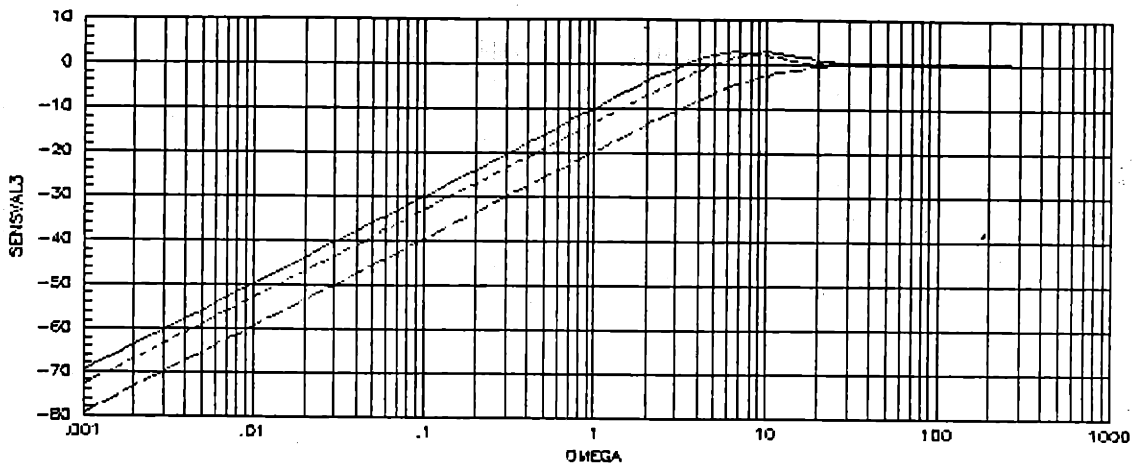

Figure 5.3-12
Frequency Response of Sensitivity TFM, $[\underline{I}+\underline{G}_a(s)\underline{K}(s)]^{-1}$ - First Design
$(\nu=0.01,\ \rho=0.0001)$

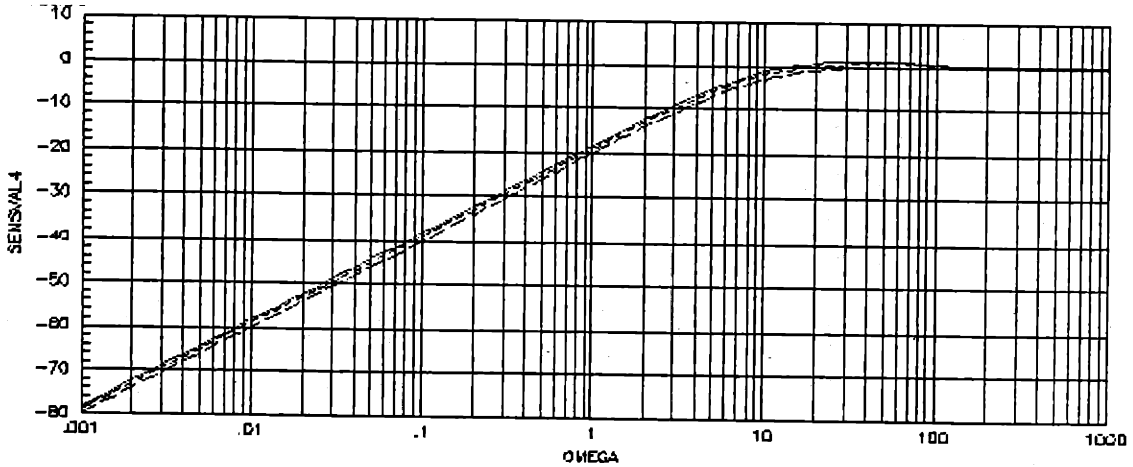

Figure 5.3-13
Frequency Response of Sensitivity TFM, $[\underline{I}+\underline{G}_a(s)\underline{K}(s)]^{-1}$ - Second Design
$(\nu=0.01,\ \rho=10^{-6})$

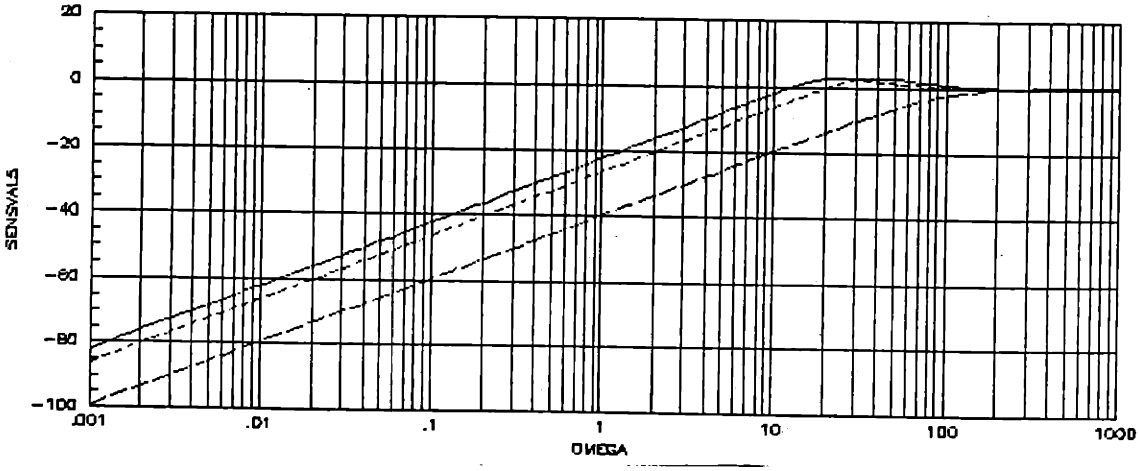

Figure 5.3-14
Frequency Response of Sensitivity TFM, $[\underline{I}+\underline{G}_a(s)\underline{K}(s)]^{-1}$ - Third Design
$(\nu=10^{-4},\ \rho=10^{-6})$

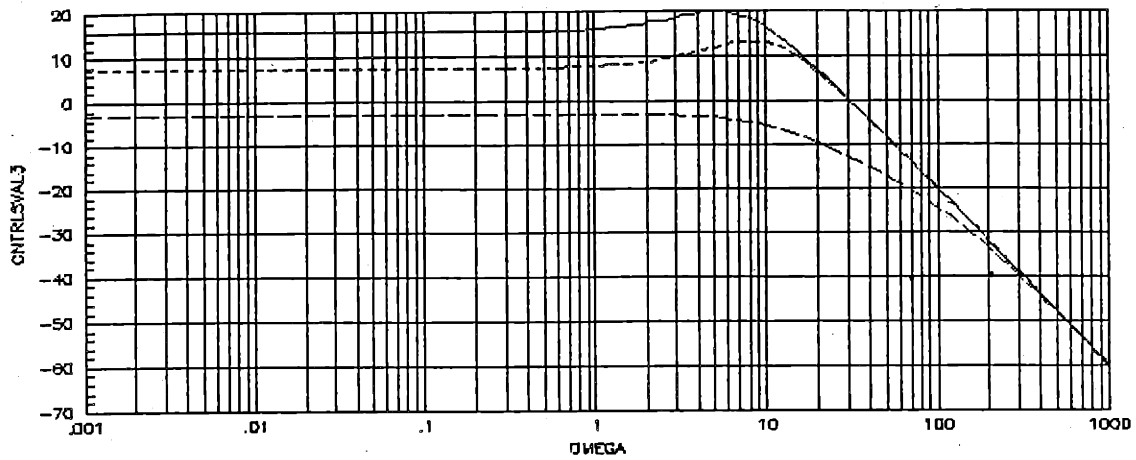

Figure 5.3-15
Frequency Response of Reference Command, $\underline{r}$, to Plant Input, $\underline{u}$, of First Design (υ=0.01, ρ=0.0001)

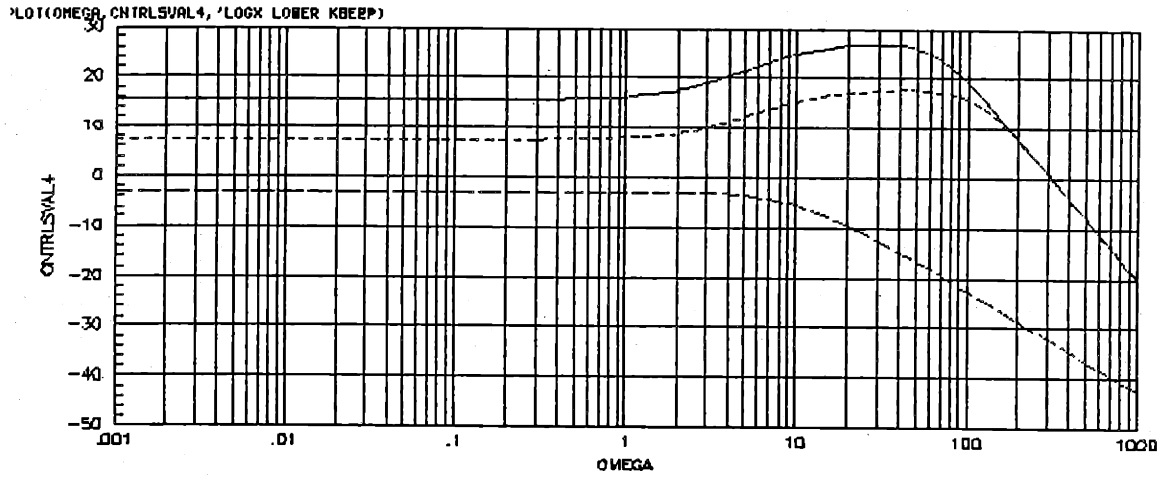

Figure 5.3-16
Frequency Response of Reference Command, $\underline{r}$, to Plant Input, $\underline{u}$, of Second Design (υ=0.01, $\rho=10^{-6}$)

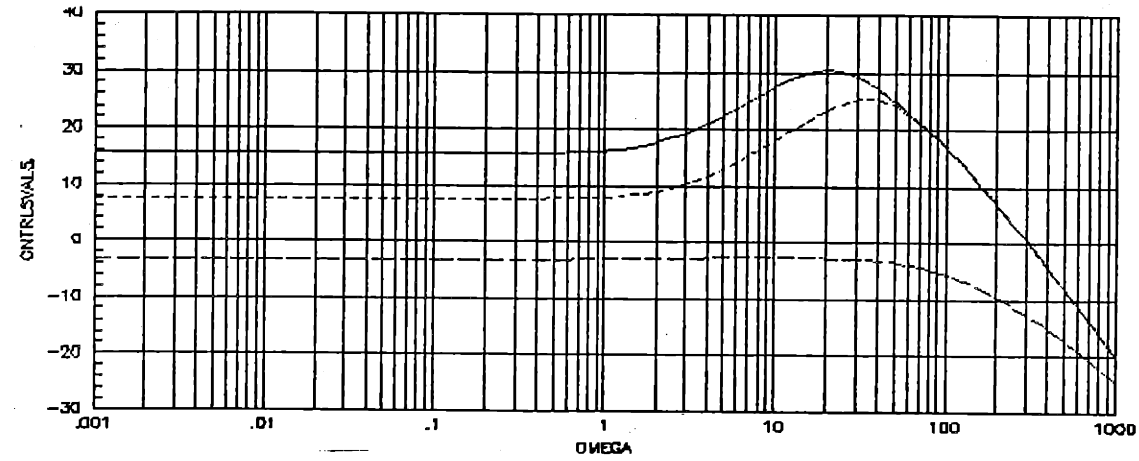

Figure 5.3-17
Frequency Response of Reference Command, $\underline{r}$, to Plant Input, $\underline{u}$, of Third Design ($\upsilon=10^{-4}$, $\rho=10^{-6}$)

plotted in dB, are spread in the frequency range from d.c. to past 100 rad/sec. This indicates that the response of the control inputs to reference commands (or disturbances) is not uniform for all directions. In the faster designs, we also see that commands in two directions at a frequency of approximately 12 rad/sec will be amplified at the plant input. This is seen clearly in Figure 5.3-17 as the frequency response peaks at +30 dB at 12 rad/sec. All of these plots do tend to roll-off at higher frequencies and, although some indicate that reference inputs up to approximately 300 rad/sec will appear at the engine controls (i.e., the frequency response of the loop is at or above 0 dB and therefore will not attenuate inputs up to this frequency), none of the designs appear to be overly sensitive to the reference inputs.

Thus far, all designs appear to be acceptable. The transient response characteristics of the various designs must also be evaluated.

5.4 SYSTEM TIME RESPONSES

This section presents the results of the time simulations when the compensators are connected to the linear and nonlinear plant models. The compensators were first connected to the linear plants and a reference command input was applied. This command input held N2 and N25 at the equilibrium values (i.e., N2=0 and N25=0 for the linear

simulations and N2=5382 rpm and N25=7236 rpm for the nonlinear simulations) and commanded thrust as shown in Figure 5.4-1. The nonlinear plant was the substituted in place of the linear plant and a similar input command was given.

5.4.1 LINEAR SIMULATIONS

The time responses of the Thrust output and the two rotor speeds are shown in Figures 5.4-2 through 5.4-4. All three of the designs appear to meet the specifications with regard to command following, response time and overshoot limitations.

There are very small perturbations (less than 0.1%) in the speeds at the times when the step changes in command input are applied. This type of momentary perturbation is not unexpected for the type of command inputs applied.

An expanded view of the Thrust output response is provided in Figure 5.4-5. This figure superimposes the responses of all three systems at the first step change in commanded thrust. From this figure, the effects of the dominant poles (see section 5.5) can be seen.

The time responses of the plant control inputs are shown in Figures 5.4-6 thru 5.4-8. These figures indicate that all three compensators will keep the control inputs within acceptable bounds and that there is no significant overshoot to be concerned with.

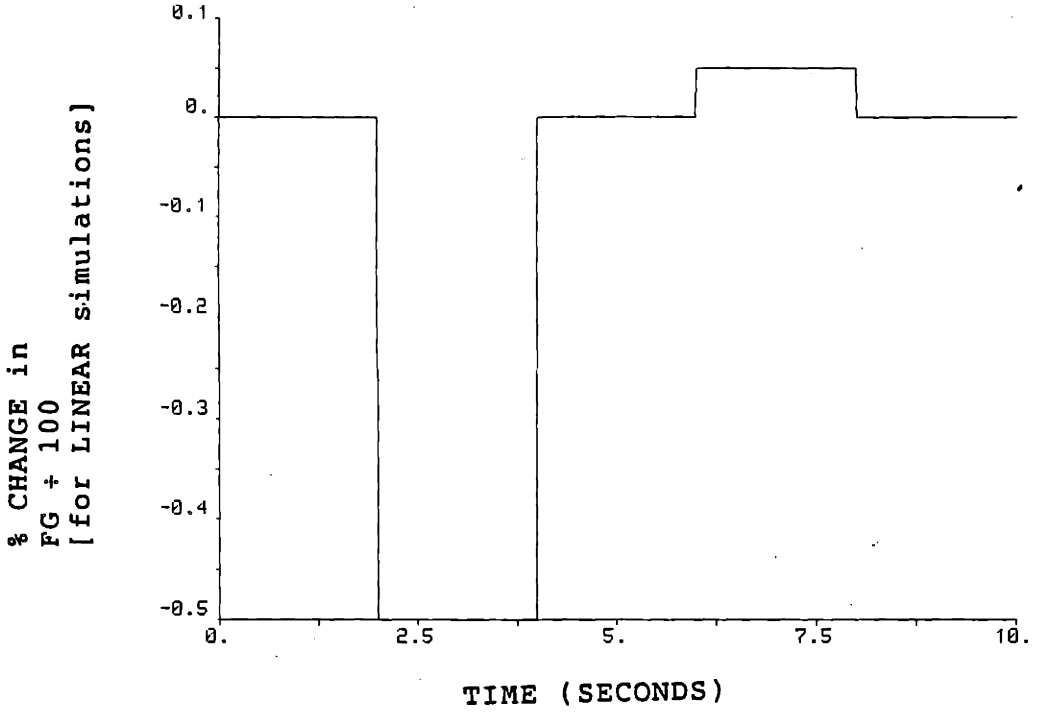

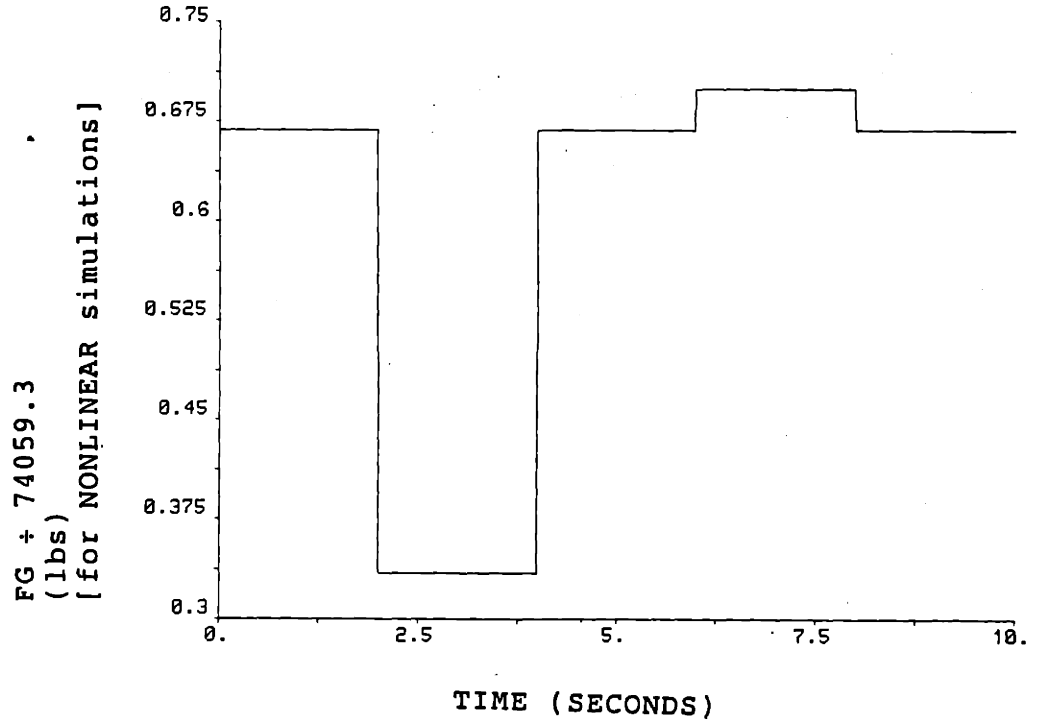

Figure 5.4-1
Commanded Thrust Changes for Linear and Nonlinear Simulations

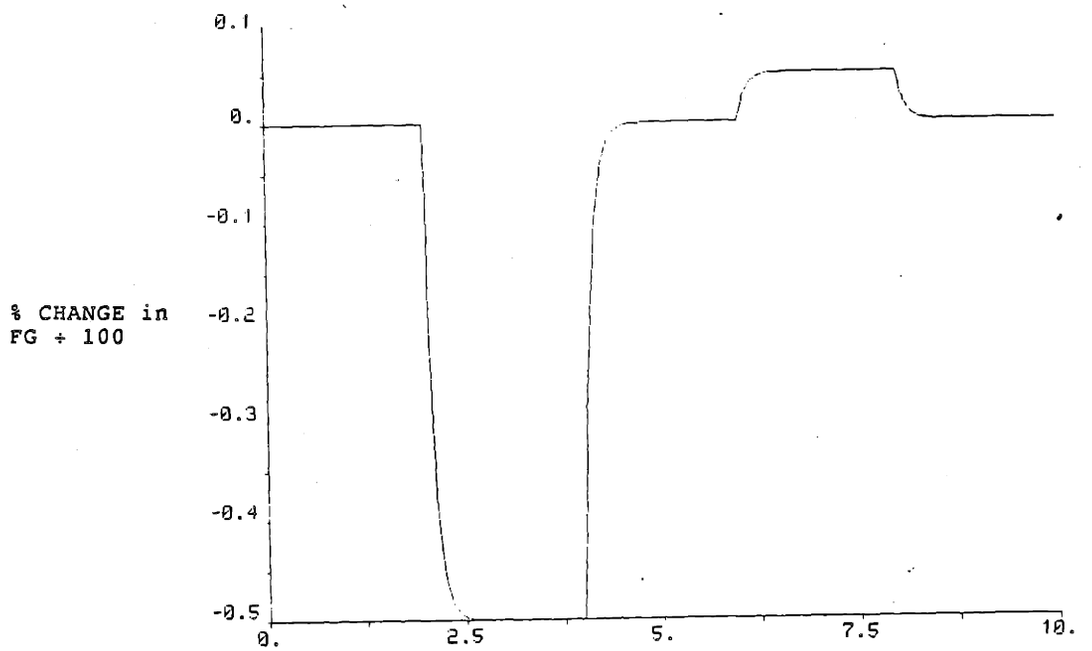

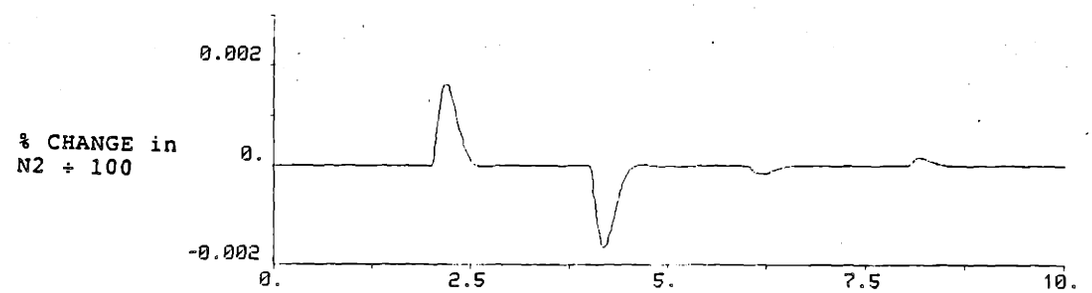

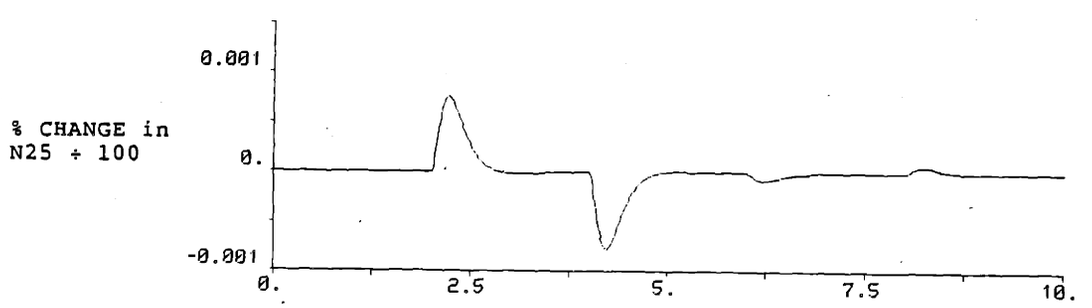

Figure 5.4-2
Output Responses of Linear Model - First Design

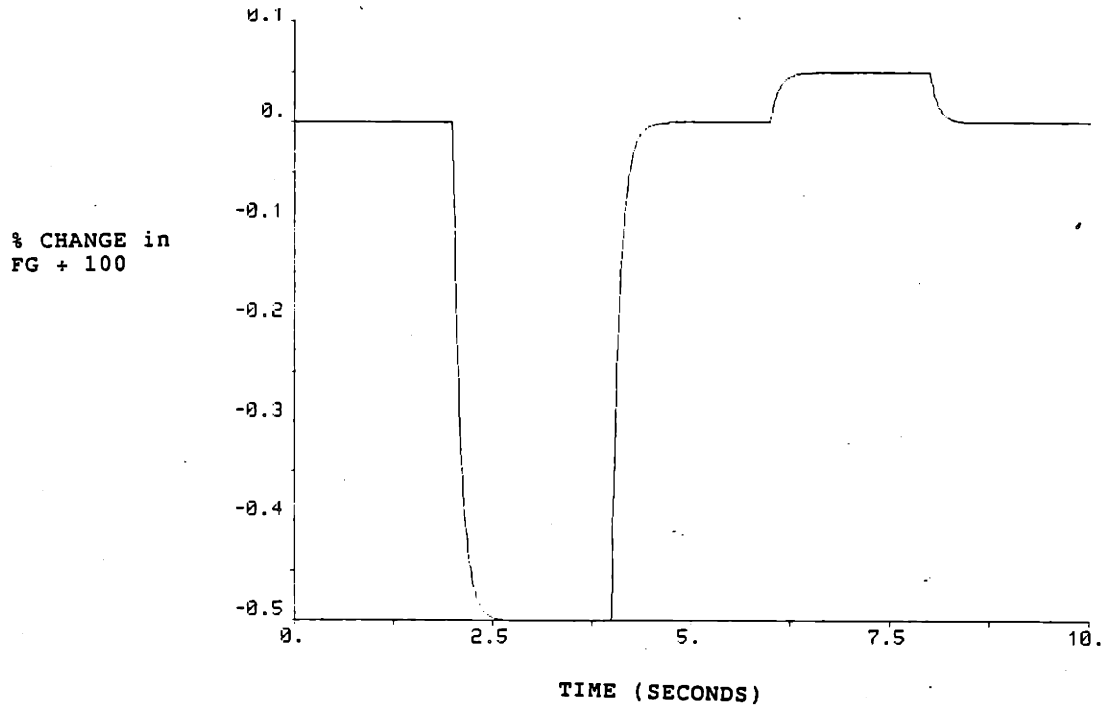

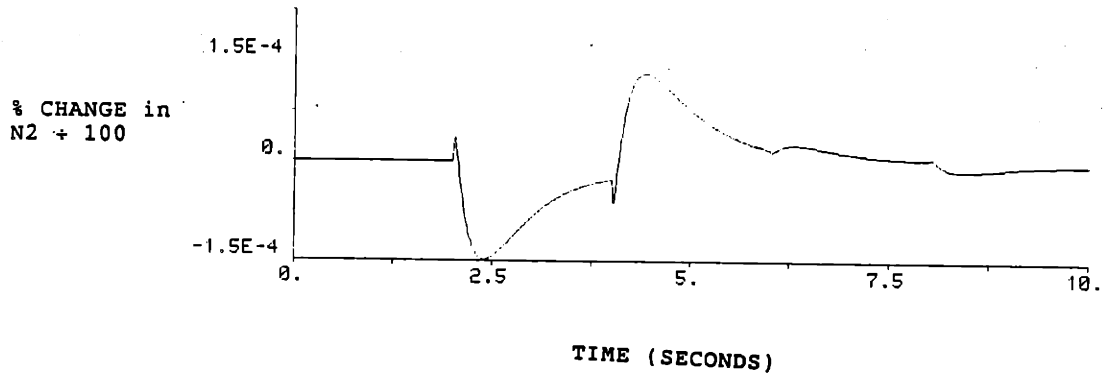

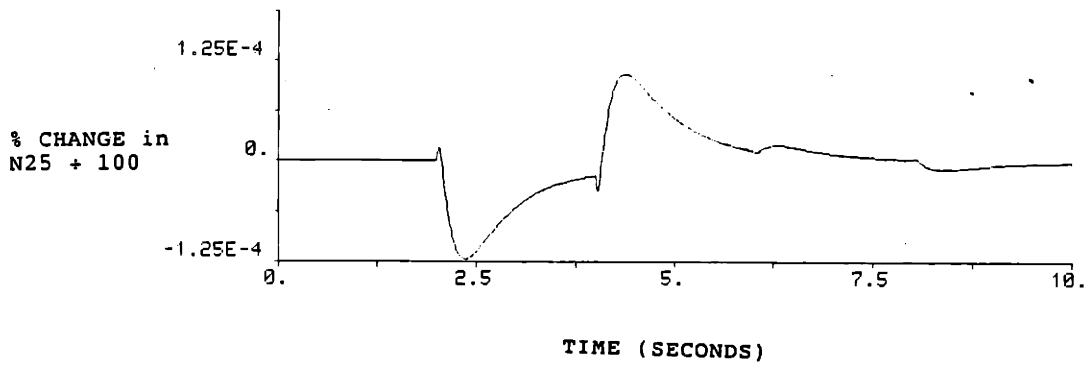

Figure 5.4-3
Output Responses of Linear Model - Second Design

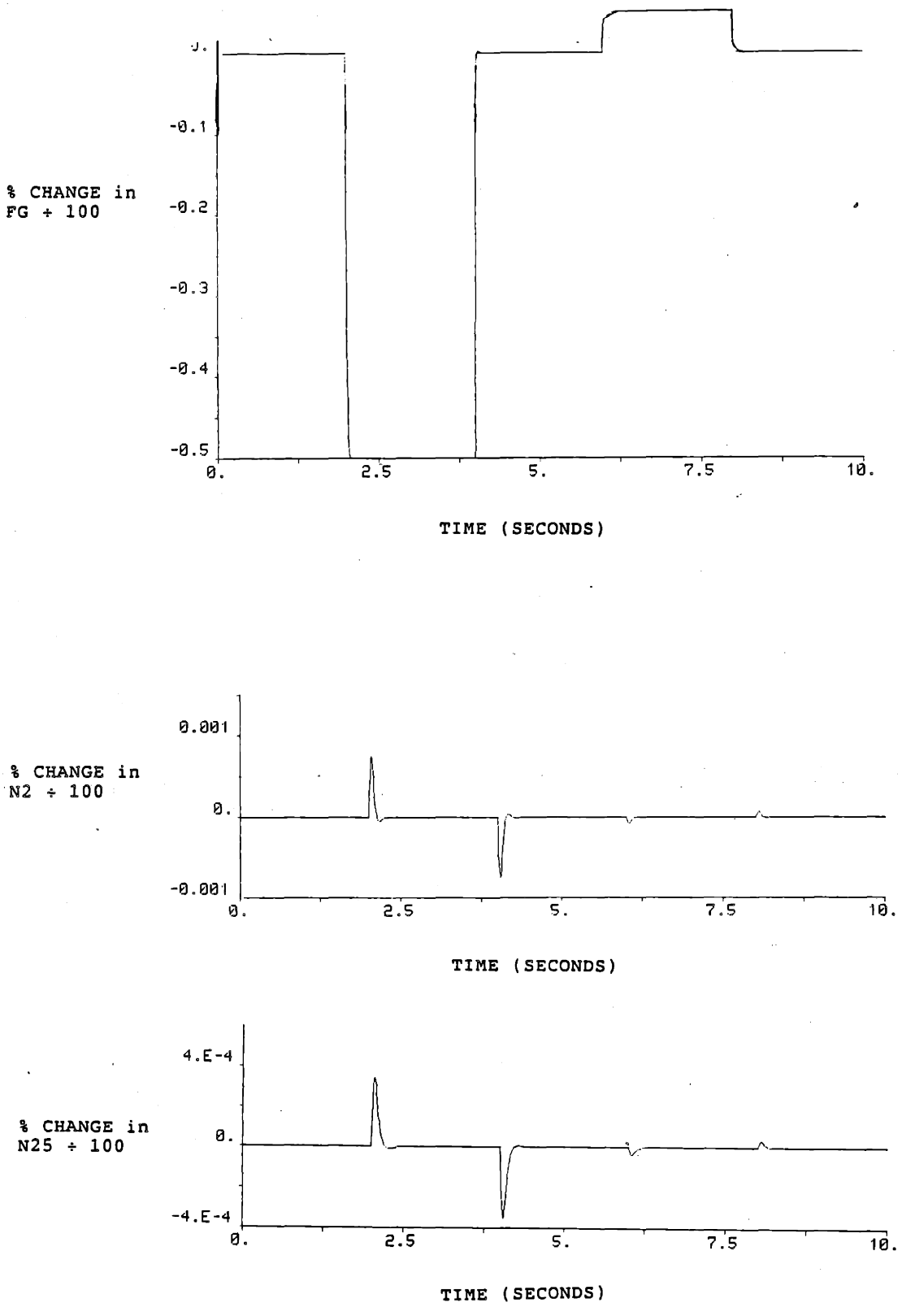

Figure 5.4-4
Output Responses of Linear Model - Third Design

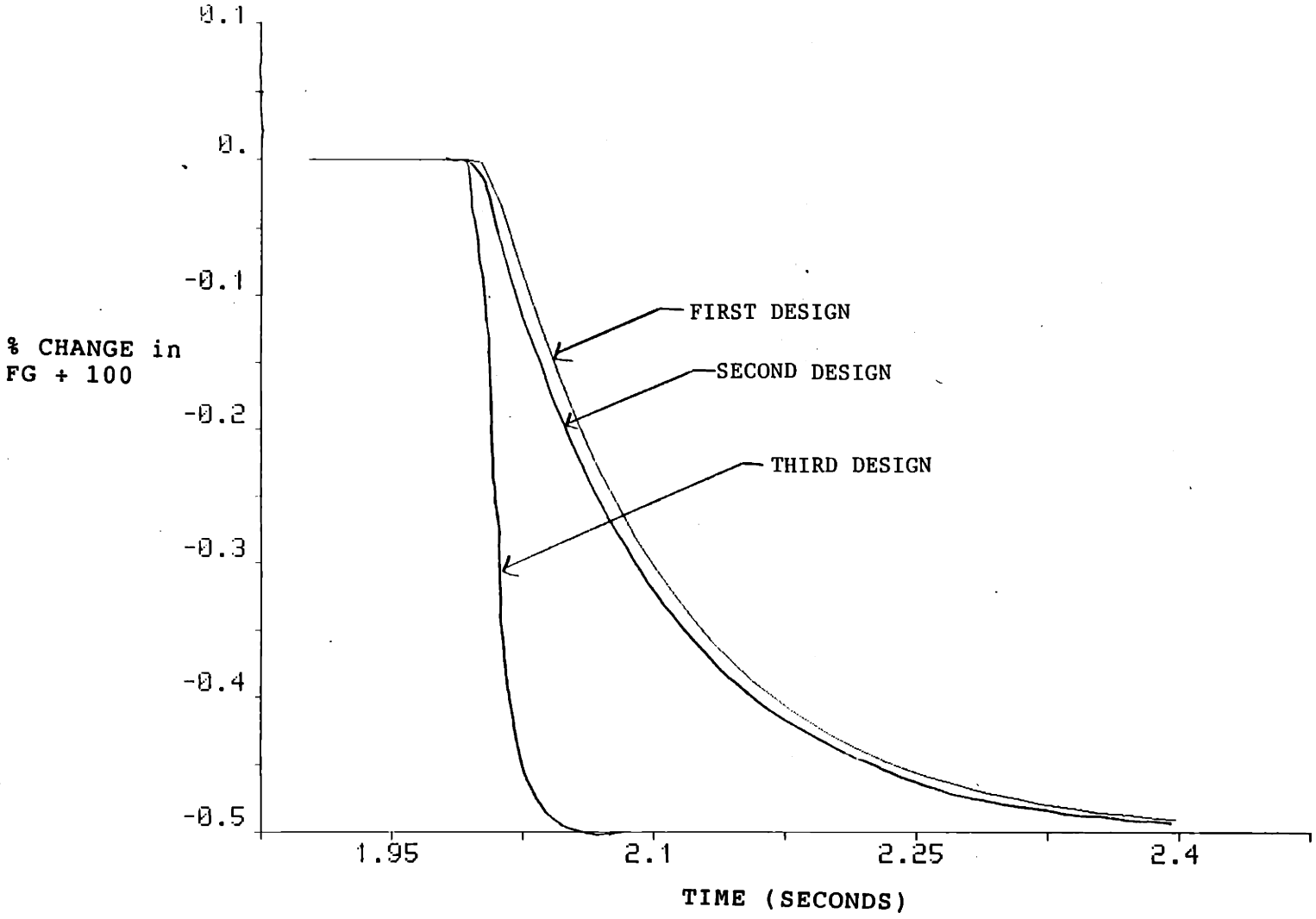

Figure 5.4-5
Comparison of Thrust Output Response of
Linear Model for all Three Designs

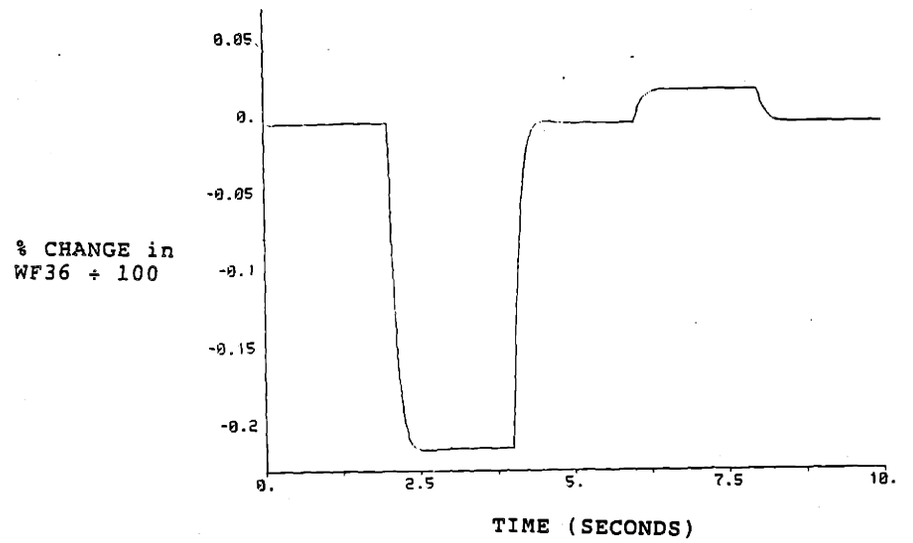

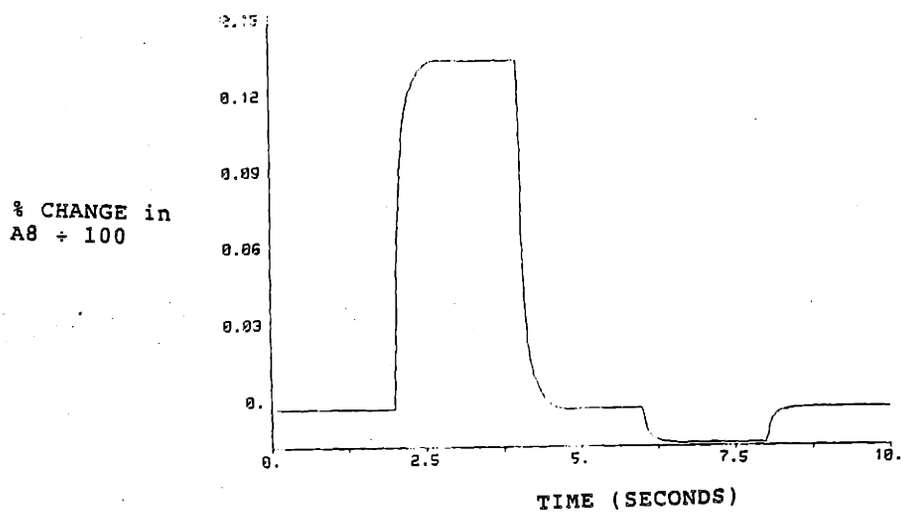

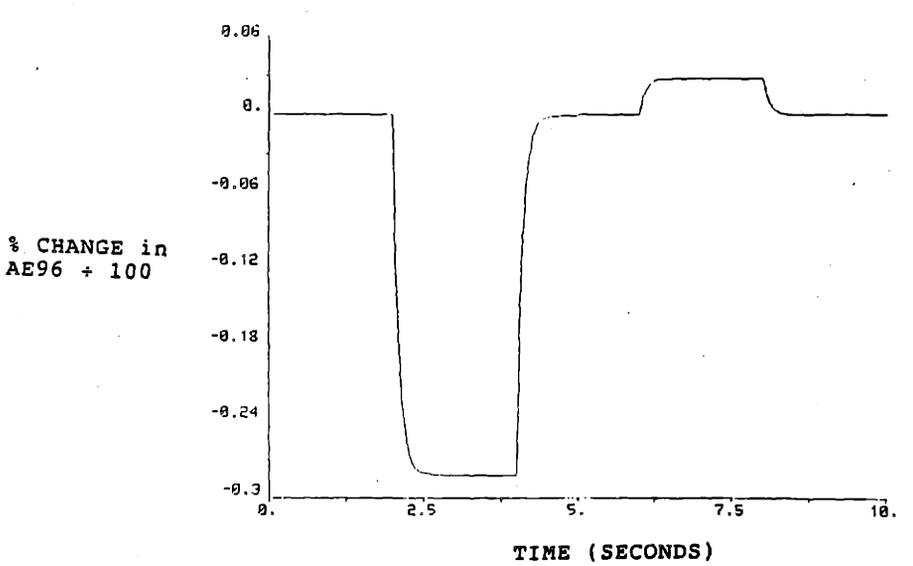

Figure 5.4-6
Response of Control Inputs for Linear Plant - First Design

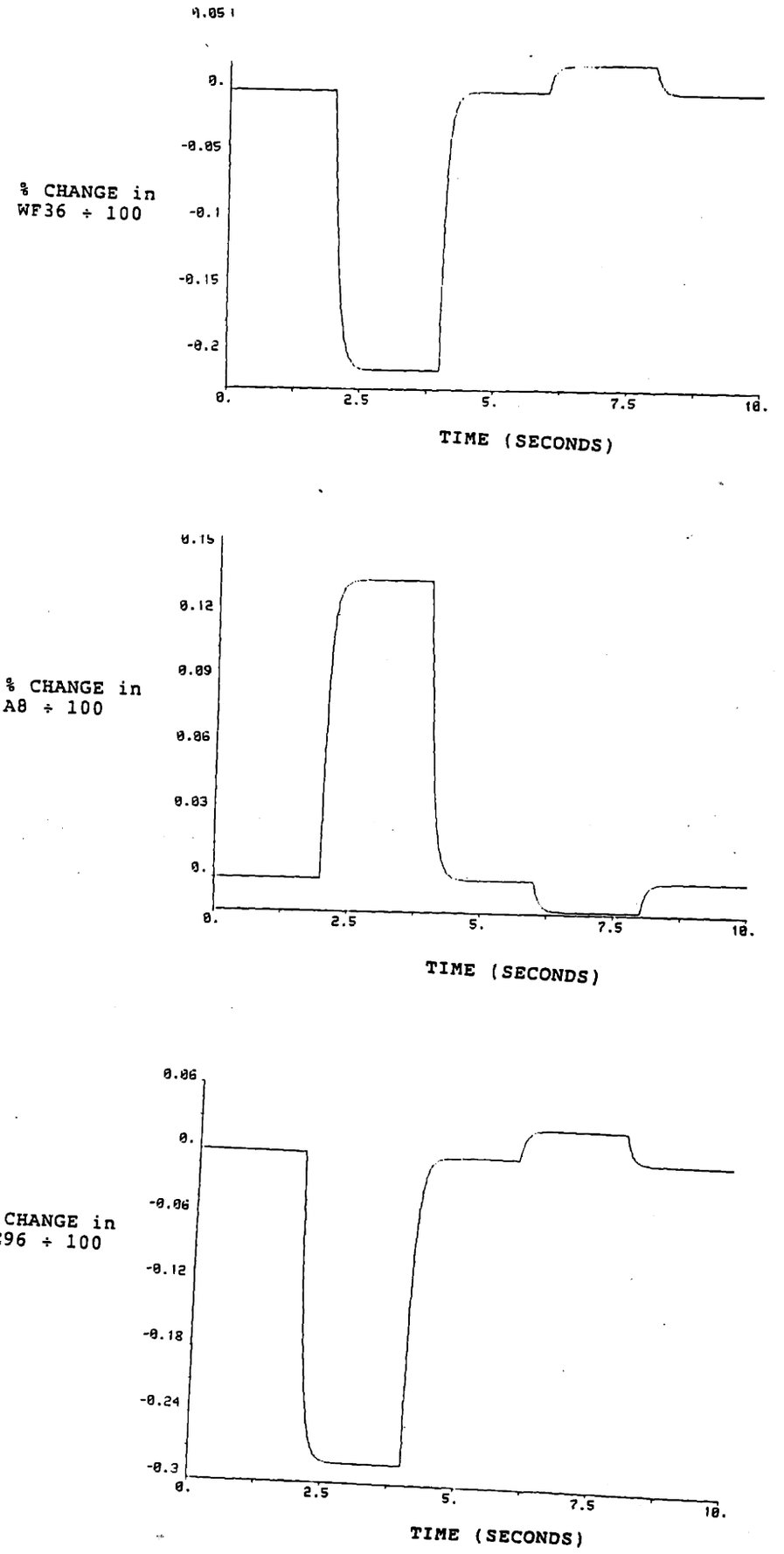

Figure 5.4-7
Response of Control Inputs for Linear Plant - Second Design

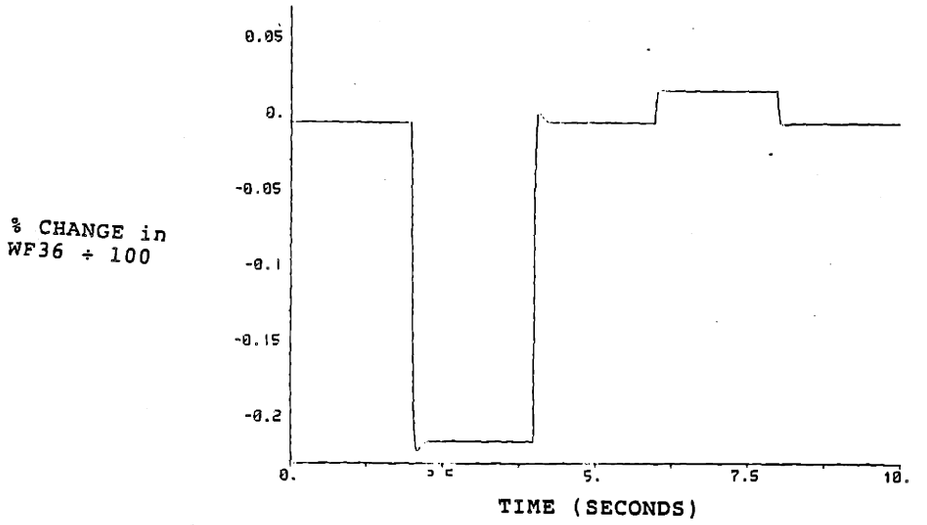

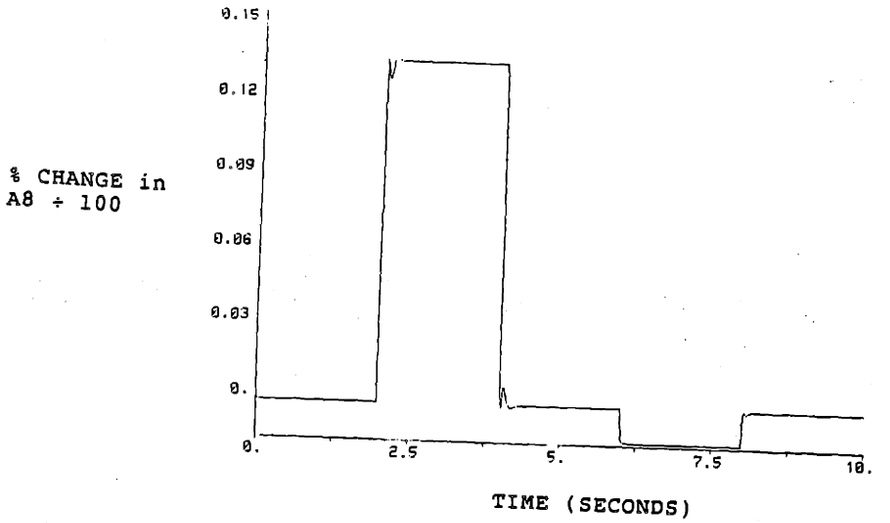

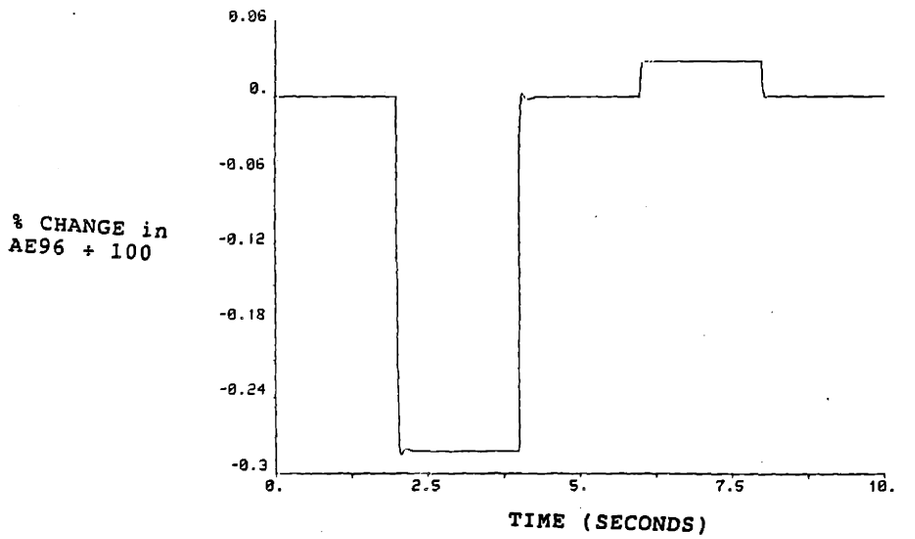

Figure 5.4-8
Response of Control Inputs for Linear Plant - Third Design

An important point to note here is that the simulations using the reduced linear plant do not provide any indication as to the status of the temperatures, pressures or stall margins of the actual plant. Since the plant model was reduced to the 3 x 3 system in section 3.3, the nonlinear simulations must be used to obtain this additional information.

5.4.2 NONLINEAR SIMULATIONS

The nonlinear plant was substituted in place of the linear model and the time simulations were repeated. The compensator states were initialized to provide the plant with the required inputs to establish an equilibrium at the desired operating point. For these simulations, the variables in the nonlinear model were all scaled using the physical maximum values.

The output response of the first design is shown in Figure 5.4-9. Notice that the command following for the rotor speeds and the thrust is good, but that the response time specification is not met. The thrust output requires approximately 1 second to settle to the final value. This is not a totally unexpected result since the linear model was simply an approximation of the nonlinear plant.

In rough terms, the response indicates that the closed loop dynamics of the nonlinear system are slower than those indicated in the linear model or that the commands to the

nonlinear plant occur in the "slow" directions of the frequency response curves presented in the previous section.

The response of the nonlinear plant to the commanded input using the second compensator is shown in Figure 5.4-10. As in the linear simulations, this design is slightly faster than the first, but still does not meet the response time specifications. Notice, also, that there does not appear to be a problem with overshoot or undershoot on any of the control inputs.

The output response of the third design is shown in Figure 5.4-11. The command following of this design is excellent and the response time specification has been met. In addition, the control variables, see Figure 5.4-12, are kept within the acceptable system bounds which indicates that there is no need for limit protection.

An expanded view of the Thrust output response is provided in Figure 5.4-13. This figure superimposes the response of all three nonlinear simulations at the first step change in commanded thrust. Notice that these simulations indicate that the engine thrust can be varied very rapidly (in less than 0.125 seconds with no actuators) while the speeds are held constant.

Finally, the turbine temperature, compressor pressure and stall margins are shown in Figure 5.4-14. These figures indicate that all of these parameters remain within the acceptable operating ranges for this system. If any of these parameters had exceeded the bounds of the system, then the

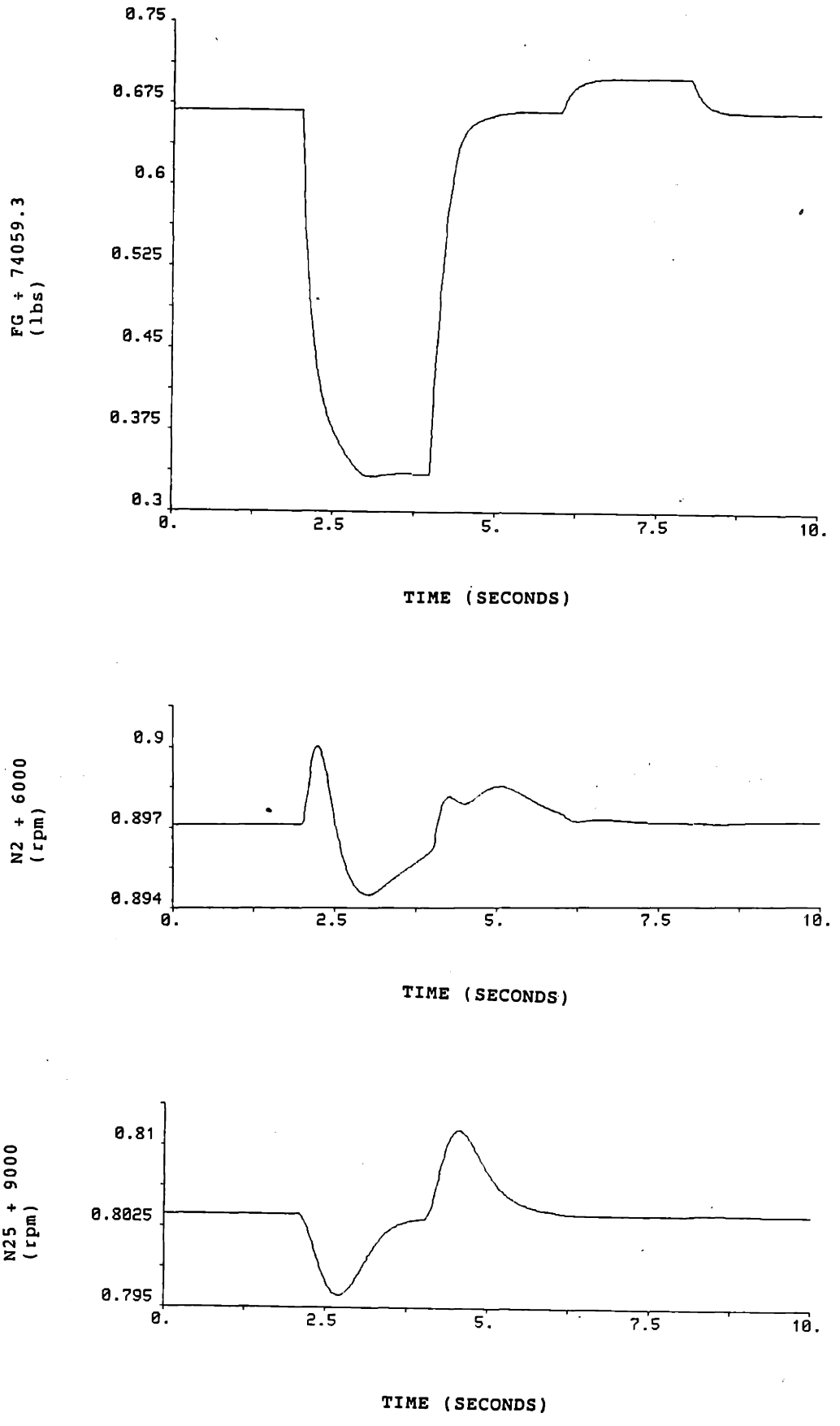

Figure 5.4-9
Output Responses of Nonlinear Model - First Design

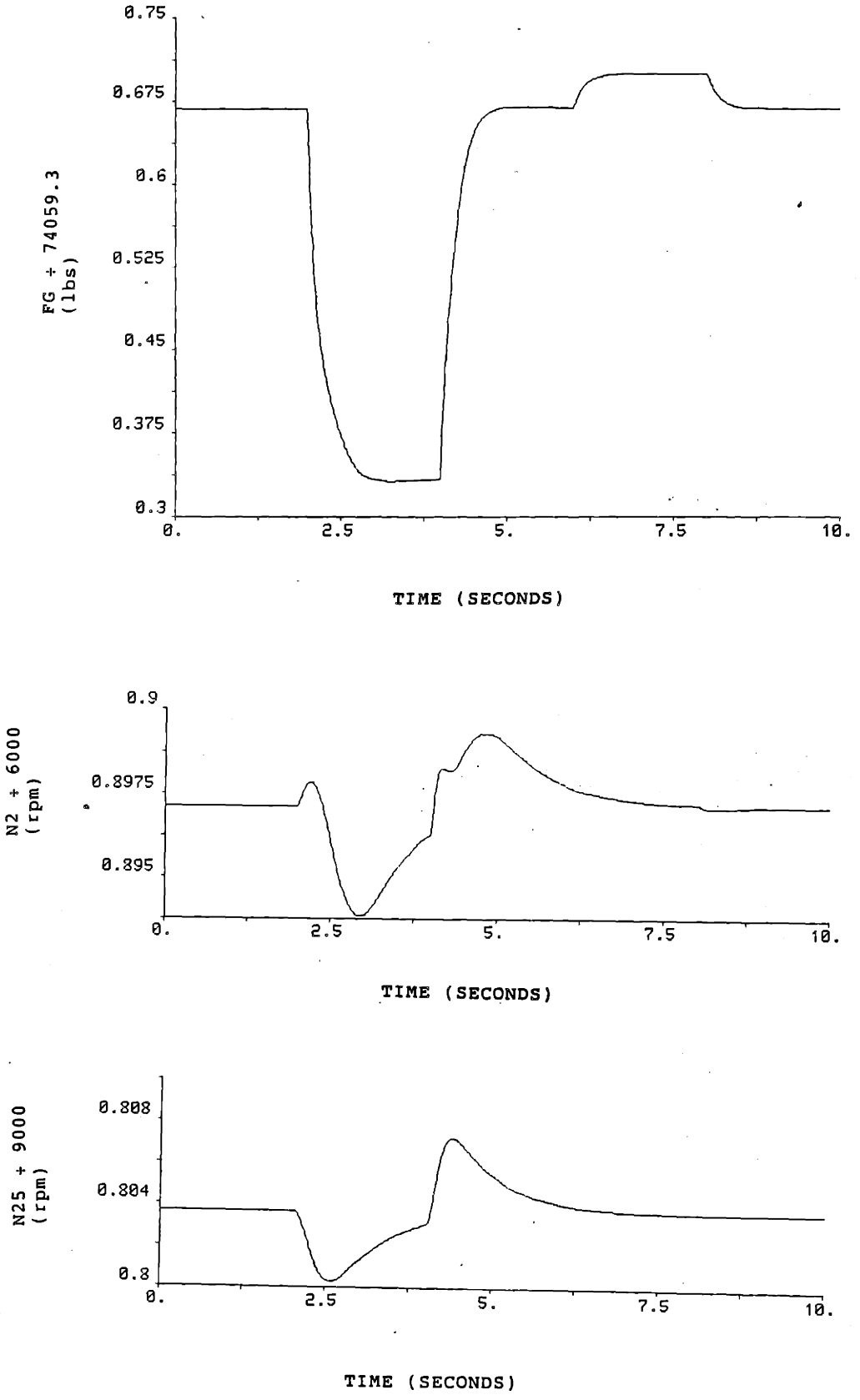

Figure 5.4-10
Output Responses of Nonlinear Model - Second Design

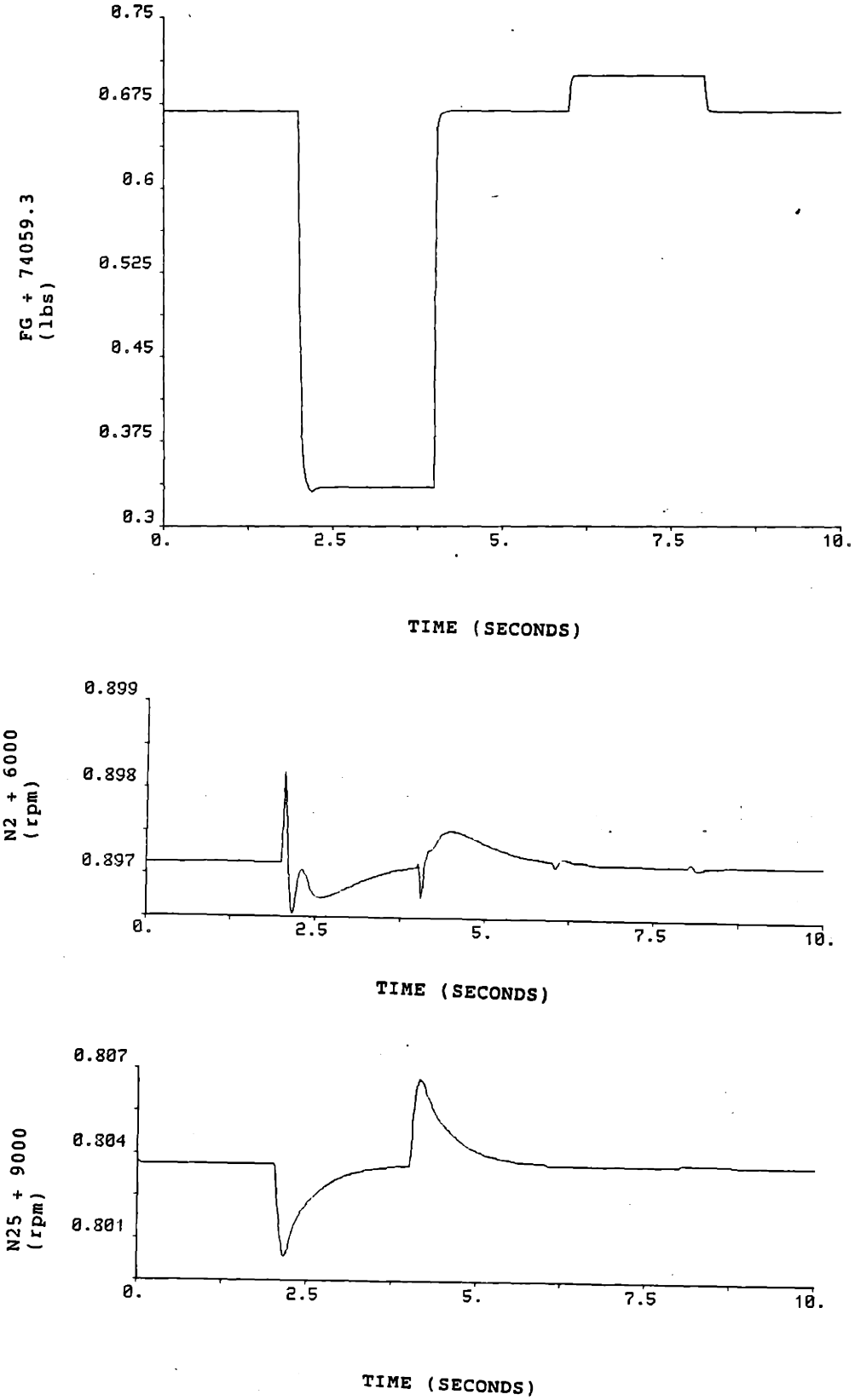

Figure 5.4-11
Output Responses of Nonlinear Model - Third Design

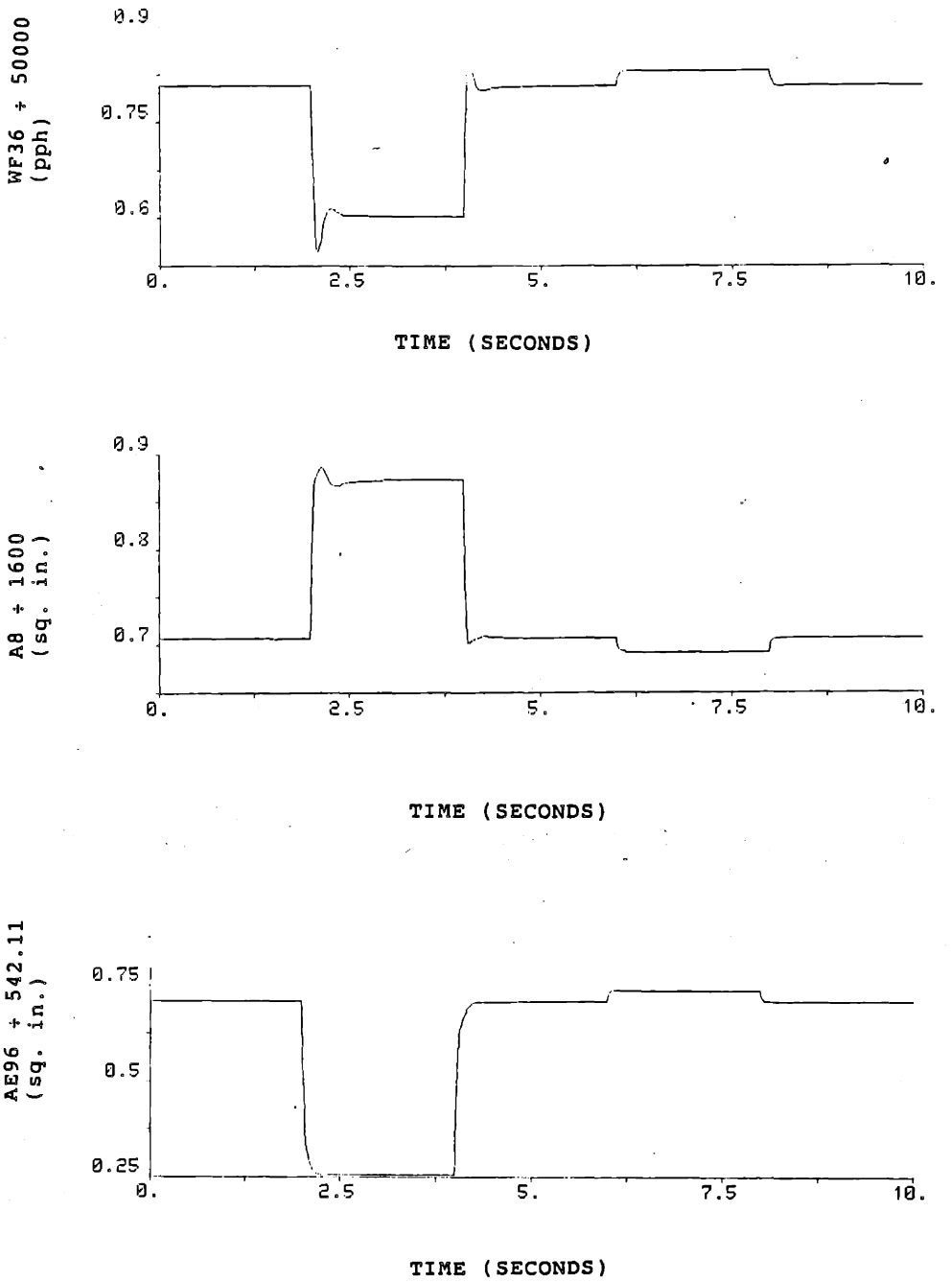

Figure 5.4-12
Response of Control Inputs for Nonlinear Plant - Third Design

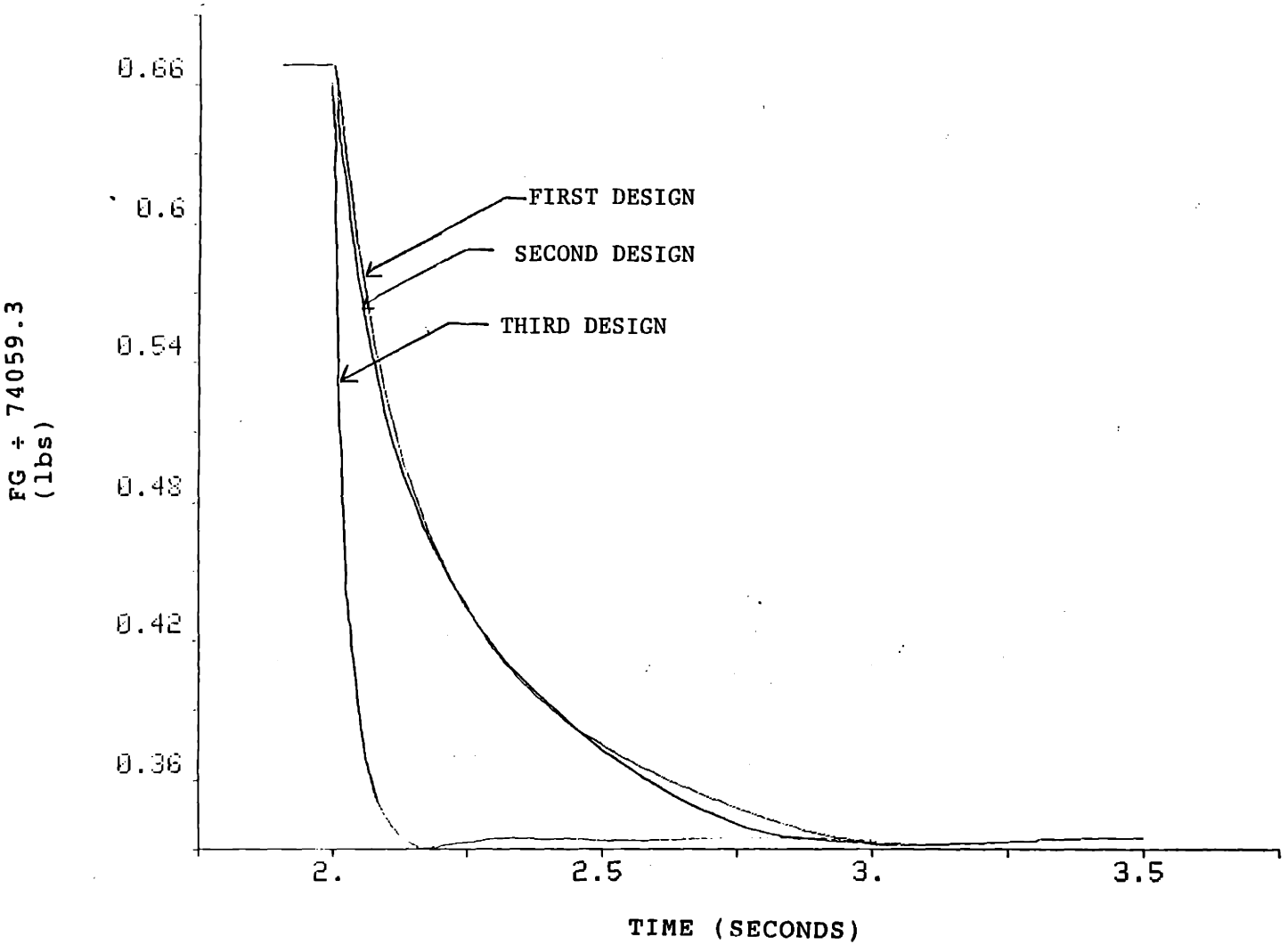

Figure 5.4-13
Comparison of Thrust Output Response of
Nonlinear Model for all Three Designs

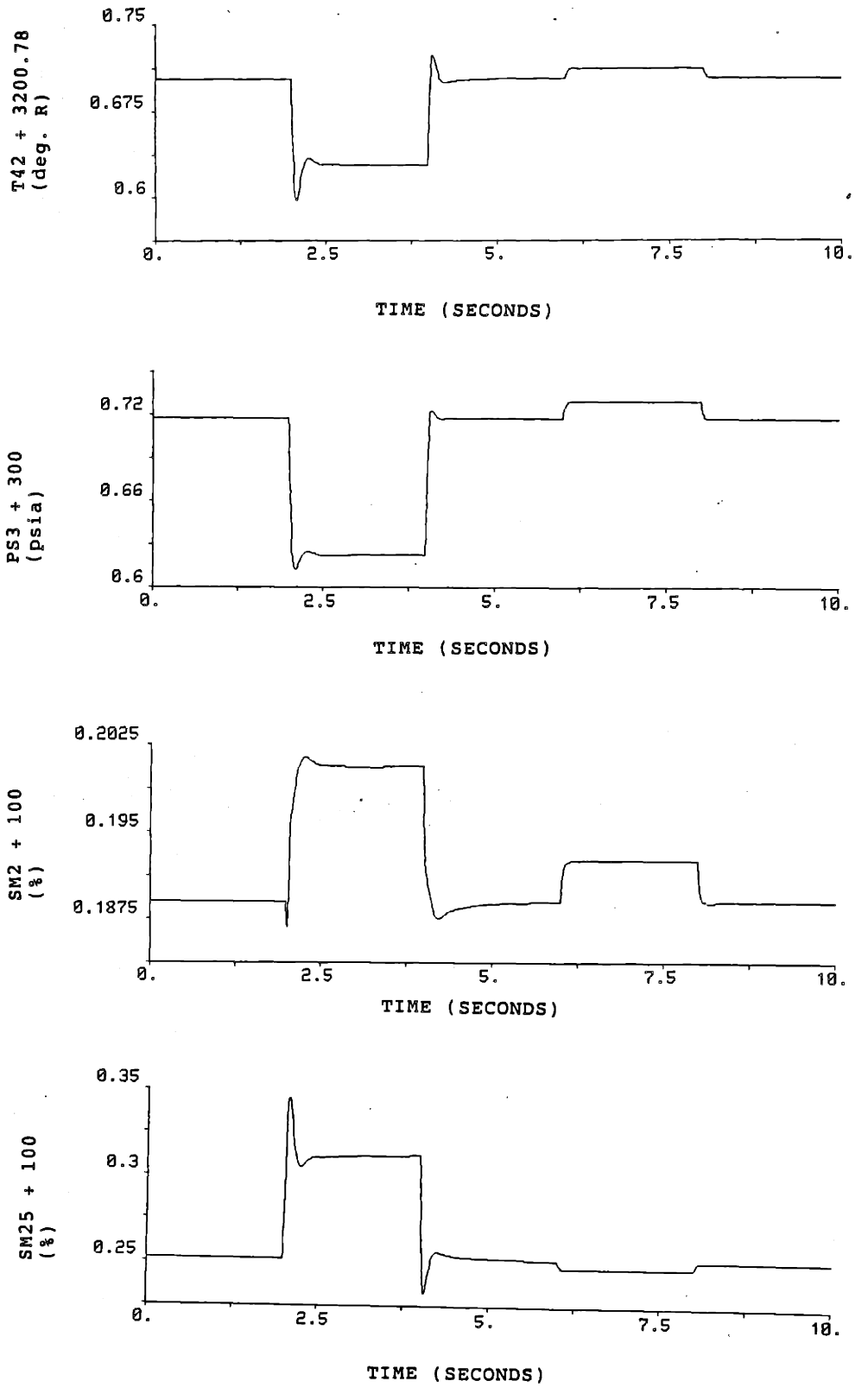

Figure 5.4-14
Response of Critical Engine Parameters During Nonlinear Simulation for Third Design

design process would simply be repeated; but the parameter which exceeded its limit would be included in the linear model. Once the 3 x 3 case shown here is applied, it is a straight forward procedure to increase the number of inputs and outputs.

5.5 POLES, ZEROS AND PRACTICAL IMPLEMENTATION

The poles and zeros for the above systems are presented in Tables 5.5-1 through 5.5-3. From these tables it is easily seen that the zeros of the compensator approach the poles of the linear plant - this is characteristic of this type of compensator. The numerical values of the matrices used in these simulations are given in the appendices.

The three design examples used were selected to illustrate another important aspect of the poles and zeros of the compensator. Notice that as the loop is taken from the partial recovery of the first design to the full recovery of the second design the closed loop poles move to higher frequencies. The response of each design is affected by the dominant poles and zeros of the system.

From Table 5.5-1, the dominant poles in the first design are the two complex pairs $-4.76 \pm j4.41$ and $-8.12 \pm j7.85$. These low frequency poles will limit the response time of the system since the original plant poles at -2.55 and -2.80 rad/sec are cancelled by the zeros of the compensator. Notice, also, that the complex pole pairs are critically

damped; another characteristic of using an LQG based design.

In order to achieve quicker response times of the system, the "slow" closed loop poles must be moved higher in frequency. Table 5.5-2 shows the poles and zeros of the system with a 10 rad/sec crossover which is recovered to 10 rad/sec. Notice that in the limit as the loop is fully recovered, the dominant poles become those of the target loop. In this design, the target loop had poles at 10 rad/sec. In addition to moving the dominant poles from 5 rad/sec to 10 rad/sec, the full recovery procedure has moved all of the poles out to higher frequencies. The high frequency pole created by the design procedure that was at -134 rad/sec is now at -13413 rad/sec. The very high frequency poles can be "dropped" using a technique which is shown in section 5.6.

Another practical issue involved in the recovery procedure is that as $\rho \to 0$, entries in the control gain matrix, $\underline{G}$, and in the $\underline{A}_c$ matrix of the compensator ($\underline{A}_c = \underline{A}_a - \underline{B}_a\underline{G} - \underline{H}\ \underline{C}_a$) become large. In most cases, the size of these entries may not be a problem. But, there are times when the size of the matrix entries causes computational problems when implemented on a computer with a fixed word length.

The third design illustrates a technique of overcoming the problem of large gains. This technique is to simply "over design" the target loop and then only partially recover. The poles and zeros of this design are shown in Table 5.5-3. Notice that in this design, the dominant closed

OPEN LOOP SYSTEM	COMPENSATOR (W/ INTEGRATORS)	CLOSED LOOP SYSTEM
$\{\underline{G}(s)\}$	$\{\underline{K}(s)\ \underline{I}/s\}$	$\{[\underline{I}+\underline{G}_a(s)\underline{K}(s)]^{-1}\underline{G}_a(s)\underline{K}(s)\}$
POLES	POLES	POLES
-2.55	-144.13	-134.1
-2.80	-13.11 $\pm$ j10.85	-10
	-9.76 $\pm$ j6.49	-10
* note:	0	-10
actuators and	0	-8.12 $\pm$ j7.85
sensors not used	0	-4.76 $\pm$ j4.41
in simulations.		-2.55
		-2.80
ZEROS	ZEROS	ZEROS
none	-2.55	-2.55
	-2.80	-2.80

Table 5.5-1
POLES AND ZEROS OF FIRST DESIGN

OPEN LOOP SYSTEM	COMPENSATOR (W/ INTEGRATORS)	CLOSED LOOP SYSTEM
$\{\underline{G}(s)\}$	$\{\underline{K}(s)\ \underline{I}/s\}$	$\{[\underline{I}+\underline{G}_a(s)\underline{K}(s)]^{-1}\underline{G}_a(s)\underline{K}(s)\}$
POLES	POLES	POLES
-2.55	-13423.0	-13413.0
-2.80	-85.0 $\pm$ j85.0	-80.0 $\pm$ j80.0
	-51.0 $\pm$ j50.0	-46.0 $\pm$ j46.0
* note:	0	-10
actuators and	0	-10
sensors not used	0	-10
in simulations.		-2.55
		-2.80
ZEROS	ZEROS	ZEROS
none	-2.55	-2.55
	-2.80	-2.80

Table 5.5-2
POLES AND ZEROS OF SECOND DESIGN

OPEN LOOP SYSTEM	COMPENSATOR (W/ INTEGRATORS)	CLOSED LOOP SYSTEM
$\{\underline{G}(s)\}$	$\{\underline{K}(s)\ \underline{I}/s\}$	$\{[\underline{I}+\underline{G}_a(s)\underline{K}(s)]^{-1}\underline{G}_a(s)\underline{K}(s)\}$
POLES	POLES	POLES
-2.55	-1441.3	-1341.3
-2.80	-93.5	-25.3 $\pm$ j25.2
	-75.3 $\pm$ j25.8	-14.6 $\pm$ j14.5
* note:	-35.7	-100
actuators and	0	-100
sensors not used	0	-100
in simulations.	0	-2.55
		-2.80
ZEROS	ZEROS	ZEROS
none	-2.55	-2.55
	-2.80	-2.80

Table 5.5-3
POLES AND ZEROS OF THIRD DESIGN

loop poles are the complex conjugate pair at -14.6 $\pm$ j14.5 rad/sec. The highest frequency pole created is at -1341 rad/sec and the target loop poles are at -100 rad/sec. This loop will obviously be faster than either of the previous two designs (this can be seen from the time simulations presented in section 5.4).

The third design also has smaller entries in the $\underline{A}_c$ and $\underline{G}$ matrices than the second design (see Appendix B for the numerical values of the matrices used). Notice that the zeros of the third compensator cancel with the poles of the plant and, even though the loop was not fully recovered, the complex pole pairs are still critically damped. The one draw back to this partial recovery technique is that the properties listed in section 4.2.1 are weakened by not recovering fully. However, by examining the appropriate

singular value frequency responses, the designer can still decide if the design is adequate. In addition, those properties apply to linear designs and when the nonlinear plant is placed in the loop these properties are not fully guaranteed. It is still up to the designer to analyze the appropriate simulation results and decide if the design meets the specifications.

5.6 REDUCED COMPENSATOR

As metioned previously, the recovery procedure creates some high frequency poles in the closed loop response. Typically these poles are well above the required crossover and do not contribute significantly to the response of the system. Since these poles are not required by the system, it is advantageous to omit them from the final compensator design.

There are two basic reasons why the designer may wish to eliminate these high frequency poles: 1) the overall order of the compensator would be reduced, requiring fewer integrator stages to implement and hence a lower cost and 2) the implementation of the compensator on a computer would be easier and more efficient (i.e., less chance of numerical instability) if the high frequency terms were eliminated.

One such technique was demonstrated by Kappos [4, 39] on a linear design for the F100 engine. This same technique is valid for this research using the nonlinear model of the GE21

engine.

The technique centers on the residue method of expansion of multivariable systems. The transfer matrix of the compensator is expanded as

$$\underline{K}(s)=\hat{\sum}_{i=1} (\underline{R}_i/\lambda_i)/((s/\lambda_i)-1) \qquad (5.1)$$

where

$$\underline{R}_i = \underline{C}_a\underline{u}_i\underline{v}^T{}_i\underline{B} \qquad (5.2)$$

and the vectors $\underline{u}_i$ and $\underline{v}_i$ are the right and left eigenvectors of the compensator $\underline{A}$ matrix and the λ_i are distinct eigenvalues of this matrix.

The main purpose at this stage is to transform the original $\underline{A}$, $\underline{B}$, $\underline{C}$ and $\underline{D}$ matrices of the compensator into another set of system matrices $\underline{F}$, $\underline{G}$, $\underline{H}$ and $\underline{J}$ which describe a lower order "equivalent" compensator. The procedure for reducing the compensator is described below:

I) Expand the Compensator TFM into the residue matrix sum described in equation (5.1) and find the magnitude of the residue term (any norm can be used). Based on the crossover specifications and the magnitude of the residues, decide which poles can be eliminated. The reduced model has the remaining eigenvalues of the original $\underline{A}$ matrix, arranged in a suitable order $[\lambda_1, \ldots, \lambda_r]$.

II) Define a transformation matrix

$$\underline{T} = \begin{bmatrix} \underline{T}_1 & & \underline{0} \\ & \ddots & \\ \underline{0} & & \underline{T}_j \end{bmatrix} \qquad (5.3)$$

where

$\underline{T}_k = 1$ for each real eigenvalue retained

$$\underline{T}_k = \begin{bmatrix} 1/2 & -j/2 \\ 1/2 & j/2 \end{bmatrix}$$ for each complex pair of eigenvalues retained.

and $\dim(\underline{T})=r$.

III) Compute a matrix $\underline{K}$ as

$$\underline{K} \equiv \left(\underline{T}^{-1}\right) \begin{bmatrix} \underline{v}_1^T \\ \cdot \\ \cdot \\ \underline{v}_r^T \end{bmatrix} \qquad (5.4)$$

and a matrix $\underline{M}$ as

$$\underline{M} \equiv [\underline{u}_1 \; . \; . \; . \; \underline{u}_r] \; \underline{T} \qquad (5.5)$$

with $\underline{u}_i$ and $\underline{v}_i$ as define in equation (5.2).

IV) Compute the reduced state-space matrices as

$$\begin{aligned} \underline{F} &= \underline{K} \; \underline{A} \; \underline{M} \\ \underline{G} &= \underline{K} \; \underline{B} \\ \underline{H} &= \underline{C} \; \underline{M} \\ \underline{J} &= \sum_{i=1}^{n} \underline{R}_i/(-\lambda_i) \end{aligned} \qquad (5.6)$$

V) Plot the singular values vs frequency of the reduced model and compare them with the original model. If the reduced model is not acceptable, redefine the set of eigenvalues to be retained and repeat the procedure.

Note that this transformation will provide a state-space description for the reduced order compensator and that the $\underline{F}$, $\underline{G}$, $\underline{H}$ and $\underline{J}$ matrices all contain real elements (assuming that the original $\underline{A}$, $\underline{B}$, $\underline{C}$ and $\underline{D}$ matrices were real).

5.6.1 REDUCED COMPENSATOR EXAMPLE

The above procedure was applied to the compensator

derived for the third design. The residues computed are presented in Table 5.6-1. From this table, it appears that only the pole at 1441 rad/sec can be easily dropped. This pole was dropped and the reduced state-space matrices were computed and substituted in place of the original matrices. The frequency response of the compensator and the open loop system are shown in Figures 5.6-1 and 5.6-2.

EIGENVALUE	$\|\| \underline{R}_i \|\| / \|\lambda_i\|$ *
-1441.3	0.0694
-93.5	1.5889
-75.3 + j25.8	1.9350
-75.3 - j25.8	1.9350
-35.7	1.6557

Table 5.6-1
Eigenvalues and Residue Norms for Third Compensator

* Norm scaled by 1000. Free integrator poles not included.

There is no discernable difference between these two responses and those shown in Figures 5.3-11 and 5.3-7. This indicates that this pole did not contribute very strongly to the response of the compensator. The reduced compensator was then substituted for the original compensator in the nonlinear simulations. The results of the nonlinear simulations are shown in Figures 5.6-3 and 5.6-4. Again, there is no discernable difference between the response of the system using the reduced order compensator and that using the original compensator.

This example demonstrates that the method used by Kappos

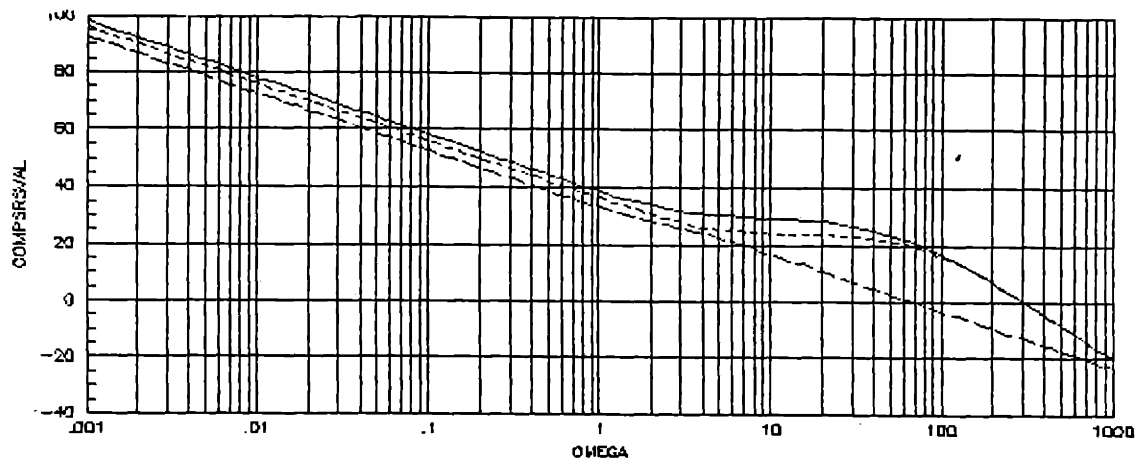

Figure 5.6-1
Frequency Response of Reduced Compensator, $\underline{K}_r(s)\underline{I}/s$

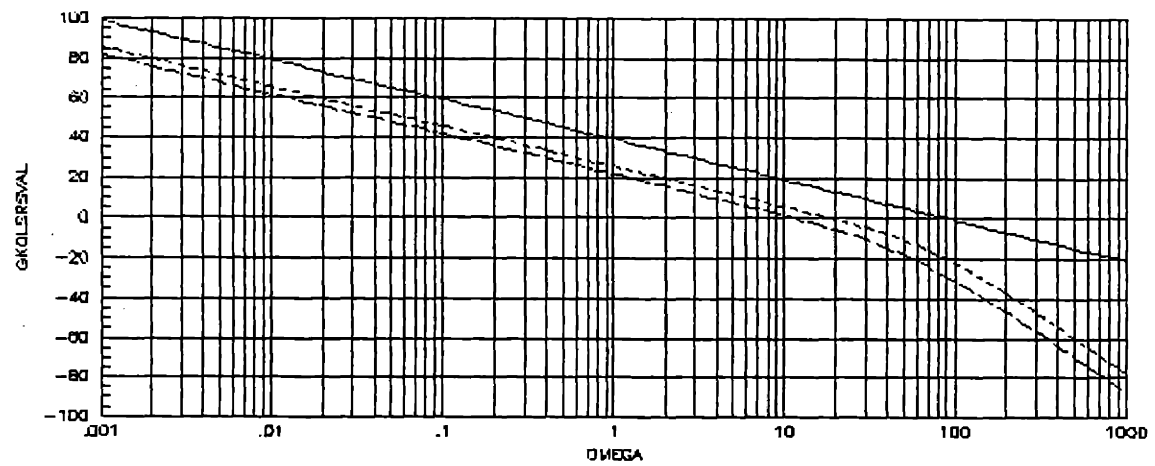

Figure 5.6-2
Frequency Response of $\underline{G}_a(s)\underline{K}_r(s)$

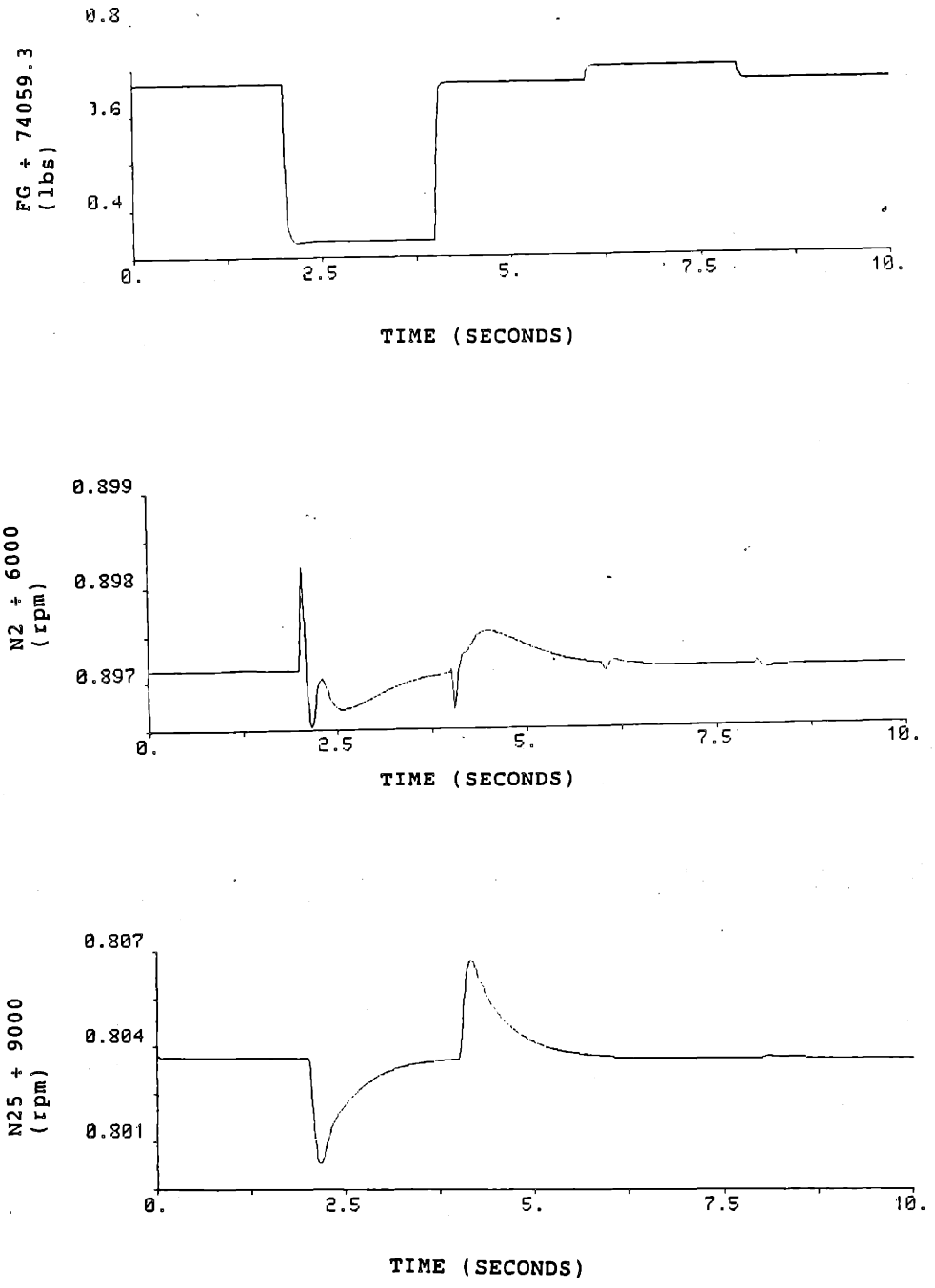

Figure 5.6-3
Output Response of Nonlinear Model Using Reduced Compensator

in [4] will extend to use in the nonlinear designs. For a more detailed description of this reduction technique see [39].

5.7 RESPONSE TO COMMANDS IN DIFFERENT DIRECTIONS

The main purpose of the compensator designs presented in the previous sections was to rapidly vary the thrust output of the engine while holding the rotor speeds constant. However, the compensators could be used to control the engine when commands in different directions are applied.

Section 3.6 presented a discussion of the plant behavior at steady state. From this discussion, there are basically three directions of interest. These are:

1. N2, N25 and FG move in the same direction.
2. N2 and N25 move in the same direction but FG moves in the opposite direction from the speeds.
3. N2 and N25 move in opposite directions.

To complete the discussion of the compensator performance, a few sample trials, obtained by providing commands in different directions, were run.

There are a few issues to keep in mind when applying the compensators to command the speeds to change. First, recall that the bandwith of the control loop for the third design was pushed to around 14 rad/sec. This loop is rather fast for controlling the low speed inertia terms in the jet engine response. Typically, spinning the core or fan speed up or

down requires on the order of 1.8 to 2.5 seconds. This would imply that there will be significant overshoot in the response of the control system due to the fact that the compensator is responding very quickly to changes in the system outputs.

Since the loop bandwith of the third design is most likely too fast for the control of the rotor speeds, one would expect the first design to be more appropriate. The bandwith of the first loop is around 3 rad/sec, therefore the overshoot on the control inputs should be less than that observed using the third design.

The output response, using the third (reduced) compensator, to a step input which commanded N2, N25 and FG to decrease is presented in Figure 5.7-1. The command following is good and the thrust decrease is fairly quick, though not as rapid or as smooth as in Figure 5.4-11. The response of the control inputs for this simulation are shown in Figure 5.7-1. Comparing this to Figure 5.4-12, we notice significant overshoot on the fuel and outer nozzle control inputs. This type of response is generally not desireable since it places additional stress on the physical actuators used to supply these inputs.

Using the reduced compensator, N2 and N25 could not be commanded in opposite directions since the response of the control inputs caused the model of the engine to stall. For this case, limits on the inputs would be needed to prevent stall.

The fan speed and thrust could be commanded to decrease while the core speed was held constant without using limits on the control inputs. The output response for this case is shown in Figure 5.7-3. The response of the control inputs to this command are shown in Figure 5.7-4. Again, there is significant overshoot on all the control inputs.

An attempt to move N2 and N25 in one direction while moving FG in the opposite direction using the reduced compensator also caused the engine model to stall. This was again due to the rapid response and unacceptable overshoot on the control inputs.

The first (slow) compensator was then substituted in place of the reduced compensator and commands in the different directions were applied. Figure 5.7-5 displays the response of the plant outputs when N2, N25 and FG are all commanded to decrease. The control responses to this command are shown in Figure 5.7-6. Notice that there is very little overshoot on the controls and that the thrust still reaches the final value in approximately 1 second.

The command to increase N2 and N25 and decrease FG was then applied to the system using the First compensator and the output response is presented in Figure 5.7-7. The response of the control inputs to this command are shown in Figure 5.7-8. Notice, again, that the command following is very good and that there is very little overshoot on the control inputs.

Finally, the command to increase N2 and FG but decrease

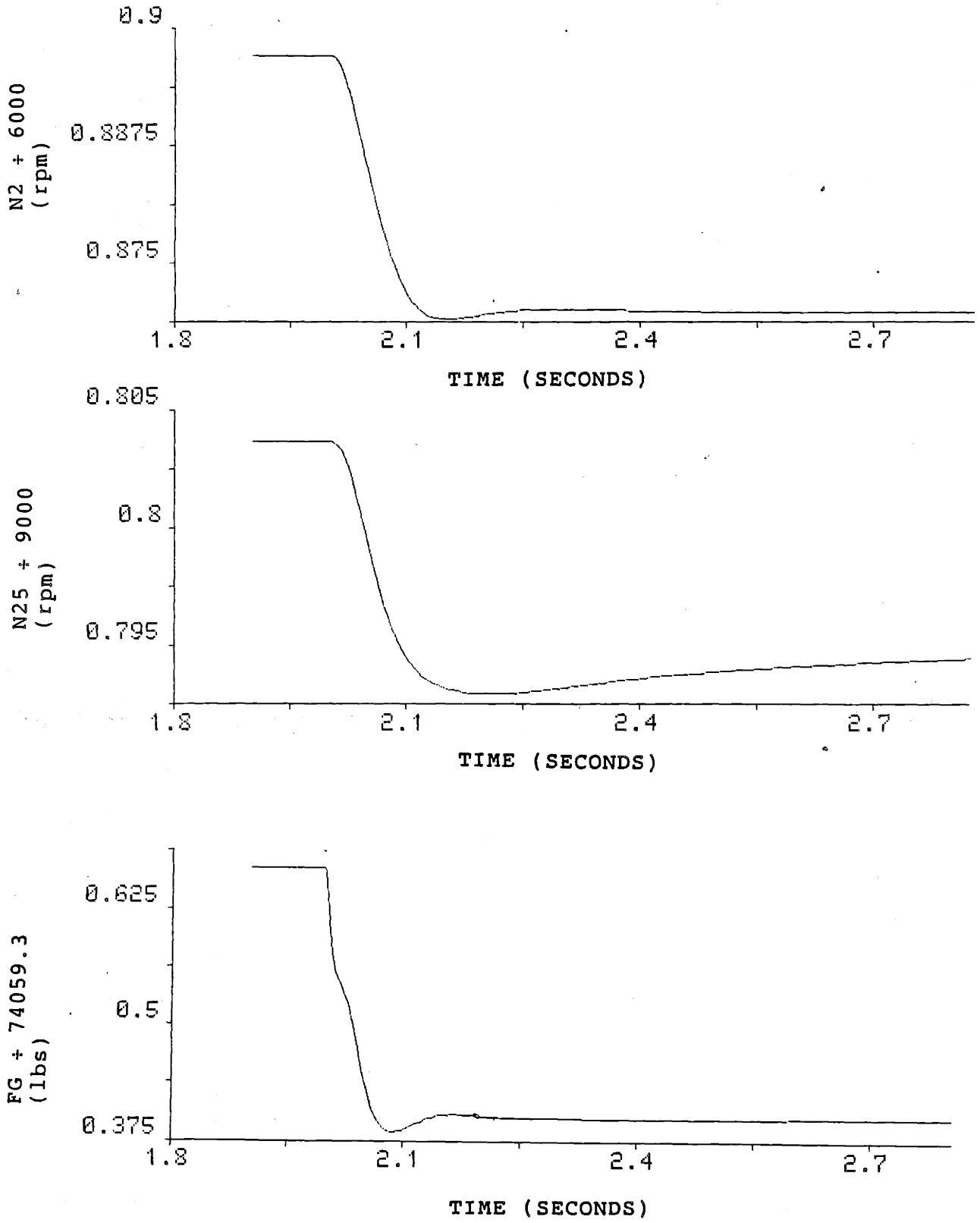

Figure 5.7-1
Output Response to Step Decrease in N2, N25 and FG
using the Reduced Compensator

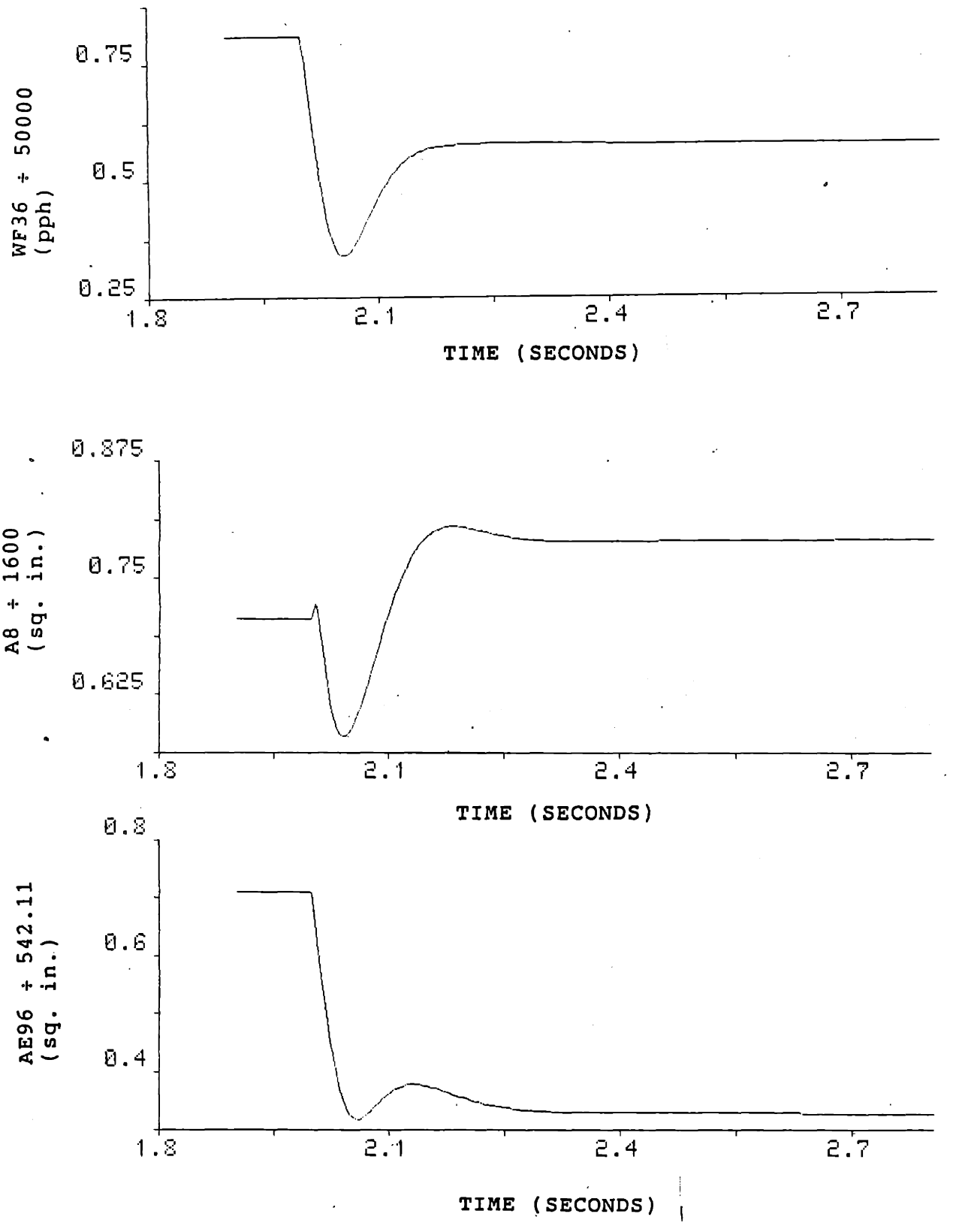

Figure 5.7-2
Control Input Response to Step Decrease in
N2, N25 and FG using the Reduced Compensator

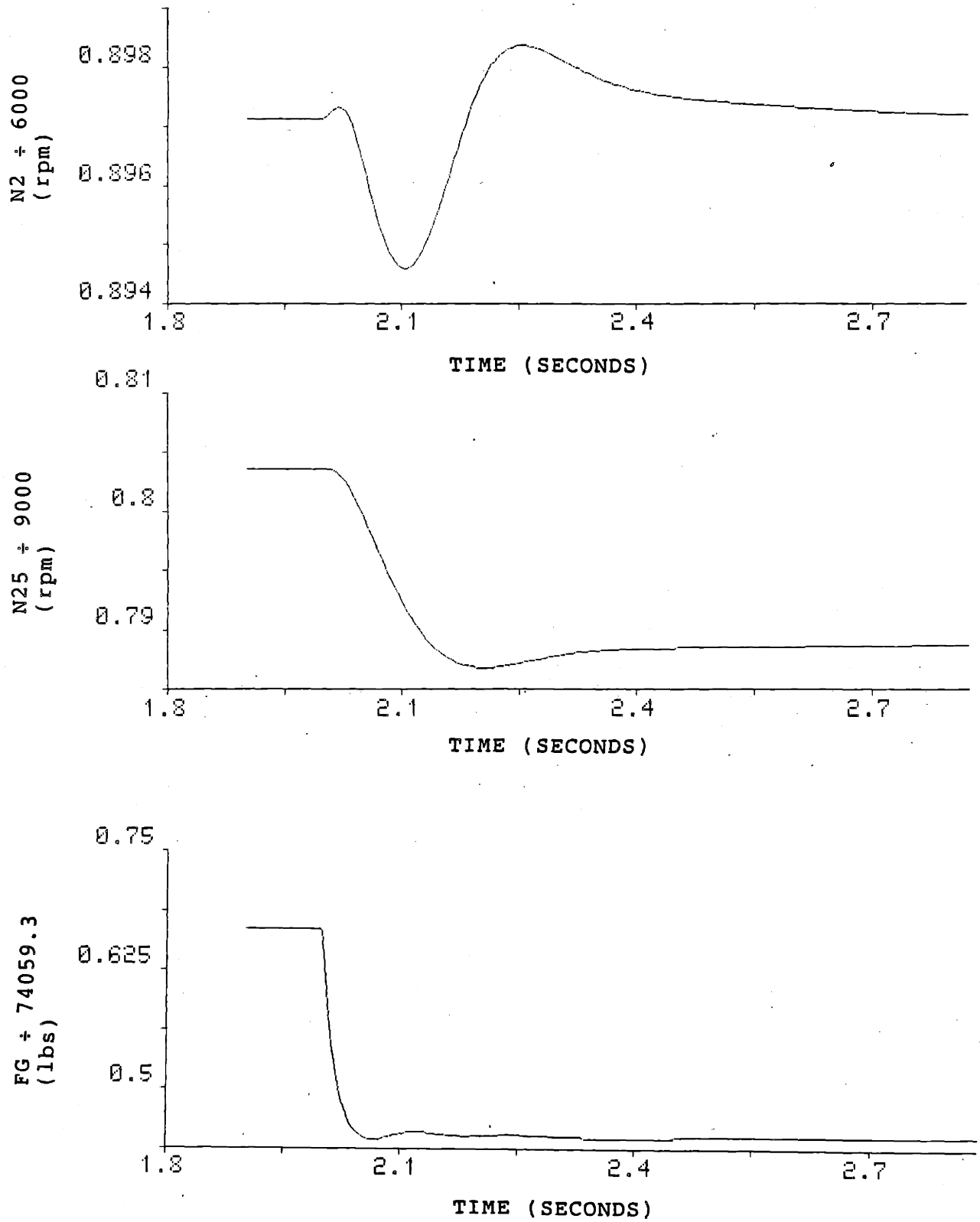

Figure 5.7-3
Output Response to Step Decrease in N25 and FG
with N2 Held Constant using the Reduced Compensator

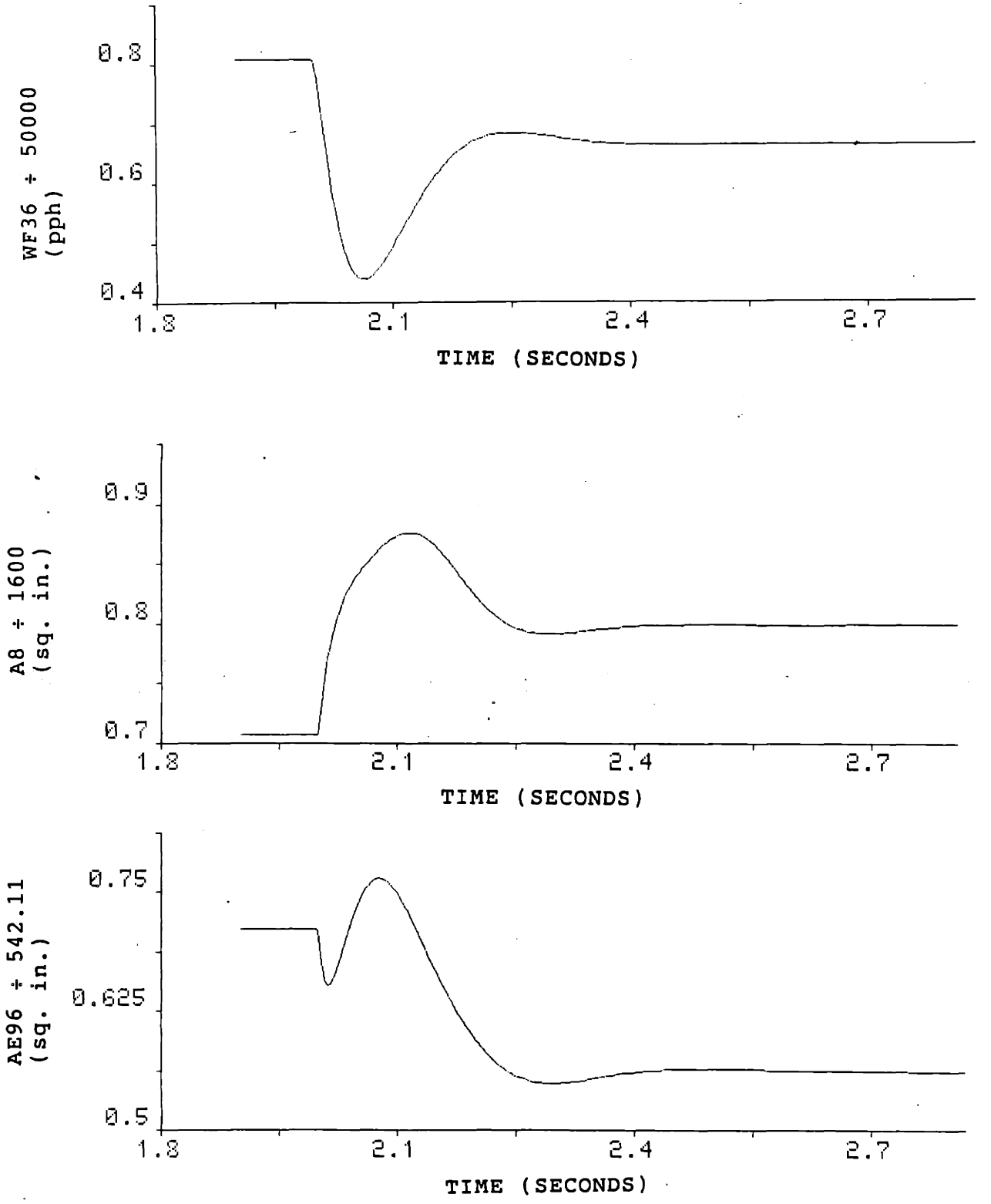

Figure 5.7-4
Control Input Response to Step Decrease in N25 and FG
with N2 Held Constant using the Reduced Compensator

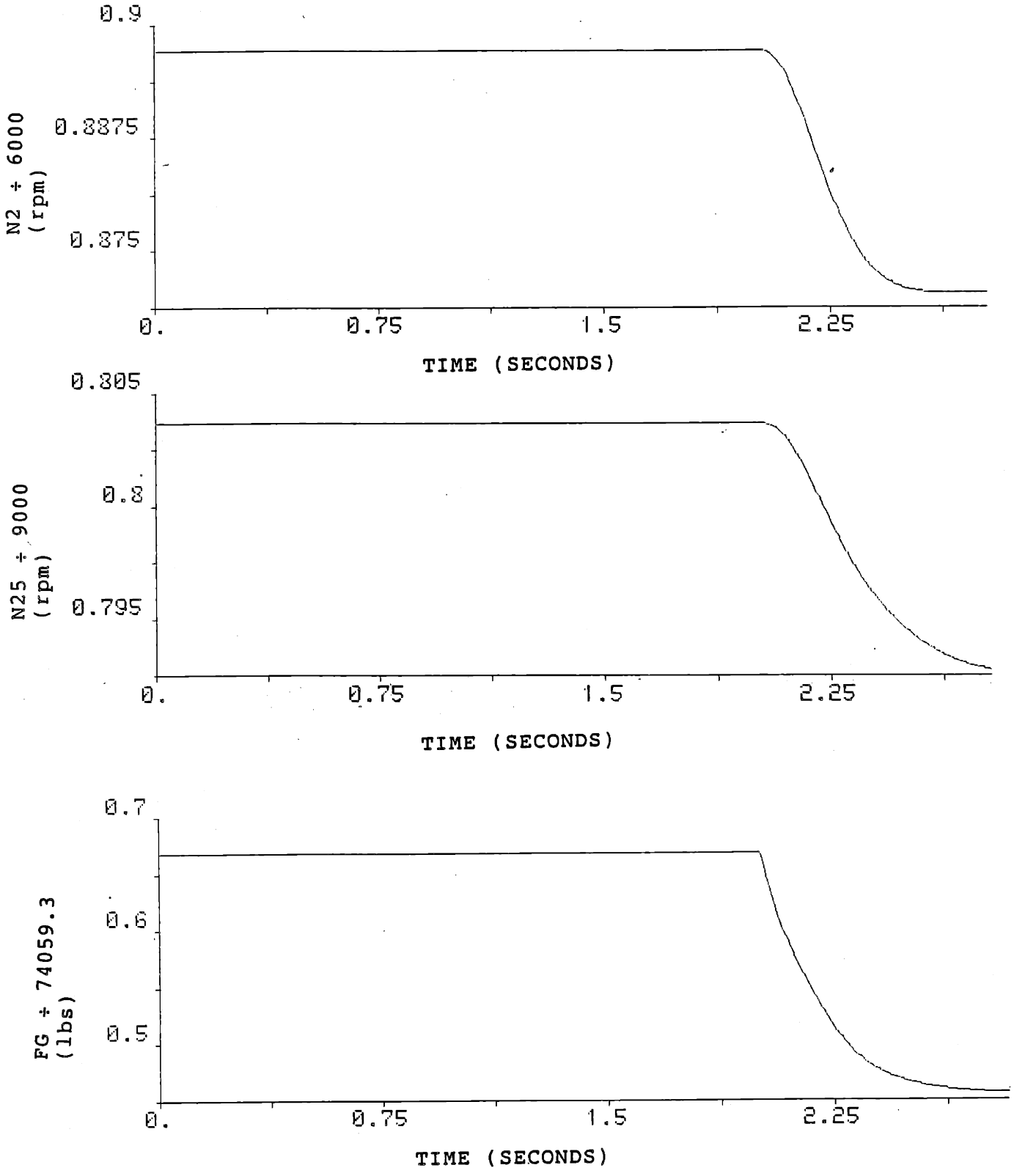

Figure 5.7-5
Output Response to Step Decrease in N2, N25 and FG
using the First Compensator

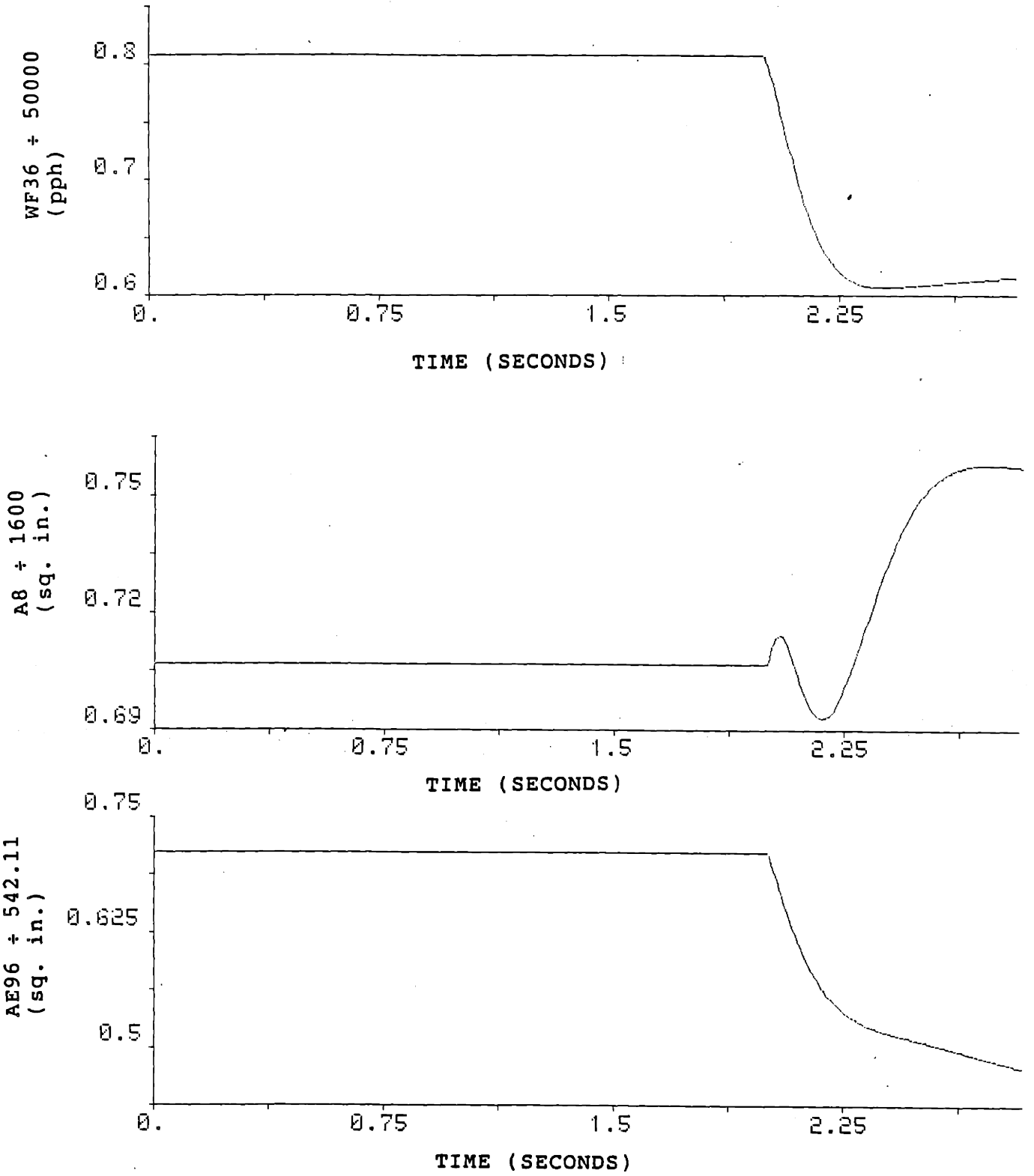

Figure 5.7-6
Control Input Response to Step Decrease in
N2, N25 and FG using the First Compensator

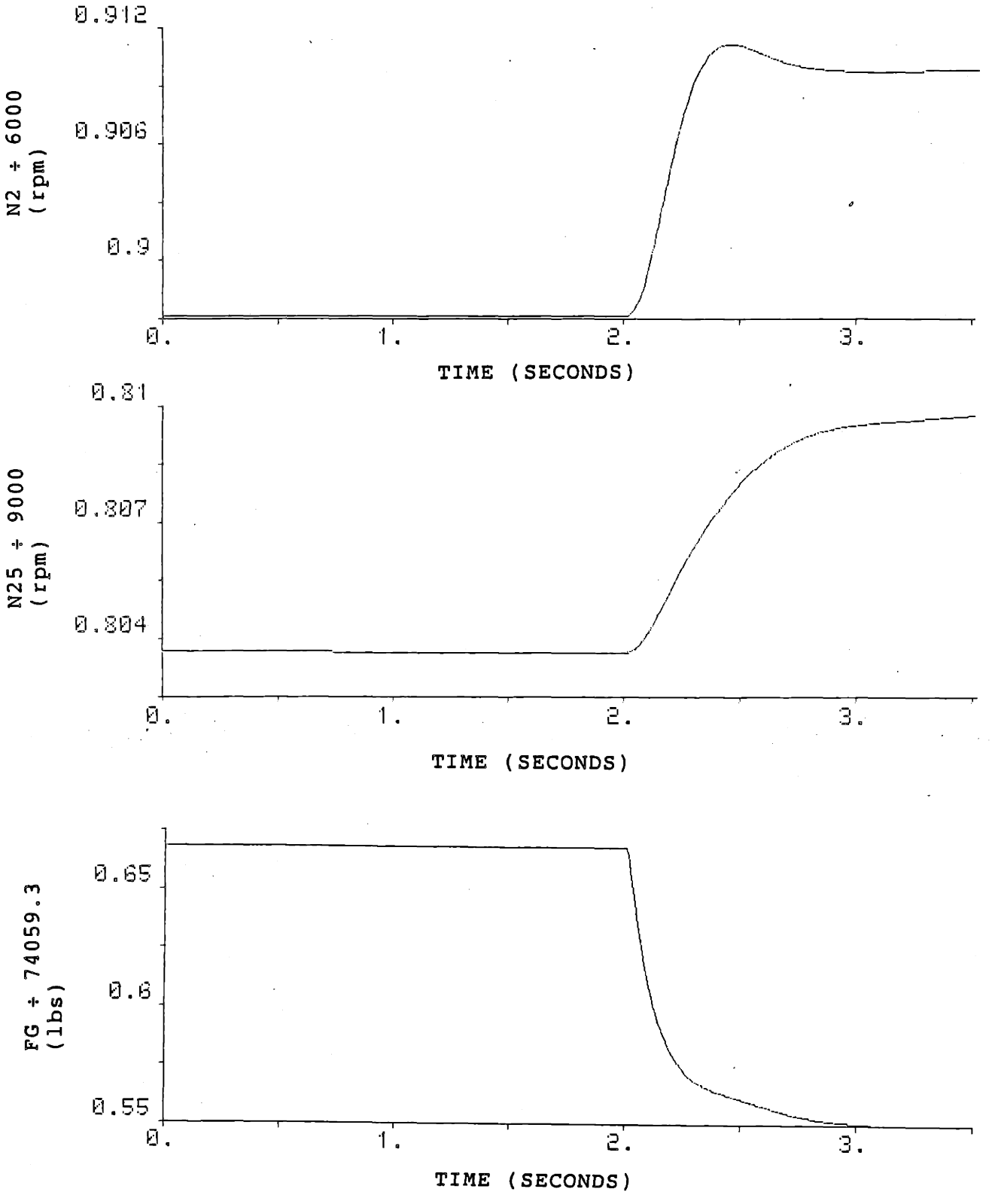

Figure 5.7-7
Output Response to Step Increase in N2 and N25 and
Step decrease in FG using the First Compensator

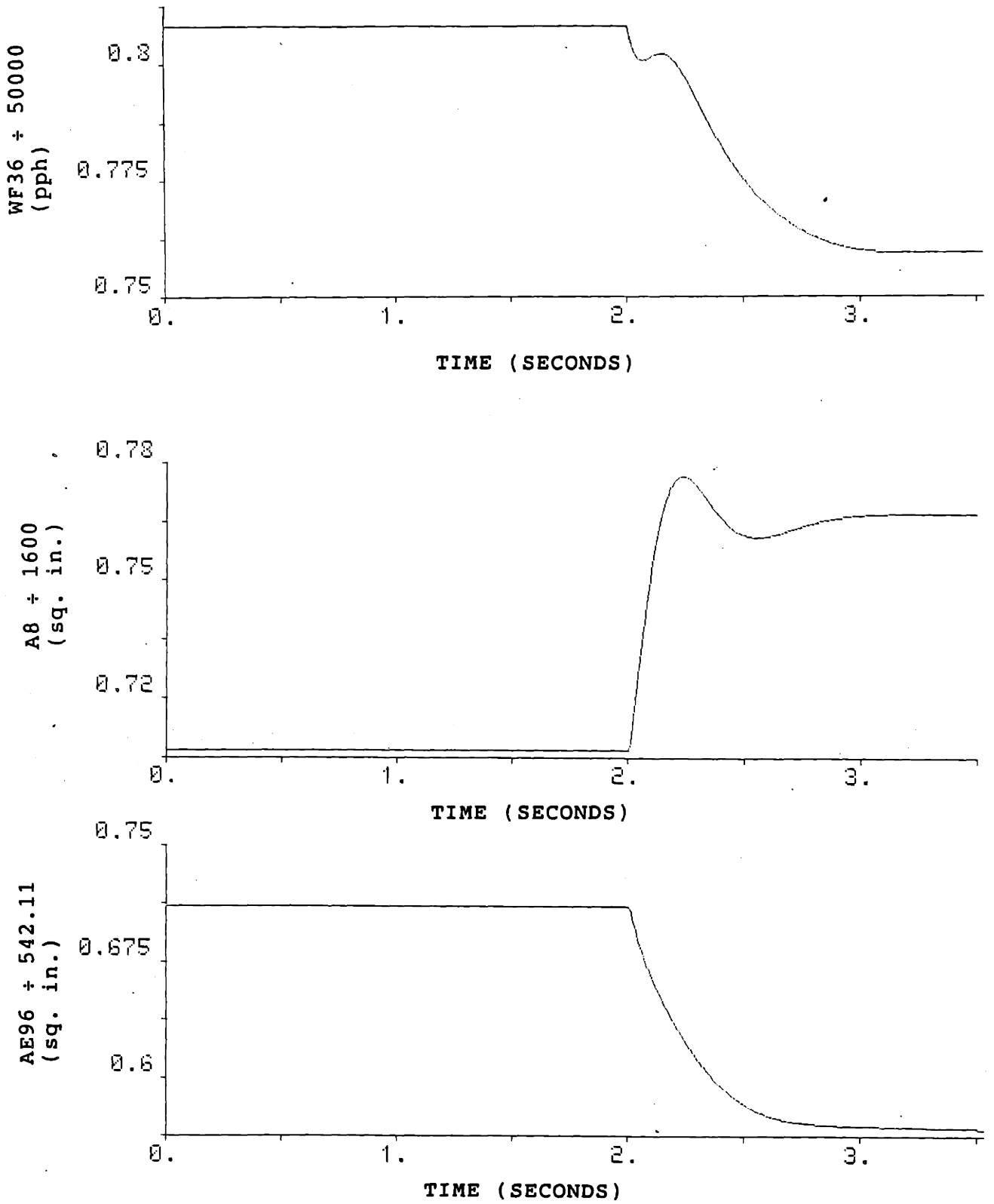

Figure 5.7-8
Control Input Response to Step Increase in N2 and N25 and Step decrease in FG using the First Compensator

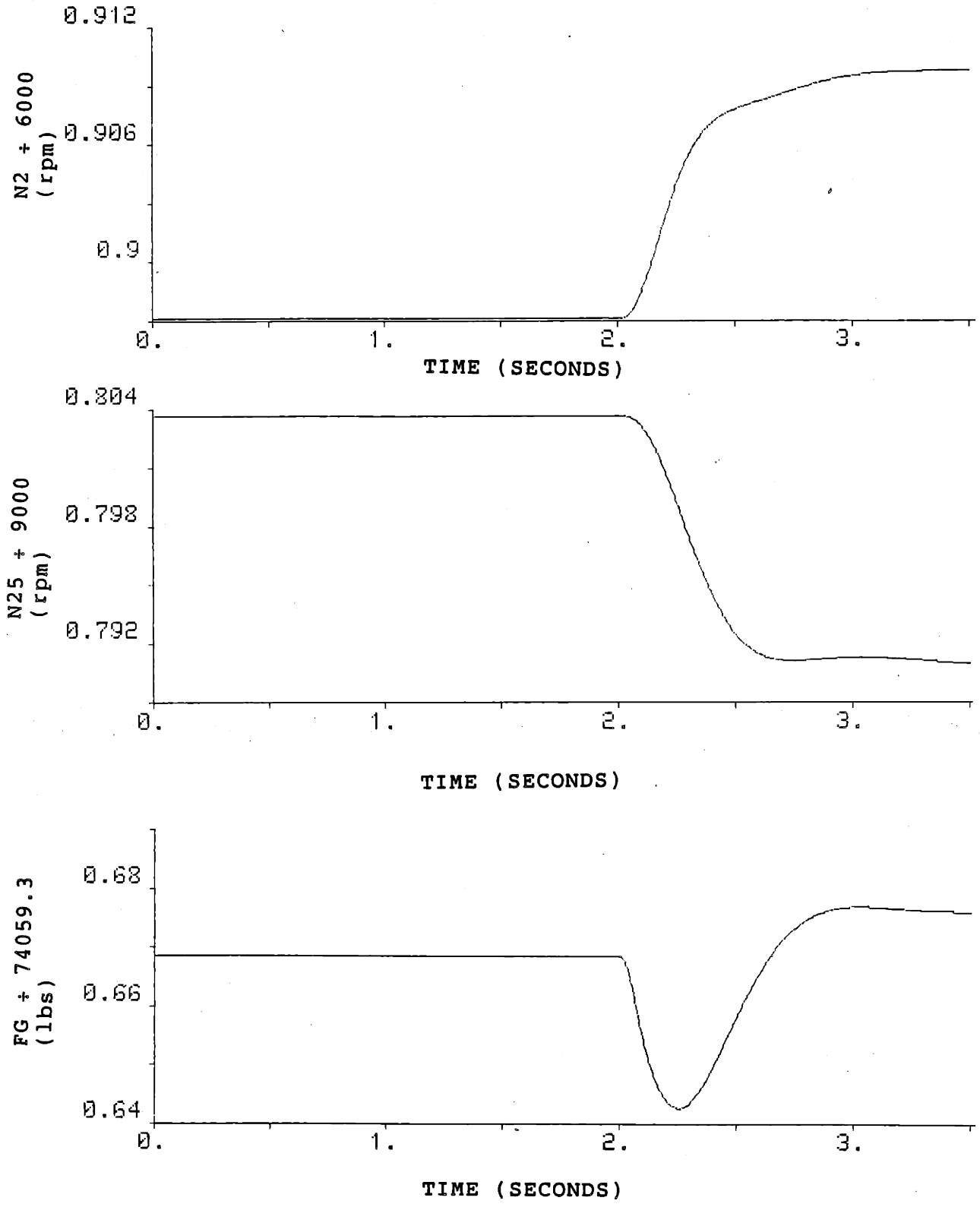

Figure 5.7-9
Output Response to Step Increase in N2 and FG and
Step decrease in N25 using the First Compensator

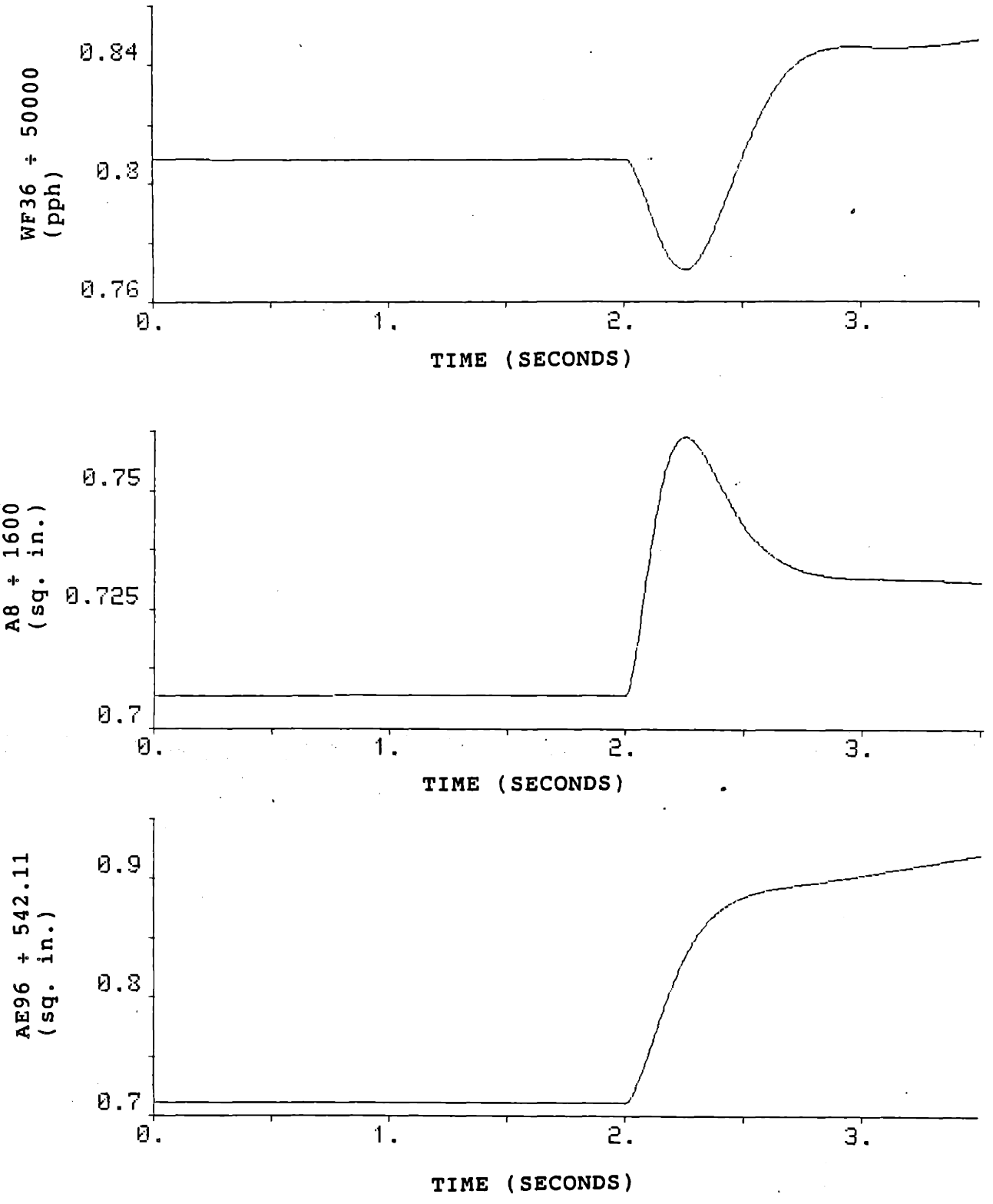

Figure 5.7-10
Control Input Response to Step Increase in N2 and FG and
Step decrease in N25 using the First Compensator

N25 was applied to the system. The response of the system output is shown in Figure 5.7-9 and 5.7-10. The system displayed adequate command following, however there appears to be significant overshoot on all the control inputs. This mode of operation is presented purely for academic interest since there is no forseen reason why one would wish to operate the engine in this manner.

It is clear that use of the first design is more appropriate for operating the engine in the "traditional" mode of operation (i.e., when the rotor speeds are used to adjust thrust) and that the third or reduced designs are more appropriate for operating in the Thrust Modulation mode. For implementation on the engine, both compensators could be provided and the pilot would choose which compensator is used by defining the mode of operation required.

5.8 RESPONSE TO SINUSOIDAL THRUST COMMANDS

As a final simulation, the reduced order compensator was connected to the nonlinear model and a sinusoidal input was provided as the commanded thrust reference. The speeds, N2 and N25 were commanded to stay at their equilibrium values (N2=5382 rpm and N25=7236 rpm) throughout the simulations.

For the first simulation, the thrust reference input shown in Figure 5.8-1 was applied to the system. This reference input commands the average thrust to decrease from the nominal value of 48900 lbs down to 41000 lbs.

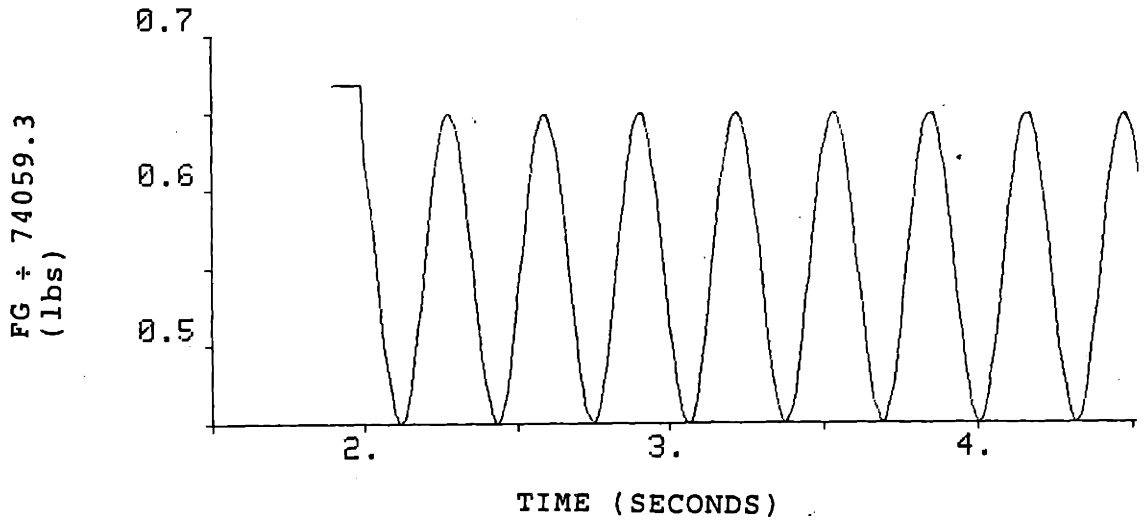

Figure 5.8-1
Commanded Thrust Change Using 5 rad/sec Sinusoidal Input

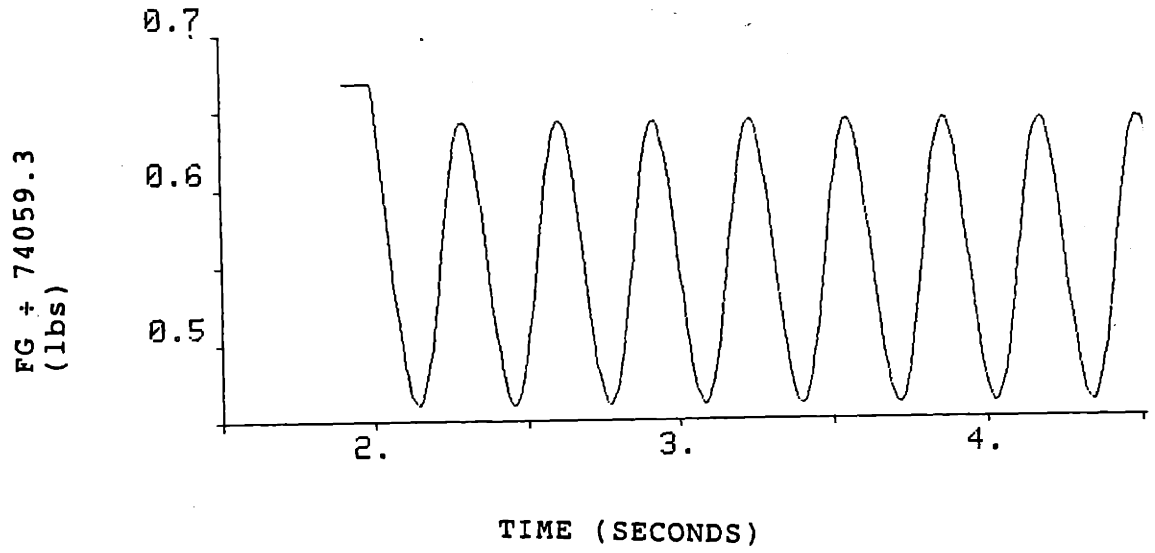

Figure 5.8-2
System Thrust Output Response To 5 rad/sec Sinusoidal Input
Using the Reduced Order Compensator

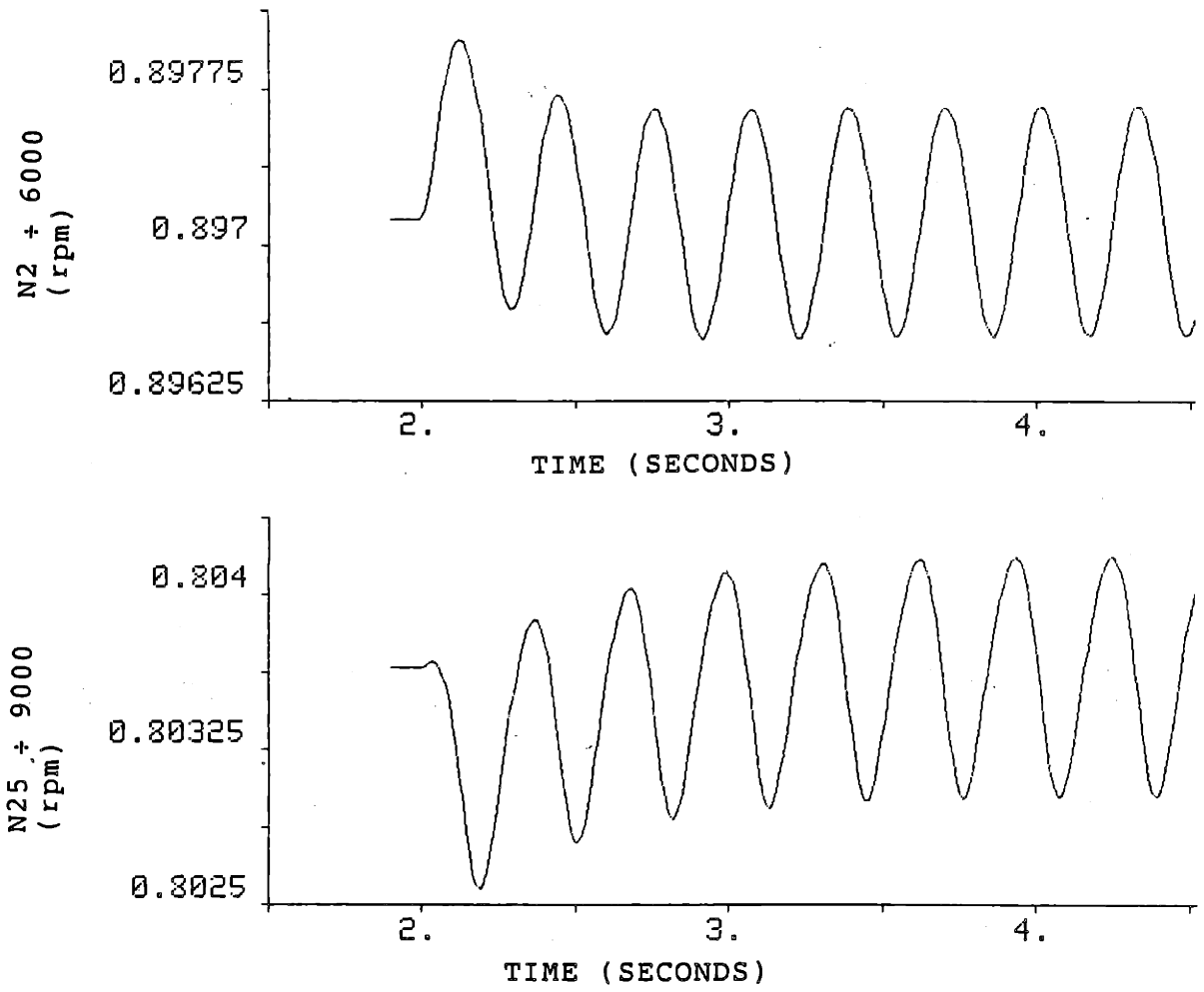

Figure 5.8-3
Rotor Speed Response To 5 rad/sec Sinusoidal Thrust Input
and Constant Commanded Speeds Using Reduced Compensator

Superimposed on this average change in thrust is a 15000 lb peak-to-peak sinusoidal reference at a frequency of 5 rad/sec. This implies that the steady state operation of the system will be to sinusoidally vary thrust from 33500 lbs to 48500 lbs at a frequency of 5 rad/sec.

The thrust output response for this simulation is shown in Figure 5.8-2. The response of the two rotor speeds and are shown in Figure 5.8-3. It can be seen from these figures that the command following response of the system is excellent. The thrust output follows the commanded input exactly and the rotor speeds remain constant (note the scale in Figure 5.8-3 - the rotor speeds change less than 0.01%).

In order to test the disturbance rejection properties of the loop, the same type of input was again applied to the system except the frequency was increased to 2000 rad/sec. We expect the loop respond to the average decrease in thrust as if it were a step input, but the sinusoidal portion of the input should be attenuated. The commanded thrust input for this case is shown in Figure 5.8-4 and the thrust output response is presented in Figure 5.8-5. These figures, as expected, show that the thrust output of the engine does followed the average commanded decrease of 7900 lbs thrust but the sinusoidal component of this input is rejected. For this case, again, the speeds were held constant and the output responses of N2 and N25 are shown in Figure 5.8-6. Again, note the scale on Figure 5.8-6; the rotor speeds change less that 0.01% in response to this commanded input.

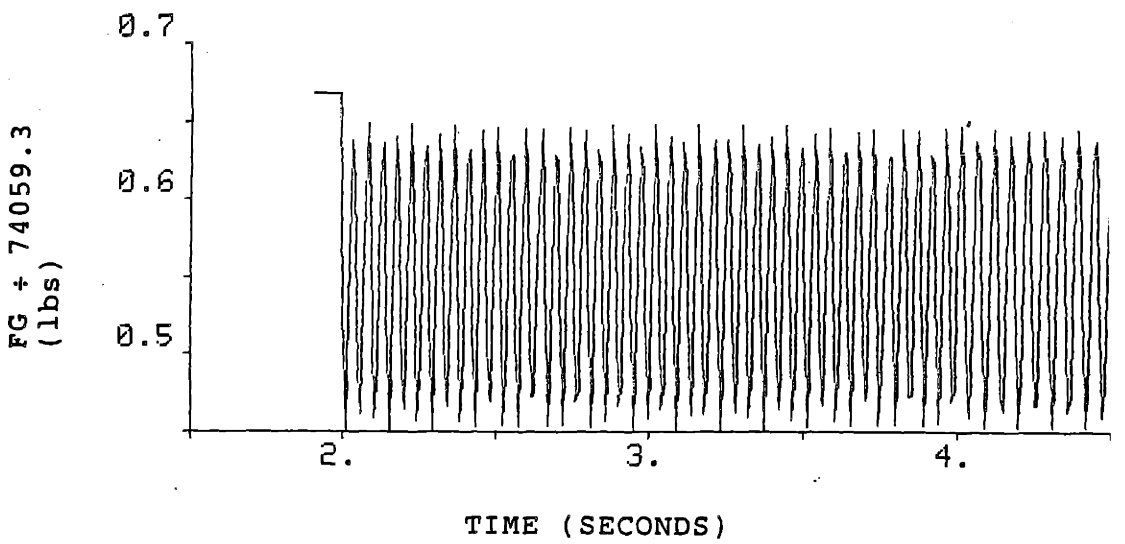

Figure 5.8-4
Commanded Thrust Change Using 2000 rad/sec Sinusoidal Input

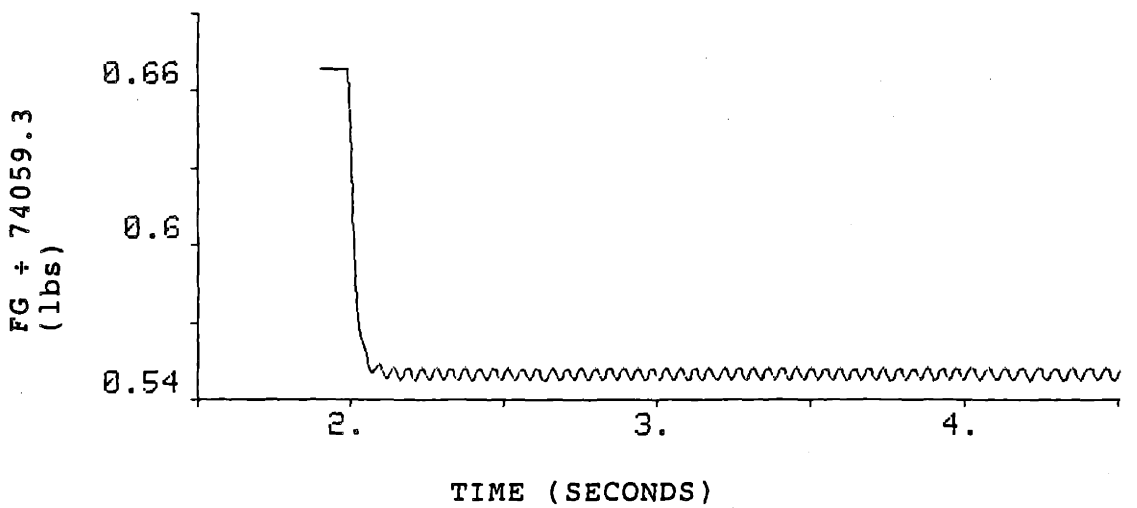

Figure 5.8-5
System Thrust Output Response To 2000 rad/sec Sinusoidal Input
Using the Reduced Order Compensator

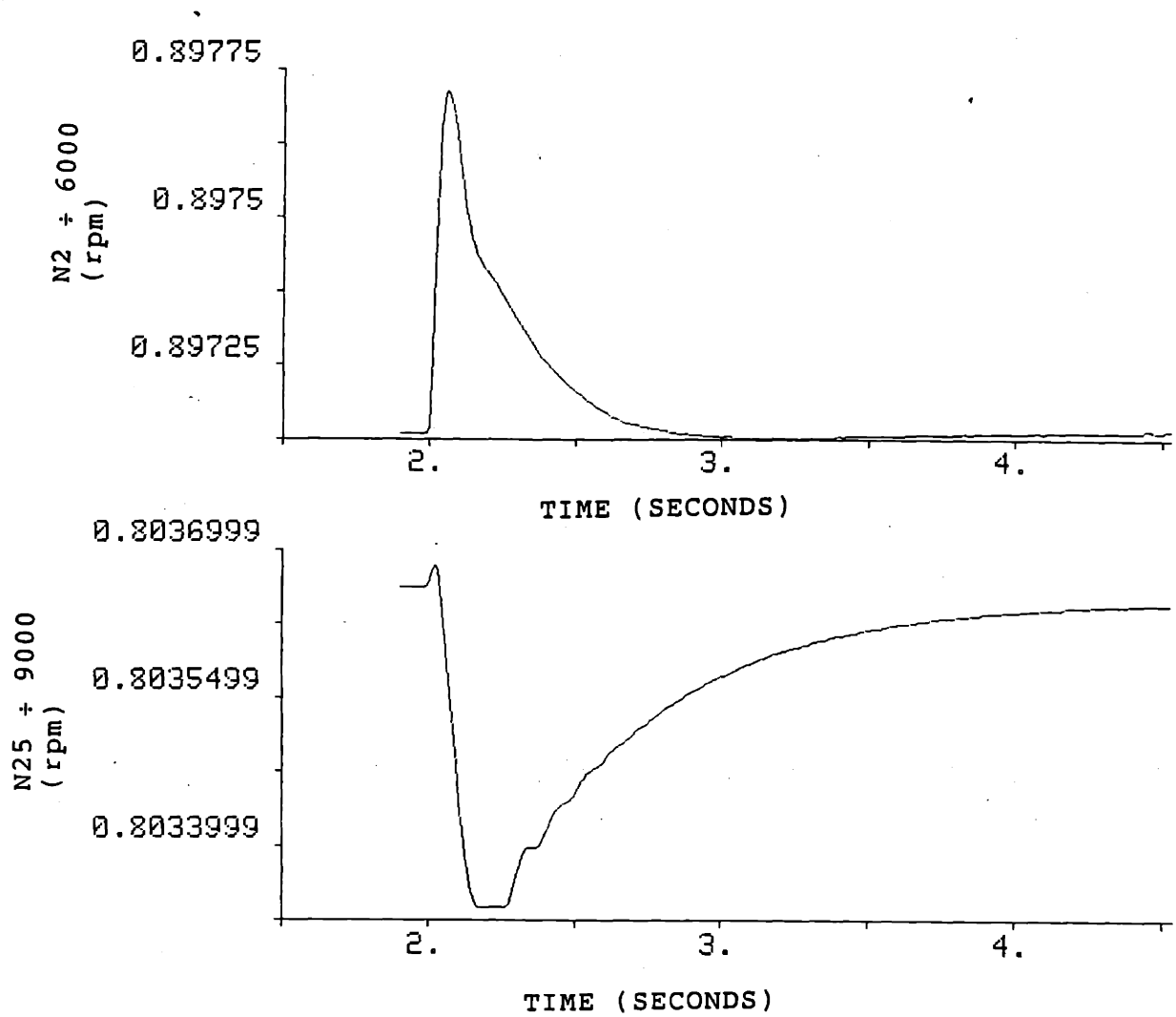

Figure 5.8-6
Rotor Speed Response To 2000 rad/sec Sinusoidal Thrust Input
and Constant Commanded Speeds Using Reduced Compensator

5.9 SUMMARY

This chapter has presented three compensator design examples using the GE21 engine. The three designs were used to illustrate the issues involved in the design of an LQG/LTR based compensator.

The ideas of partial versus full recovery were presented as well as the issues relating to dominant poles and the size of the numerical entries in the compensator system matrices. The technique of over designing the target loop and performing only partial recovery was illustrated by example. The costs and benefits of this type of design were reviewed.

In addition, the technique of reducing the compensator was illustrated using one of the design examples. The combination of the techniques of over designing the loop and reducing the compensator was shown to produce a compensator that met the design specifications, was of lower order than the original compensator and contained reasonable size entries in the compensator system matrices.

The overall discussion was rounded-out by providing a few examples of the system command following properties when commands in different directions were provided as reference inputs.

CHAPTER 6

SUMMARY AND DIRECTIONS FOR FURTHER RESEARCH

6.1 SUMMARY

This thesis has presented a set of control system design examples for the MIMO control of the GE21 jet engine using the LQG/LTR methodology. The major points presented in the thesis were the:

I. Linearization of the nonlinear model around a defined operating point and comparison of the input/output response of resulting linear and nonlinear models.

II. Scaling of the input, output and state variables, various methods of scaling, definition of a scaling transformation and the effects of scaling on the control system design.

III. Use of the singular value decomposition (SVD) in the selection of inputs and outputs as well as in the design of the control system.

IV. Evaluation of the plant chatacteristics at steady state using the plant transfer function matrix (TFM) and the SVD of the plant TFM at s=0.

V. Overview of the LQG/LTR methodology and a discussion of the practical issues, such as the size of the entries in the compensator system matrices.

VI. Design examples using the LQG/LTR methodology which demonstrate the issues involved in partial vs full recovery.

VII. Technique of over designing the target loop and only using partial recovery to obtain the desired performance while keeping the numerical entries in the compensator matrices "small."

VIII. Reduction of the compensator order.

Operation of the engine in the thrust modulation mode, varying thrust from nominal down to 50% of nominal and back up to nominal thrust again while holding the fan and core speeds constant, was also shown to be possible with the compensators obtained using LQG/LTR design methodology. Thrust could be varied by 50% in less than 0.125 seconds without exceeding limits on any of the control inputs when actuators were not used. The speed of the response when using actuators and sensors would depend on the time constants of the particular actuators and sensors used. The overall approach to the problem would remain the same and the actuator and sensor dynamics would simply be modelled as part of the plant during the compensator design.

6.2 DIRECTIONS FOR FURTHER RESEARCH

This research has demonstrated that the LQG/LTR methodology provides an excellent design procedure for the design of control systems for linear plants or for nonlinear plants restricted to a certain operating range. There is still a great deal of work needed in order to develop more systematic nonlinear control system design procedures.

Since it is apparent that the develpoment of nonlinear design methodologies will not be available in the near future, work extending the linear techniques over many different operating points, either by gain sheduling in the controller, see [1] for example, or by switching between

different controllers based on the operating point of the system can be expanded.

The effects of saturation, physical limits or other nonlinearities on the robustness, stability and operation of LQG/LTR based compensators should be evaluated. Both theoretical analysis and design examples in this area are scarce.

The singular value decomposition (SVD) of the plant transfer function matrix has been used to provide very useful information about the coupling of inputs and outputs of the system at steady state. However, the singular values and the singular vectors will change with frequency. Additional research into how the SVD changes with frequency and how the input/output coupling of the plant changes with frequency could also yield valuable information.

In addition, more work is needed in developing less conservative error measures in the LQG/LTR designs. The current error measures are conservative even when the problem specifications are spacially round. In fact, the methods of scaling used tend to force the error response of the system to be "round." However, some of the models developed during the course of this research were actually "better" when operated in certain directions; and these were the directions that were most needed in the system operation. This would mean that the error bounds placed on the control design were probably more conservative than needed. Theoretical work in this area has been started [38], but the design synthesis and

examples have not been attempted.

Finally, the issues of partial vs full recovery should have a careful review. The effects of partial recovery on the stability and robustness of the systems should be qualified by detailed analysis and quantified by more design examples.

Appendix A

Definitions of Variables used in the GE21 Nonlinear Computer Model

This appendix contains a list of the variables used in the nonlinear dynamic computer model of the GE21 engine. The variables used in the component level model, used in this research, are identified with an asterisk (*).

DEFINITION OF VARIABLES FOR THE GE-21 MODEL

	VARIABLE	UNSCALED UNIT	DESCRIPTION
*	A8	SQ. IN.	OUTER NOZZLE EFFECTIVE AREA
*	A88	SQ. IN.	INNER NOZZLE EFFECTIVE AREA
*	AE14B	SQ. IN.	FORWARD VABI AREA FOR FLOW W14B
*	AE16	SQ. IN.	REAR VABI AREA FOR FLOW W16
*	AE56	SQ. IN.	REAR VABI AREA FOR FLOW W56
*	AE96	SQ. IN.	FORWARD VABI AREA FOR FLOW W96
	ALT	FT	ALTITUDE
	AP16	LBS	PS58 * AE16
	AP56	LBS	PS58 * AE56
	BPR94		BYPASS RATIO OF 1ST BLOCK FAN
	BPR94X		DIFFERENT CALCULATION OF BPR94
*	DN2	RPM/SEC	LP ROTOR SPEED DERIVATIVE
*	DN25	RPM/SEC	HP ROTOR SPEED DERIVATIVE
	DLP13	PSI	
	DLP93	PSI	
*	DPQP13		
*	DPQP3		
*	DPQP93		
	DPW2	BTU/SEC	UNBALANCED LP ROTOR POWER
	DPW25	BTU/SEC	UNBALANCED HP ROTOR POWER
*	E14	PSI	ERROR IN STATIC PRESS. AT FWD VABI
*	E4	PSI	ERROR IN COMBUSTOR PRESSURE
*	E4D36		
*	E41	(LBS-SQ. IN.)/SEC	ERROR IN HPT CORRECTED AIRFLOW
*	E49	(LBS-SQ. IN.)/SEC	ERROR IN LPT CORRECTED AIRFLOW
	E48	PSI	ERROR IN HPT PRESSURE
	E56	DEG. R	ERROR IN LPT TEMPERATURE
	E56	PSI	ERROR IN STATIC PRESS. AT REAR VABI
*	E7		
*	E87		
	E93	PSI	ERROR IN 1ST BLOCKER FAN PRESSURE
	ER94		ERROR IN 1ST BLOCK FAN BYPASS RATIO
*	FAR36		
	FAR4		FUEL/AIR RATIO IN COMBUSTOR
*	FAR41		
*	FAR42		
*	FAR49		
*	FAR5		
*	FAR56		
*	FAR6		
*	FAR68		
*	FAR7		
	FFG		
*	FG	LBS	THRUST
	FGR67		FUEL/AIR RATIO IN AFTERBURNER

	VARIABLE	UNSCALED UNIT	DESCRIPTION
	G877		INTERMEDIATE VARIABLE
*	H14B		
*	H16		
*	H25		
*	H3		
*	H41		
*	H41R		
*	H41RX		
*	H42		
*	H49		
*	H49R		
*	H49RX		
*	H5		
*	H56		
*	H6		
*	H7		
	HB27		
*	HCL49		
*	MS058		
*	N2	RPM	LP ROTOR SPEED
*	N2R		
*	N22R		
*	N25	RPM	HP ROTOR SPEED
*	N25R		
*	N41R		
*	N49R		
*	P13	PSI	2ND BLOCK FAN PRESSURE
	P13Q22		2ND BLOCK FAN PRESSURE RATIO
	P14	PSI	2ND BLOCK FAN BYPASS AIR PRESSURE
*	P14B		
	P14Q13		PRESSURE RATIO P14/P13
*	P15B		
*	P16	PSI	BYPASS AIR PRESSURE AT REAR VABI
	P16QAM		PRESSURE RATIO P16/PAMB
*	P2	PSI	INLET AIR PRESSURE
*	P21		
*	P2102		1ST BLOCK FAN PRESSURE RATIO
*	P22	PSI	AIR PRESSURE ENTERING 2ND BLOCK FAN
*	P23		
*	P23Q22		
*	P25	PSI	AIR PRESSURE ENTERING COMPRESSOR
*	P3	PSI	COMPRESSOR OUTPUT PRESSURE
*	P3Q25		COMPRESSOR PRESSURE RATIO

	VARIABLE	UNSCALED UNIT	DESCRIPTION
*	P4	PSI	COMBUSTOR PRESSURE
*	P4X	PSI	P4 CALCULATED DIFFERENTLY
*	P42		
	P42	PSI	HPT EXIT PRESSURE
	P48X	PSI	P48 CALCULATED DIFFERENTLY
	P4204		HPT PRESSURE RATIO
*	P5		
*	P56	PSI	LPT EXHAUST PRESSURE
*	P58		
	P5048		LPT PRESSURE RATIO
	P6	PSI	REAR VABI AIR PRESSURE
*	P7	PSI	AFTER BURNER PRESS. (OUTER NOZZEL)
	P7C	PSI	P7 CHOKED
*	P7X		
*	P7Y		
*	P7Z		
	P7OAM		PRESSURE RATIO P7/PAMB
*	P87		
*	P87X		
*	P87Y		
*	P87Z		
	P93	PSI	1ST BLOCK FAN PRESSURE
	P93X	PSI	P93 CALCULATED DIFFERENTLY
	P9314B		
*	P96		
*	PAMB	PSI	AMBIENT PRESSURE
	PC		POWER CODE
	PCN22R	RPM/DEG. R	CORRECTED SPEED OF 2ND BLOCK FAN
	PCN2R	RPM/DEG. R	CORRECTED SPEED OF 1ST BLOCK FAN
	PRQN2	(DEG. R)/RPM	RATIO OF P2102/PCN2R
*	PS13	PSI	STATIC PRESSURE OF P13
*	PS14B	PSI	STATIC PRESSURE OF P14BO
	PS1409		RATIO OF PS96/PS93
*	PS16	PSI	STATIC PRESSURE OF P16
*	PS3	PSI	STATIC PRESSURE OF P3
	PS58	PSI	STATIC PRESSURE OF P58
*	PS93	PSI	STATIC PRESSURE OF P93
*	PS96		
*	PW2		
*	PW22		
*	PW25		
*	PW4		
*	PW48		
*	PX15B		
*	SM2		
*	SM22		
*	SM25		
*	SQRT14		
*	SQRT15		
*	SQRT16		
*	SQRT25		

	VARIABLE	UNSCALED UNIT	DESCRIPTION
*	SQRT49		
*	SQRT56		
*	SQRTT2		
*	SQRTT22		
*	SQRTT23		
*	SQRTT4		
*	SQRTT41		
*	SQRTT42		
*	SQRTT6		
*	SQRTT7		
	SQT15B	DEG. R	T15B
*	SQTQ21		
*	SQTQ22		
*	SQTQ25		
	SQTT13	DEG. R	T13
	SQTT16	DEG. R	T16
	SQTT2	DEG. R	T2
	SQTT3	DEG. R	T3
	SQTT4	DEG. R	T4
	SQTT48	DEG. R	T48
	SQTT56	DEG. R	T56
	SQTT6	DEG. R	T6
	SQTT7	DEG. R	T7
	SQTT93	DEG. R	T93
	STP2	SQ. IN	1ST BLOCK FAN STATOR VANE AREA
*	STP22	SQ. IN	2ND BLOCK FAN STATOR VANE AREA
*	STP48	SQ. IN	COMPRESSOR STATOR VANE AREA
	T13	DEG. R	2ND BLOCK FAN OUTLET TEMP.
*	T14B		
*	T15B	DEG. R	FWD VABI OUTLET AIR TEMP.
*	T16	DEG. R	BYPASS AIR TEMP. AT REAR VABI
*	T2	DEG. R	INLET OUTLET TEMP.
*	T22		
*	T2202		
*	T25		
*	T2522		
*	T3	DEG. R	COMPRESSOR OUTLET TEMP.
*	T3025		
*	T4	DEG. R	COMBUSTOR OUTLET TEMP.
*	T41		
*	T42		
	T48	DEG. R	HPT OUTLET TEMP.
	T4804		HPT TEMPERATURE RATIO
*	T49		
*	T5		
*	T56	DEG. R	LPT OUTLET TEMP.
	T56X	DEG. R	SAME AS T56, CALCULATED DIFFERENTLY
	T5648		LPT TEMPERATURE RATIO
*	T6	DEG. R	REAR VABI AIR TEMP.
*	T7	DEG. R	HOT STREAM EXHAUST NOZ. INLET TEMP.
	T93	DRG. R	1ST BLOCK FAN OUTLET TEMP.
*	TS58		
*	V58		
*	W13R	PPS	CORRECT. AIRFLOW THRU 2ND BLOCK FAN
*	W14B	PPS	BYPASS AIRFLOW THRU 2ND BLOCK FAN

	VARIABLE	UNSCALED UNIT	DESCRIPTION
	W14BR	PPS	CORRECTED AIR FLOW W14B
*	W14RQA		
*	W15B	PPS	AIR FLOW THRU FWD VABI
	W15BR	PPS	CORRECTED AIR FLOW W15B
*	W15RQA		
*	W16	PPS	BYPASS AIRFLOW ENTERING REAR VABI
	W16R	PPS	CORRECTED AIR FLOW W16
*	W16RQA		
*	W2	PPS	AIR FLOW THRU 1ST BLOCK FAN
*	W21R		
*	W22	PPS	AIR FLOW AT INLET OF 2ND BLOCK FAN
*	W22R	PPS	CORRECTED AIR FLOW W22
*	W23R		
*	W25	PPS	AIR FLOW ENTERING COMPRESSOR
*	W25R	PPS	CORRECTED AIR FLOW W25
*	W2R	PPS	CORRECTED AIR FLOW W2
*	W3		
*	W3R	PPS	CORRECTED COMP. AIRFLOW AT OUTLET
*	W3RQ		
*	W4	PPS	AIR FLOW AT COMBUSTOR OUTPUT
*	W4R		
*	W41		
	W41R	PPS	AIR FLOW AT HPT INLET
	W41RX	PPS	CORRECTED AIR FLOW W41R
*	W42		
*	W42R		
	W48	PPS	AIR FLOW AT LPT INLET
*	W49		
	W49R	PPS	CORRECTED AIR FLOW W49
	W49RX	PPS	W49R CALCULATED DIFFERENTLY
*	W5		
*	W56	PPS	AIR FLOW AT LPT OUTLET
*	W56SQA		
*	W58RQA		
*	W6	PPS	AIR FLOW AT REAR VABI OUTLET
	W6R	PPS	CORRECTED AIR FLOW W6
	W7	PPS	GAS FLOW AT AFTERBURNER OUTLET
	W7SQ	PPS SQ.	W7 SQUARED
*	W87	PPS	AIR FLOW AT INNER NOZZEL INLET
*	W87R		
	W87RQ7		RATIO OF CORRECTED FLOW AT EXHAUST
	W87XR	PPS	CORRECTED AIR FLOW W87 AT P16
*	W93R		
	W94	PPS	BYPASS AIR FLOW AT 1ST BLOCK FAN
	W94R	PPS	CORRECTED AIR FLOW W94
*	W96		
*	W96RQA		
*	WA36		
*	WA41		
*	WA42		
*	WA49		

	VARIABLE	UNSCALED UNIT	DESCRIPTION
*	WA5		
*	WA56		
*	WA6		
*	W8L16Q		RATIO OF W87/W16B
*	WF36	PPH	MAIN BURNER FUEL FLOW
*	WF6	PPH	AFTER BURNER FUEL FLOW
	WQAP14	PPS/(IN. SQ.)	W1413R/AE1413
*	WRQA8		
*	WRQA88		
	WSQTT7	PPS - DEG. R	W7 * T7
*	WTQA8		
*	WTQA88		
*	WV16		(W16*W16*T16)/AP16
*	WV56		(W56*W56*T56)/AP56
	WV6		(W6*W6*T6)/PS58
	XN41R	RPM/DEG. R	CORRECTED COMPRESSOR SPEED
	XN49R	RPM/DEG. R	CORRECTED HP ROTOR SPEED
	XRPCN2	RPM/DEG. R	CORRECTED HP ROTOR SPEED
	XM		MACH NO.
	ALT	FT	ALTITUDE

Appendix B

Numerical Values of Matricies Used in the Simulations

This appendix contains the linear models used in this research. The linear models of the plant are given for the 7 x 7 system. To obtain the model of the 3 x 3, simply omit the rows and columns corresponding to the variables not used. The linear models for the plant are derived using operating point 9 of the nonlinear model. This operating point corresponds to maximum power without afterburner at sea level static conditions.

CONTROL INPUTS	STATES	PLANT OUTPUTS
WF36 (MAIN FUEL FLOW)	N2 (LP ROTOR SPEED)	N2 (LP ROTOR SPEED)
STP22 (STATOR POS.)	N25 (HP ROTOR SPEED)	N25 (HP ROTOR SPEED)
STP48 (STATOR POS.)		FG (THRUST)
A8 (OUTER NOZZLE AREA)		T42 (TURBINE TEMP.)
A88 (INNER NOZZLE AREA)		PS3 (STATIC PRESSURE)
AE16 (REAR VABI AREA)		DPQP3 (COMB. PRES.)
AE96 (FWD VABI AREA)		DPQP13 (FAN. PRES.)

UNSCALED PLANT MATRICES FOR GE21 AT OPERATING POINT 9

A =

```
   -3.3756D+00   1.3118D+00
   -4.7310D-01  -1.9336D+00
```

B =

```
     COLUMNS  1 THRU  6
5.8910D-02  -1.3227D+01  -6.9833D+01   4.2934D+00   9.9861D-01 -2.3686D+00
7.4672D-02   3.1149D+01   7.4723D+01   7.9008D-01   1.7097D+00  5.6932D-01

     COLUMNS  7 THRU  7
   2.0959D+00
  -4.0069D+00
```

C =

```
   1.0000D+00   0.0000D+00
   0.0000D+00   1.0000D+00
   2.6937D+00   1.7633D+01
  -1.1710D-01  -9.9419D-02
   3.5899D-02   2.9047D-02
   9.8955D-06   7.1774D-06
  -3.8373D-05   8.6732D-05
```

D =

```
     COLUMNS  1 THRU  6
0.0000D+00   0.0000D+00   0.0000D+00   0.0000D+00   0.0000D+00   0.0000D+00
0.0000D+00   0.0000D+00   0.0000D+00   0.0000D+00   0.0000D+00   0.0000D+00
8.8192D-01  -2.3357D+02   1.6245D+02  -2.9382D+01   3.3180D+01   4.2507D+01
2.9971D-02   4.6387D-01  -4.9315D+00   1.4675D-01   5.3228D-01   2.7009D-01
1.5466D-03  -2.4597D-01  -1.4231D-01  -3.3014D-02  -9.7645D-02  -4.3791D-02
-7.672D-07  -8.1638D-05   8.8711D-06  -7.1546D-06  -2.1981D-05  -1.0356D-05
-7.180D-07   1.9343D-04  -1.3043D-04   2.2569D-05   6.3532D-05   2.6651D-05

     COLUMNS  7 THRU  7
   0.0000D+00
   0.0000D+00
   1.3943D+02
   5.5325D-02
   9.3046D-02
   1.4377D-05
  -3.4836D-05
```

MATRICIES USED FOR SCALE FACTORS

$\underline{S}_x^{-1}$ =

```
   6000.          0.
      0.       9000.
```

$\underline{S}_u^{-1}$ =

```
      COLUMNS  1 THRU  6
5.0000D+04   0.0000D+00   0.0000D+00   0.0000D+00   0.0000D+00   0.0000D+00
0.0000D+00   6.0000D+01   0.0000D+00   0.0000D+00   0.0000D+00   0.0000D+00
0.0000D+00   0.0000D+00   1.3725D+02   0.0000D+00   0.0000D+00   0.0000D+00
0.0000D+00   0.0000D+00   0.0000D+00   1.6000D+03   0.0000D+00   0.0000D+00
0.0000D+00   0.0000D+00   0.0000D+00   0.0000D+00   5.0000D+02   0.0000D+00
0.0000D+00   0.0000D+00   0.0000D+00   0.0000D+00   0.0000D+00   5.2259D+02
0.0000D+00   0.0000D+00   0.0000D+00   0.0000D+00   0.0000D+00   0.0000D+00

      COLUMNS  7 THRU  7
    0.0000D+00
    0.0000D+00
    0.0000D+00
    0.0000D+00
    0.0000D+00
    0.0000D+00
    5.4211D+02
```

$\underline{S}_y^{-1}$ =

```
      COLUMNS  1 THRU  6
6.0000D+03   0.0000D+00   0.0000D+00   0.0000D+00   0.0000D+00   0.0000D+00
0.0000D+00   9.0000D+03   0.0000D+00   0.0000D+00   0.0000D+00   0.0000D+00
0.0000D+00   0.0000D+00   7.4059D+04   0.0000D+00   0.0000D+00   0.0000D+00
0.0000D+00   0.0000D+00   0.0000D+00   3.2008D+03   0.0000D+00   0.0000D+00
0.0000D+00   0.0000D+00   0.0000D+00   0.0000D+00   3.0000D+02   0.0000D+00
0.0000D+00   0.0000D+00   0.0000D+00   0.0000D+00   0.0000D+00   2.0000D-01
0.0000D+00   0.0000D+00   0.0000D+00   0.0000D+00   0.0000D+00   0.0000D+00

      COLUMNS  7 THRU  7
    0.0000D+00
    0.0000D+00
    0.0000D+00
    0.0000D+00
    0.0000D+00
    0.0000D+00
    2.0000D-01
```

SCALED SYSTEM MATRICIES OF GE21 AT OPERATING POINT 9

A =

```
  -3.3756D+00   1.9677D+00
  -3.1540D-01  -1.9336D+00
```

B =

```
     COLUMNS  1 THRU  6
4.9092D-01  -1.3227D-01  -1.5974D+00   1.1449D+00   8.3218D-02  -2.0630D-01
4.1484D-01   2.0766D-01   1.1395D+00   1.4046D-01   9.4986D-02   3.3058D-02

     COLUMNS  7 THRU  7
   1.8937D-01
  -2.4136D-01
```

C =

```
   1.0000D+00   0.0000D+00
   0.0000D+00   1.0000D+00
   2.1823D-01   2.1428D+00
  -2.1950D-01  -2.7955D-01
   7.1797D-01   8.7141D-01
   2.9687D-01   3.2298D-01
  -1.1512D+00   3.9029D+00
```

D =

```
     COLUMNS  1 THRU  6
0.0000D+00   0.0000D+00   0.0000D+00   0.0000D+00   0.0000D+00   0.0000D+00
0.0000D+00   0.0000D+00   0.0000D+00   0.0000D+00   0.0000D+00   0.0000D+00
5.9542D-01  -1.8923D-01   3.0106D-01  -6.3478D-01   2.2401D-01   2.9994D-01
4.6819D-01   8.6954D-03  -2.1146D-01   7.3359D-02   8.3148D-02   4.4098D-02
2.5776D-01  -4.9195D-02  -6.5107D-02  -1.7607D-01  -1.6274D-01  -7.6281D-02
-1.918D-01  -2.4491D-02   6.0878D-03  -5.7237D-02  -5.4953D-02  -2.7061D-02
-1.795D-01   5.8029D-02  -8.9505D-02   1.8055D-01   1.5883D-01   6.9637D-02

     COLUMNS  7 THRU  7
   0.0000D+00
   0.0000D+00
   1.0206D+00
   9.3703D-03
   1.6814D-01
   3.8970D-02
  -9.4425D-02
```

COMPENSATOR (W/OUT INTEGRATORS) MATRICIES FOR THIRD DESIGN

A =

-3.1770D+02	2.9400D+02	-4.8970D+02	-5.9450D+02	-2.2847D+03
2.8350D+02	-3.5220D+02	4.9730D+02	-7.7220D+02	1.5312D+03
-4.8030D+02	5.0510D+02	-8.4580D+02	-8.0910D+02	-1.2297D+03
5.0000D-01	1.1000D+00	2.0000D-01	-1.0340D+02	1.8000D+00
4.0000D-01	1.0000D-01	-2.0000D-01	-3.0000D-01	-1.0190D+02

B =

3.8434D+01	2.2996D+02	4.2094D+01
2.6750D+02	-1.6899D+02	-2.7378D+01
9.2899D+01	-5.0193D+02	5.6396D+01
1.0000D+02	0.0000D+00	0.0000D+00
0.0000D+00	1.0000D+02	0.0000D+00

C =

2.9260D+02	-2.6720D+02	4.4680D+02	5.3410D+02	1.9419D+03
-2.6720D+02	3.3480D+02	-4.6930D+02	5.1890D+02	-1.2889D+03
4.4680D+02	-4.6930D+02	7.8820D+02	6.8680D+02	1.5805D+03

TRANSFORMATION MATRICIES USED FOR COMPENSATOR REDUCTION OF THIRD DESIGN

T =

COLUMNS 1 THRU 3

1.0000D+00 +0.0000D+00i	0.0000D+00 +0.0000D+00i	0.0000D+00 +0.0000D+00i
0.0000D+00 +0.0000D+00i	5.0000D-01 +0.0000D+00i	0.0000D+00 -5.0000D-01i
0.0000D+00 +0.0000D+00i	5.0000D-01 +0.0000D+00i	0.0000D+00 +5.0000D-01i
0.0000D+00 +0.0000D+00i	0.0000D+00 +0.0000D+00i	0.0000D+00 +0.0000D+00i

COLUMNS 4 THRU 4

0.0000D+00 +0.0000D+00i
0.0000D+00 +0.0000D+00i
0.0000D+00 +0.0000D+00i
1.0000D+00 +0.0000D+00i

K =

-8.5426D-01	3.5026D-01	7.2373D-01	-5.2039D+00	2.3790D+01
-5.4333D-01	-8.8384D-01	-2.2275D-01	4.4253D+01	7.5643D+00
5.3168D-01	8.7789D-01	2.2043D-01	-2.4115D+00	1.6155D+00
-6.2359D-03	2.2488D-03	5.1051D-03	-2.7666D-01	1.3957D+00

M =

-7.0370D-01	7.8704D-03	5.0559D-01	1.0719D+01
2.8794D-01	4.9268D-02	8.3705D-01	-5.4785D+00
6.0370D-01	2.6864D-03	2.0159D-01	-1.1626D+01
1.1065D-03	2.2924D-02	2.3127D-02	-1.7002D-01
-5.5969D-03	4.4900D-03	4.7572D-03	7.8203D-01

REDUCED COMPENSATOR MATRICIES

F =

-3.5120D+01	-5.5511D-16	-1.0270D-14	-4.4054D-13
1.9651D-14	-7.5296D+01	2.4971D+01	-4.9027D-13
-1.7125D-14	-2.4971D+01	-7.5296D+01	3.4817D-13
1.3878D-17	4.1633D-17	-5.5511D-17	-9.4080D+01

G =

-3.9229D+02	1.7601D+03	-4.7331D+00
4.1473D+03	8.9266D+02	-1.1235D+01
3.4594D+01	2.4813D+01	1.0777D+01
-2.6829D+01	1.3519D+02	-3.6158D-02

H =

-2.3381D+01	1.1302D+01	3.5939D+01	8.3348D+02
8.8994D+00	1.9239D+01	5.6411D+01	-3.3835D+02
1.8212D+01	5.3532D+00	1.5370D+01	-6.8418D+02

D =

-1.6438D-01	-9.7189D-02	3.0869D+01
1.7455D-01	1.0320D-01	-3.2780D+01
-2.8104D-01	-1.6616D-01	5.2777D+01

FILTER GAIN MATRIX, H, and CONTROL GAIN MATRIX, G, for FIRST DESIGN
(υ=0.01, ρ=0.0001)

$$\underline{H} = \begin{bmatrix} 3.8434 & 22.9958 & 4.2094 \\ 26.7497 & -16.8993 & -2.7378 \\ 9.2900 & -50.1934 & 5.6396 \\ 10.0000 & 0.0000 & 0.0000 \\ 0.0000 & 10.0000 & 0.0000 \end{bmatrix}$$

$$\underline{G} = \begin{bmatrix} 35.0364 & -24.0269 & 43.9901 & 45.8328 & 180.7654 \\ -24.0269 & 39.1416 & -44.3330 & 33.6626 & -113.9700 \\ 43.9901 & -44.3330 & 80.3469 & 58.3002 & 170.1850 \end{bmatrix}$$

FILTER GAIN MATRIX, H, and CONTROL GAIN MATRIX, G, for SECOND DESIGN
(υ=0.01, ρ=10^{6})

$$\underline{H} = \begin{bmatrix} 3.8434 & 22.9958 & 4.2094 \\ 26.7497 & -16.8993 & -2.7378 \\ 9.2900 & -50.1934 & 5.6396 \\ 10.0000 & 0.0000 & 0.0000 \\ 0.0000 & 10.0000 & 0.0000 \end{bmatrix}$$

$$\underline{G} = \begin{bmatrix} 2734 & -2770 & 4508 & 5600 & 19932 \\ -2770 & 3119 & -4786 & 5916 & -13464 \\ 4508 & -4786 & 7806 & 7237 & 15214 \end{bmatrix}$$

FILTER GAIN MATRIX, H, and CONTROL GAIN MATRIX, G, for THIRD DESIGN
(υ=10^{-4}, ρ=10^{6})

$$\underline{H} = \begin{bmatrix} 38.4344 & 229.9582 & 42.0940 \\ 267.4970 & -168.9931 & -27.3782 \\ 92.8995 & -501.9340 & 56.3958 \\ 100.0000 & 0.0000 & 0.0000 \\ 0.0000 & 100.0000 & 0.0000 \end{bmatrix}$$

$$\underline{G} = \begin{bmatrix} 292.6 & -267.2 & 446.8 & 534.1 & 1941.9 \\ -267.2 & 334.8 & -469.3 & 518.9 & -1288.9 \\ 446.8 & -469.3 & 788.2 & 686.8 & 1580.5 \end{bmatrix}$$

Appendix C

Physical Values of the Variables in the GE21 Model

This appendix contains the physical values of the control inputs and states of the GE21 nonlinear models. For reference, the values of the variables are given at all 9 defined engine operating points. The operating points were provided by the General Electric Company and correspond to various steady state operating points of the engine. Operating point 1 corresponds to ground idle, operating points 2 through 8 correspond to various intermediate power setting (e.g., flight idle, climb, cruise) and operating point 9 corresponds to the maximum non-augmented power.

MAXIMUM PHYSICAL VALUES OF CONTROL AND OUTPUT VARIABLES

WF36	= 50,000 pph	N2	= 6000 rpm
STP22	= 60 in^2	N25	= 9000 rpm
STP48	= 137.25 in^2	FG	= 74059.3 lbs
A8	= 1600 in^2	T42	= 3200.78 ^oR
A88	= 500 in^2	PS3	= 300 psia
AE16	= 522.6 in^2	DPQP3	= 0.2
AE96	= 542.11 in^2	DPQP13	= 0.2

Note that the value of each parameter listed above is used as the scale factor for the respective variable.

PHYSICAL VALUES OF CONTROL INPUTS AT THE 9 OPERATING POINTS

VARIABLE:	WF36	STP22	STP48	A8	A88	AE16	AE96
UNITS:	pph	in^2	in^2	in^2	in^2	in^2	in^2
OP. POINT							
1	4050	40.2	109.39	1430.4	341.5	242.5	330.14
2	5850	40.2	109.66	1430.4	294	418.1	362.13
3	7800	40.2	98.82	1296	33.5	401.8	389.23
4	9950	40.2	95.53	1286.4	32	366.3	404.41
5	12750	40.2	94.56	1393.6	32.5	334.5	419.59
6	15450	40.2	95.53	1430.4	90	259.2	428.26
7	17450	40.2	92.64	1131.2	325.5	58.0	429.35
8	26950	30.0	95.8	1131.2	261.5	58.0	414.17
9	40400	19.98	98.68	1131.2	203.5	70.5	385.44

PHYSICAL VALUES OF PLANT OUTPUTS AT THE 9 OPERATING POINTS

VARIABLE:	N2	N25	FG	T42	PS3	DPQP3	DPQP13
UNITS:	rpm	rpm	lbs	^oR	psia	-----	------
OP. POINT							
1	3108	5283	4961	1021	51	0.0850	0.118
2	3468	5706	8813	1149	63	0.0802	0.1346
3	3552	5571	11479	1287	73	0.0744	0.0986
4	3840	5760	14811	1389	86	0.0722	0.0986
5	4236	6057	19700	1488	105	0.0714	0.1026
6	4536	6282	22070	1575	122	0.0708	0.1062
7	4596	6318	24217	1674	127	0.0676	0.1058
8	5016	6750	32882	1936	167	0.0640	0.1212
9	5382	7236	49545	2253	215	0.0604	0.1456

Appendix D

Actuator and Sensor Linear Models

This appendix contains linear models which illustrate typical sensor and actuator dynamics. These models can be assumed to be valid for all operating points of the engine.

figures

REFERENCES

1. Kapasouris, Petros, Gain-Scheduled Multivariable Control for the GE-21 Turbofan Engine Using the LQR and LQG/LTR Methodologies, S.M. Thesis (LIDS-TH-1380), MIT, Cambridge, MA, June 1984.

2. Lehtomaki, Norman A., Practical Robustness Measures in Multivariable Control Systems Analysis, Ph.D. Thesis (LIDS-TH-1093), MIT, Cambridge, MA, May 1981.

3. Treayer, Irwin E., Aircraft Gas Turbine Engine Technology, McGraw-Hill, New York, 1979.

4. Kappos, E., Robust Multivariable Control for the F100 Engine, S.M. Thesis (LIDS-TH-1328), MIT, Cambridge, MA, September 1983.

5. Pfeil, William H., Multivariable Control for the GE T700 Engine Using the LQG/LTR Methodology, S.M. Thesis (LIDS-TH-1394), MIT, Cambridge, MA, August 1984.

6. Stewart, G.W., Introduction to Matrix Computations, Academic Press, New York, 1973.

7. Strang, Gilbert, Linear Algebra and its Applications, Academic Press, New York, 1980.

8. Cadzow, James A. and Martens, Hinrich R., Discrete Time and Computer Control Systems, Prentice-Hall Inc., Englewood Cliffs, N.J., 1984.

9. Ogata, Katsuiko, Modern Control Engineering, Prentice-Hall Inc., Englewood Cliffs, N.J., 1970.

10. Phillips, Charles L. and Nagle, H. Troy, Digital Control Systems Analysis and Design, Prentice-Hall Inc., Englewood Cliffs, N.J., 1984.

11. Aircraft Gas Turbine Guide, General Electric Co., AEG-607R (10/80).

12. Preliminary Design Variable Cycle Study Data - Users Manual For Steady-State Performance Computer Program, GE-R-78-AEG-374, General Electric Co., June 1978.

13. Athans, M., Lecture Notes on Multivariable Control Systems: MIT Subject 6.232, MIT, Cambridge, MA, 1984.

14. Simplified Nonlinear Dynamic Engine Model of the GE21/J11B19 Variable Cycle Engine, Aircraft Engine Business Group, General Electric Company.

15. Mette, James A., Multivariable Control of a Submarine

Using the LQG/LTR Method, S.M. Thesis (LIDS-TH-1468), MIT, Cambridge, MA, May 1985.

16. Brown, H., GE-AEBG Evendale Control Perspective, Presentation delivered at MIT, Cambridge, MA, September 24, 1985.

17. Lau, Henry and Jensen, K. F., "Evaluation of Changeover Control Policies by Singular Value Analysis - Effects of Scaling," AIChE Journal, Vol. 31, No. 1, pp. 135 - 146, January 1985.

18. Lau, Henry, Alvarez, Jesus and Jensen, K. F., "Synthesis of Control Structures by Singular Value Analysis: Dynamic Measures of Sensitivity and Interaction," AIChE Journal, Vol. 31, No. 3, pp. 427 - 439, March 1985.

19. Grosdidier, P, Morari, M. and Holt, B.R., "Integral Controllability Failure Tolerance, Robustness and the Relative Gain Array," Proceedings of the 1984 American Control Conference, Vol. 3, pp. 1290 - 1295, 1984.

20. Brown, H. and Fisk, W., "Integrated Flight and Propulsion Operating Modes for Advanced Fighter Engines," ASME, 83-GT-194, 1983.

21. Doyle, J.C., and Stein, G., "Multivariable Feedback Design: Concepts for Classical/Modern Synthesis," IEEE Trans. Auto Control, Vol. AC-26, No. 1, pp. 4-16, February 1981.

22. Stein, G., "LQG Based Multivariable Design: Frequency Domain Interpretation," AGARD-LS-117, 1981.

23. Stein, G. and Athans, M., "The LQG/LTR Procedure for Multivariable Feedback Control Design," LIDS-P-1384, May 1984.

24. Gill, P.E., Murray, W., and Wright, M.H., Practical Optimization, Academic Press, New York, 1981.

25. Athans, Michael, "A Tutorial On The LQG/LTR Method," Proc. American Control Conference, Seattle, WA, June 1986.

26. Forsythe, G.E., and Moler, C.B., Computer Solutions of Linear Algebraic Systems, Prentice-Hall, Englewood Cliffs, N.J., 1967.

27. Tomlin, J.A., "On Scaling Linear Programming Problems," Math. Program. Study, Vol. 4, No. 146, 1975.

28. SAE Aerospace Recommended Practices, ARP755A, Revision 4-15-74.

29. SAE Aerospace Standard, AS681C, Revision 4-15-74.

30. Kwakernaak, H. and Sivan, R., Linear Optimal Control Systems, Wiley, New York, N.Y., 1972.

31. Kwakernaak, H. and Sivan, R., "The Maximally Achievable Accuracy of Linear Regulators and Linear Optimal Filters," IEEE Trans. Auto Control, Vol. AC-17, No. 1, pp. 79-85, Februrary 1972.

32. Lehtomaki, N., Sandell, N., and Athans, M., "Robustness Results in Linear-Quadratic Gaussian Based Multivariable Control Designs," IEEE Trans. Auto Control, Vol. AC-26, No. 1, Februrary 1981.

33. Quinn, Wilma, Multivariable Control of A Forward Swept Wing Aircraft, S.M. Thesis (LIDS-TH-1530), MIT, Cambridge, MA, January 1986.

34. Rosenbrock, H., Computer-Aided Control Systems Design, Academic Press, New York, 1974.

35. Dehoff, R. L., Hall, W. E., Adams, R. J., Gupta, N. K., F100 Multivariable Control Systhesis Program, AFAPL-TR-77-33-Vol. 1.

36. Edmunds, J. M., "Control Systems Design and Analysis Using Nyquist and Bode Arrays," International Journal of Control, Vol. 30, pp. 773-802, 1979.

37. Sain, M. K., Alternatives for Multivariable Control, NEC, Chicago, 1978.

38. Stein, G., "Beyond Singular Values and Loop Shapes," LIDS-P-1504, August 1985.

39. Athans, M., Kapasouris, P., Kappos, E., Spang, H. A., "Linear-Quadratic-Gaussian with Loop-Transfer-Recovery Methodology for the F100 Engine," AIAA Journal of Guidance, Control, and Dynamics, pp. 45 - 52, Vol. 9, No. 1, January 1986.

40. Kapasouris, P., Athans, M., Spang, H. A., "Gain Scheduled Multivariable Control for the GE-21 Turbofan Engine Using the LQG/LTR Methodology," Proc. American Control Conference, pp 109-118, Boston, MA, June 1985.

41. Pfeil, W. H., Athans, M., and Spang, H. A., "Multivariable Control of the GE T700 Engine Using the LQG/LTR Design Methodology," Proc. American Control Conference, Seattle, WA, June 1986.